Electrochemical Studies at Carbon-Based Electrodes

By

KOK DIAN PATRICK GAN

Chemistry Department & St Catherine's College, Oxford

Supervisors: JOHN S FOORD; RICHARD G COMPTON

A thesis submitted for the degree of Doctor of Philosophy
to the Board of Physical Sciences at the University of Oxford

Trinity Term, 2015

Electrochemical Studies at Carbon-Based Electrodes

Kok Dian Patrick Gan, St Catherine's College, Oxford
Doctor of Philosophy, Trinity Term 2015

Abstract

Carbon electrodes have found widespread use in electrochemistry due to its broad versatility and low cost amongst other advantages. Recent innovations in carbon materials have added new dimensions to their utility in electrochemical applications. This thesis aims to investigate aspects of carbon materials, in particular boron-doped diamond (BDD) and nanocarbon composites, mainly for electrochemical analysis and energetics studies.

The electrochemical behaviour of estradiol and other endocrine disrupting compounds was examined on the BDD electrode with different surface pretreatments, as well as on a nanocarbon-modified BDD electrode. It was shown that the precise control of surface chemical termination enabled the electrode to be tuned to exhibit diffusional or adsorptive voltammetry at oxidised and hydrogenated BDD interfaces respectively. Adsorption effects were also observed on the modified electrode leading to significant pre-concentration of the analyte onto the nanocarbon and a corresponding lowering of the limit of detection by ca three orders of magnitude to nanomolar levels.

Surface modification of the BDD electrodes was then explored using a simple and convenient dropcast technique to deposit microcrystalline copper phthalocyanine onto the electrode. The influence of the surface chemical termination towards the interaction with the modifier compound was demonstrated in relation to the oxygen reduction reaction. Hydrogen terminated BDD modified in such a manner was able to significantly decrease the overpotential for the cathodic reaction by ca 500 mV when

compared to the unmodified electrode while modified oxidised BDD showed no such electrocatalysis, signifying greater interaction of the phthalocyanine modifier with the hydrogenated surface. The lack of a further conversion of the peroxide product was attributed to its rapid diffusion away from the triple phase boundary (comprising the phthalocyanine microcrystallite, aqueous solution and BDD electrode) at which the reaction is expected to exclusively occur.

Next carbon composites were studied in the form of carbon paste electrodes (CPEs). The practicality of a nanocarbon paste was established by cyclic voltammetry with several well-characterised redox systems commonly used to test electrode activity and was found to exhibit comparable behaviour to the more typical graphitic formulation. Reversible uptake of some analytes was observed at the CPEs, giving rise to complex double peak voltammetry. This uptake phenomenon was then further examined at the nanocarbon paste electrode to monitor the transfer of species between two dissimilar liquid phases. The interfacial behaviour gave rise to voltammetric peaks which were assigned to species originating from the aqueous, binder and carbon phases respectively and this enabled the measurement of Gibbs energies of transfer between oil and aqueous phases.

Finally the effect of different ionic liquids as binder for carbon-ionic liquid composite electrodes was studied. Some ionic liquids were demonstrated to offer benefits in comparison to oil in the fabrication of carbon paste type electrode due to an increased adsorption of analytes. The ionic “liquid” (with a melting point above room temperature) *n*-octyl-pyridinium hexafluorophosphate $[C_8py][PF_6]$ was shown to be useful in combination with carbon nanotubes as a composite electrode or as a modifier to a screen-printed electrode to significantly enhance the sensitivity of electrochemical detection via adsorptive stripping voltammetry.

Overall the carbon-based electrodes studied have demonstrated excellent utility as electrode materials in the areas of electrochemical sensing and energetics investigations.

Acknowledgements

I thank my supervisors Professor John S Foord and Professor Richard G Compton for taking me on as their student for my DPhil studies in Oxford. Their vast knowledge and immense experience have provided me invaluable guidance towards the development of my research skills. I would like to express my sincere appreciation for their kind understanding and great help in the final period leading to the culmination of this thesis.

I am thankful for the wonderful companionship from all the past and present group members of both the Foord and Compton research groups over the course of my studies.

I wish to give special thanks to my dear friends Lulu, Sirikarn, Tony and Jun for their generous support and much treasured friendship since the start of my time in Oxford. I also thank my friends in Singapore for keeping in touch with me from afar.

The kind assistance from Dr Hu Jingping, Dr Denise Lowinsohn, Charlie Jones, Dr Robert Jacobs and Dr Ashley Shepherd towards showing and helping me with various experimental techniques beyond my repertoire is much appreciated.

I am grateful to the National Research Foundation and the Economic Development Board of Singapore for the financial support through the Singapore-Peking-Oxford Research Enterprise (SPORE) Scholarship.

Finally, I thank my family for their love, patience and support through all these years.

Publications

The Voltammetry and Electroanalysis of Some Estrogenic Compounds at Modified Diamond Electrodes

P. Gan, R.G. Compton, J.S. Foord, Electroanalysis 25 (2013) 2423.

Nanocarbon Paste Electrodes

D. Lowinsohn, **P. Gan**, K. Tschulik, J.S. Foord, R.G. Compton, Electroanalysis 25 (2013) 2435.

The Measurement of the Gibbs Energy of Transfer Between Oil and Water Using a Nano-Carbon Paste Electrode

P. Gan, D. Lowinsohn, J.S. Foord, R.G. Compton, Electroanalysis 26 (2014) 351.

Ionic Liquid-Carbon Nanotube Modified Screen-Printed Electrodes and Their Potential for Adsorptive Stripping Voltammetry

P. Gan, J.S. Foord, R.G. Compton, Electroanalysis 26 (2014) 1886.

Surface Modification of Boron-Doped Diamond with Microcrystalline Copper Phthalocyanine: Oxygen Reduction Catalysis

P. Gan, J.S. Foord, R.G. Compton, Chemistry Open. *In press*

Contents

Abstract i
Acknowledgements iii
Publications iv
Contents v
List of Abbreviations ix
List of Figures x
List of Tables xvii

Chapter 1 Introduction 1

1.1 General overview of electrochemical applications 1
1.1.1 Electroanalysis 1
1.1.2 Electrosynthesis 2
1.1.3 Electrochemical Power 3
1.2 Carbon materials 4
1.2.1 Diamond 5
1.2.2 Graphite 10
1.2.3 Nanocarbon (carbon black) 12
1.2.4 Glassy carbon 13
1.2.5 Carbon nanotubes 14
1.3 Aims and scope of thesis 16
References 18

Chapter 2 Experimental Methods and Background 25

2.1 Introduction 25
2.2 Equilibrium electrochemistry 25
2.3 Non-equilibrium electrochemistry 29
2.4 Electrode kinetics 31
2.5 Mass transfer 34
2.5.1 Diffusion 35
2.5.2 Convection 36

2.5.3 Migration 36
2.6 Faradaic and non-faradaic processes 38
2.6.1 Electrical double layer 38
2.7 Electrochemical cell 40
2.7.1 Three-electrode cell design 41
2.8 Electrochemical techniques 42
2.8.1 Cyclic voltammetry 42
2.8.2 Square wave voltammetry 46
2.9 Electrochemical instrumentation 47
2.10 Scanning electron microscopy 48
References 50

Chapter 3 The Voltammetry and Electroanalysis of Some Estrogenic Compounds at Modified Diamond Electrodes 52

3.1 Introduction 52
3.2 Experimental 59
3.2.1 Chemicals and Materials 59
3.2.2 Apparatus 59
3.2.3 Preparation and Modification of Electrode 59
3.3 Results and Discussion 60
3.3.1 Electrochemical Studies Using an Oxidised Diamond Electrode 60
3.3.2 Electroanalytical Studies Using an Oxidised Diamond Electrode 70
3.3.3 Electrochemical Studies Using a Hydrogen Terminated Diamond Electrode 74
3.3.4 Electrode Modification with Nanocarbon 78
3.4 Conclusions 87
References 89

Chapter 4 Surface Modification of Boron-Doped Diamond with Microcrystalline Copper Phthalocyanine: Oxygen Reduction Catalysis 94

4.1 Introduction 95
4.2 Experimental 97

4.2.1 Chemicals and Materials....97
4.2.2 Apparatus....98
4.2.3 Electrode Preparation....98
4.3 Results and Discussion....99
4.3.1 Oxygen Reduction at Unmodified BDD Electrode....99
4.3.2 Effect of Surface Termination on the Interaction of Copper Phthalocyanine with BDD towards Oxygen Reduction....104
4.3.3 Reduction of Hydrogen Peroxide at the Modified H-Terminated BDD....109
4.4 Conclusions....115
References....116

Chapter 5 Nanocarbon Paste Electrodes....121

5.1 Introduction....121
5.2 Experimental section....122
5.2.1 Chemicals and Materials....122
5.2.2 Apparatus....123
5.2.3 Preparation of carbon paste electrodes....123
5.3 Results and discussion....124
5.3.1 Surface characterisation of nanocarbon....124
5.3.2 Electrochemical characterisation: $Ru(NH_3)_6^{3+/2+}$....126
5.3.3 $Fe(CN)_6^{3-/4-}$....129
5.3.4 $IrCl_6^{2-/3-}$....132
5.3.5 Ferrocenemethanol and its diffusion into the nanocarbon paste electrode....134
5.4 Conclusions....137
References....138

Chapter 6 The Measurement of the Gibbs Energy of Transfer Between Oil and Water Using a Nanocarbon Paste Electrode....141

6.1 Introduction....142
6.2 Experimental....143
6.2.1 Chemicals and materials....143
6.2.2 Preparation of the carbon paste electrodes....143
6.3 Results and discussion....144

6.3.1 Accumulation of ferrocenemethanol in an unmodified carbon paste electrode 144
6.3.2 Electrochemical behaviour of a modified carbon paste electrode 146
6.3.3 Effect of solution stirring and peak assignment.....150
6.3.4 Paste composition with different carbon content; assignment of peak P3 ..151
6.3.5 Effect of anion in supporting electrolyte 152
6.3.6 Calculation of Gibbs energy of transfer.....155
6.4 Conclusions.....158
References.....159

Chapter 7 Ionic Liquid-Carbon Nanotube Modified Screen-Printed Electrodes and Their Potential for Adsorptive Stripping Voltammetry. 162

7.1 Introduction.....163
7.2 Experimental.....164
7.2.1 Chemicals and materials 164
7.2.2 Apparatus.....165
7.2.3 Preparation of electrodes 165
7.3 Results and discussion 166
7.3.1 Effect of binder 166
7.3.2 Comparison of different ionic liquids.....170
7.3.3 Optimisation of electrode composition.....172
7.3.4 Adsorptive stripping voltammetry on MWCNTs-[C_8py][PF_6] composite electrodes 175
7.3.5 MWCNTs-[C_8py][PF_6]-modified screen printed electrodes (SPEs) 177
7.4 Conclusions.....181
References.....182

Chapter 8 Conclusions 186

List of Abbreviations

4NP	·····	4-Nonylphenol
BDD	·····	Boron-doped diamond
BPA	·····	Bisphenol A
CE	·····	Counter electrode
CNT	·····	Carbon nanotube
CPE	·····	Carbon paste electrode
CV	·····	Cyclic voltammetry
CVD	·····	Chemical vapour deposition
E1	·····	Estrone
E2	·····	17β-Estradiol
E3	·····	Estriol
EE2	·····	17α-Ethynylestradiol
IHP	·····	Inner Helmholtz plane
IL	·····	Ionic liquid
LOD	·····	Limit of detection
MWCNT	·····	Multi-walled carbon nanotube
NC/BDD	·····	Nanocarbon modified BDD
OHP	·····	Outer Helmholtz plane
PBS	·····	Phosphate buffer solution
RE	·····	Reference electrode
SEM	·····	Scanning electron microscopy
SHE	·····	Standard hydrogen electrode
SPE	·····	Screen printed electrode
SWCNT	·····	Single-walled carbon nanotube
SWV	·····	Square wave voltammetry
WE	·····	Working electrode
XPS	·····	X-ray photoelectron spectroscopy

List of Figures

Figure 1.1 Structure of diamond. 6

Figure 1.2 SEM micrograph of CVD-grown polycrystalline boron-doped diamond. 8

Figure 1.3 Cyclic voltammograms of (a) high-quality boron-doped diamond and (b) platinum electrodes in 0.5 M H_2SO_4. Scan rate: 200 mV s^{-1}. SHE: Standard hydrogen electrode. 9

Figure 1.4 Structure of graphite 11

Figure 1.5 Jenkins-Kawamura model of glassy carbon. L_a and L_c are the lengths for the intraplanar and interplanar graphitic domains. 13

Figure 1.6 Schematic diagram of a structure for a single-walled carbon nanotube (armchair configuration). Projections normal to and along the tube axis are given left and right respectively. 15

Figure 2.1 An electrode immersed in an aqueous solution containing the redox active species O and R. 26

Figure 2.2 Diagram of the energy of electrons in the solution species and in the electrode. 27

Figure 2.3 Schematic representation of some processes involved in a simple one-electron transfer electrode reaction. 30

Figure 2.4 Tafel analysis. 34

Figure 2.5 Schematic diagram of the electrical double layer 39

Figure 2.6 Schematic diagram of a three-electrode electrochemical cell. CE: counter electrode; WE: working electrode; RE: reference electrode. 42

Figure 2.7 Potential waveform in a cyclic voltammetry experiment 43

Figure 2.8 Cyclic voltammogram for a reversible electron transfer reaction 44

Figure 2.9 Potential waveform and measurement scheme for square wave voltammetry. 46

Figure 2.10 Schematic square wave voltammetric profile.....47

Figure 2.11 Schematic illustration of a scanning electron microscope 49

Figure 3.1 Examples of estrogens and some endocrine disruptors. 53

Figure 3.2 Cyclic voltammograms of estradiol (solid), 4-nonylphenol (dash) and bisphenol A (dot), Inset: estradiol (black), estriol (red), estrone (blue) and ethynylestradiol (green). 0.10 mM each in phosphate buffer pH 12.0, scan rate: 50 mV s^{-1}.....61

Figure 3.3 General reaction mechanism for the electrochemical oxidation of phenolic compounds. 61

Figure 3.4 Cyclic voltammograms (three consecutive scans: #1 black, #2 red, #3 blue) of 0.10 mM estradiol in phosphate buffer pH 12.0, scan rate: 50 mV s^{-1}.....63

Figure 3.5 Cyclic voltammograms on oxidised BDD electrode of 0.10 mM of (a) estradiol; (b) 4-nonylphenol in phosphate buffer (pH 12.0) at scan rates of 0.01 to 1.0 V s^{-1}. Insets: Plots of anodic peak current versus the square root of scan rate. 65

Figure 3.6 Influence of pH on anodic peak potential and current of 0.10 mM estradiol in phosphate buffer. Scan rate: 50 mV s^{-1}.....66

Figure 3.7 Tafel plots of 0.10 mM estradiol in phosphate buffer pH 12.0 at scan rates of 0.01 to 0.10 V s^{-1}.....68

Figure 3.8 Square wave voltammograms on oxidised BDD electrode of estradiol in phosphate buffer pH 12.0 at different (a) pulse amplitudes of 20 to 50 mV; (b) frequency of 10 to 60 Hz; (c) scan increments of 2 to 4 mV. Concentration of estradiol for: 0.10 mM. 72

Figure 3.9 (a) Square wave voltammograms on oxidised BDD electrode of estradiol in phosphate buffer pH 12.0 at different concentrations of 0.0, 5.0, 10.0, 25.0, 50.0, 75.0 and 100.0 μM estradiol. (b) Calibration curve of peak current against concentration. ..73

Figure 3.10 Cyclic voltammograms on BDD electrode in phosphate buffer pH 12 of 0.1 mM estradiol after cathodic pretreatment at−2.5 V in 0.5 M H_2SO_4 and 0.1 M HNO_3, and anodic treatment at +2.5 V in 0.1 M HNO_3. Scan rate: 50 mV s^{-1}. 75

Figure 3.11 Cyclic voltammograms on BDD electrode in phosphate buffer pH 12 of: (a) estradiol (solid line), 4-nonylphenol (dashed line) and bisphenol A (dotted line) after

hydrogen plasma pretreatment; (b) estradiol (three consecutive scans) with background scan (dashed line) after hydrogen plasma pretreatment. Concentration of each compound: 0.10 mM. Scan rate: 50 mV s^{-1}. 76

Figure 3.12 Cyclic voltammograms on BDD electrode in phosphate buffer pH 12 of 50.0 μM estradiol at scan rates of 0.01 to 0.20 V s^{-1} after hydrogen plasma pretreatment, inset: plot of anodic peak current versus scan rate. 77

Figure 3.13 Redox couples in KCl solution on oxidised and nanocarbon-modified BDD electrodes: Cyclic voltammograms of (a) 0.50 mM ferrocenemethanol and (b) 1.0 mM ferrocyanide, oxidised (dashed line), NC/BDD (solid line), scan rate: 50.0 mV s^{-1}. 79

Figure 3.14 Redox couples in KCl solution on oxidised and nanocarbon-modified BDD electrodes: Plots of the peak current versus square root of scan rate for (a) 0.50 mM ferrocenemethanol and (b) 1.0 mM ferrocyanide, insets: cyclic voltammograms at scan rates from 10.0 to 200.0 mV s^{-1}. 80

Figure 3.15 Cyclic voltammograms of 0.10 mM estradiol in phosphate buffer solution pH 12.0 on different electrode surfaces. Scan rate: 50.0 mV s^{-1}. Post-analysis: after use for analysis of estradiol.....81

Figure 3.16 Peak current of estradiol in phosphate buffer pH 12.0 on NC/BDD for (a) 0.10 mM, versus scan rate, inset: cyclic voltammograms at scan rates from 10.0 to 150.0 mV s^{-1}.....82

Figure 3.17 Cyclic voltammograms of 0.10 mM estradiol in phosphate buffer solution pH 12.0 on nanocarbon-modified BDD electrode at accumulation times of 0, 30, 60 and 120 s. Scan rate: 50.0 mV s^{-1}. Inset: Plot of peak current against accumulation times. .83

Figure 3.18 Peak currents of 0.10 mM estradiol in phosphate buffer pH 12.0 on NC/BDD with 0, 20, 40, 60, 80, 100 and 120 μL of nanocarbon for modification. Inset: cyclic voltammograms obtained with different amounts of nanocarbon. Scan rate: 50.0 mV s^{-1}.....84

Figure 3.19 Peak currents of 100.0 nM estradiol in phosphate buffer pH 12.0 on NC/BDD with 2, 5, 8, 10 and 15 μL of nanocarbon for modification. Inset: square wave voltammograms obtained with different amounts of nanocarbon. Pulse amplitude: 40 mV; frequency: 20 Hz; scan increment: 2 mV. 84

Figure 3.20 (a) Square wave voltammograms at different concentrations of 0.0, 5.0, 8.0, 20.0, 40.0, 60.0, 80.0 and 100.0 nM estradiol in 0.10 M phosphate buffer pH 12.0 on NC/BDD electrode. Pulse amplitude: 40 mV, frequency: 20 Hz, scan increment: 2 mV. (b) Calibration curve of peak current against concentration.....86

Figure 4.1 Chemical structure of copper phthalocyanine. 96

Figure 4.2 Cyclic voltammograms for hydrogen-terminated (H-BDD, solid line) and oxygen-terminated (O-BDD, dashed line) boron-doped diamond electrodes in N_2-saturated (above) and O_2-saturated (below) 0.1 M phosphate buffer pH 7. Scan rate: 100 mV s^{-1}. The potential was swept in a negative direction from 0 V.....100

Figure 4.3 Cyclic voltammograms for H-terminated BDD electrode in O_2-saturated 0.1 M phosphate buffer pH 7 showing initial scan (solid line), second scan (dashed line) and subsequent scan after stirring (dotted line). Scan rate: 100 mV s^{-1}.....102

Figure 4.4 Cyclic voltammograms for H-terminated BDD in O_2-saturated 0.1 M phosphate buffer pH 7 at scan rates from 20 to 400 mV s^{-1}. Inset: Plot of peak current against square root of scan rate.....103

Figure 4.5 Tafel plots of cathodic current for H-terminated BDD in O_2-saturated 0.1 M phosphate buffer pH 7 at scan rates from 50 to 200 mV s^{-1}. 104

Figure 4.6 SEM micrographs of copper phthalocyanine modified (a) H-terminated, (b) O-terminated BDD.....105

Figure 4.7 Cyclic voltammograms for copper phthalocyanine modified H-terminated BDD in N_2-saturated (above) and O_2-saturated (below) 0.1 M phosphate buffer pH 7. Scan rate: 100 mV s^{-1}.....106

Figure 4.8 Cyclic voltammogram for copper phthalocyanine modified O-terminated BDD in O_2-saturated 0.1 M phosphate buffer pH 7. Scan rate: 100 mV s^{-1}.....107

Figure 4.9 (a) Cyclic voltammograms for copper phthalocyanine modified H-terminated BDD in O_2-saturated 0.1 M phosphate buffer pH 7 at scan rates from 10 to 400 mV s^{-1}. (b) Plot of peak current against square root of scan rate.....108

Figure 4.10 Tafel plots of cathodic current for copper phthalocyanine modified H-terminated BDD in O_2-saturated 0.1 M phosphate buffer pH 7 at scan rates from 50 to 200 mV s^{-1}.....109

Figure 4.11 (a) Cyclic voltammograms for copper phthalocyanine modified H-terminated BDD in N_2-saturated 0.1 M phosphate buffer pH 7 containing 0.0 to 2.0 mM H_2O_2 (dashed line: 0.0 mM). Scan rate: 100 mV s^{-1}. (b) Plot of peak current against concentration of H_2O_2. 111

Figure 4.12 Schematic diagram of the possible surface formation via dropcast modification. 112

Figure 4.13 Schematic diagram showing possible outcomes of hydrogen peroxide during oxygen reduction at the triple phase boundary. 113

Figure 5.1 Schematic diagram of a carbon paste electrode. 124

Figure 5.2 (a) High, (b) intermediate and (c) low magnification SEM images of the commercial nano-carbon particles. 125

Figure 5.3 Cyclic voltammograms of 1.0 mM $Ru(NH_3)_6Cl_3$ in KCl solution at nanocarbon paste (solid line), graphite paste (dashed line) and glassy carbon electrodes (dotted line). Scan rate: 100 mV s^{-1}. 127

Figure 5.4 Cyclic voltammograms of 1.0 mM $Ru(NH_3)_6Cl_3$ in KCl solution at nanocarbon paste electrode at scan rates from 50 to 800 mV s^{-1}. 128

Figure 5.5 Plot of absolute values of cathodic peak current density for $Ru(NH_3)_6Cl_3$ against square root of scan rate at nanocarbon paste, graphite paste and glassy carbon electrodes. 129

Figure 5.6 Cyclic voltammograms of 1.0 mM potassium ferrocyanide in KCl solution at nanocarbon paste (solid line), graphite paste (dashed line) and glassy carbon electrodes (dotted line). Scan rate: 100 mV s^{-1}. 130

Figure 5.7 Plot of anodic peak current density for potassium ferrocyanide against square root of scan rate at nanocarbon paste, graphite paste and glassy carbon electrodes. 131

Figure 5.8 Cyclic voltammograms of 1.0 mM K_2IrCl_6 in KCl solution at nanocarbon paste (solid line), graphite paste (dashed line) and glassy carbon electrodes (dotted line). Scan rate: 100 mV s^{-1}. 132

Figure 5.9 Plot of anodic peak current density for K_2IrCl_6 against square root of scan rate at nanocarbon paste, graphite paste and glassy carbon electrodes. 133

Figure 5.10 Cyclic voltammograms of 0.5 mM ferrocenemethanol in KCl solution at nanocarbon paste (solid line), graphite paste (dashed line) and glassy carbon electrodes (dotted line). Scan rate: 100 mV s^{-1}. 134

Figure 5.11 Plot of anodic peak current density for ferrocenemethanol against square root of scan rate at nanocarbon paste, graphite paste and glassy carbon electrodes.....135

Figure 5.12 Cyclic voltammograms in 0.1 M KCl (A) before and (B) after 20 min the nanocarbon paste electrode was dipped in 0.5 mM ferrocenemethanol and transferred to KCl solution. Scan rate: 50 mV s^{-1}. 136

Figure 6.1 Cyclic voltammograms of the unmodified nanocarbon paste electrode in 0.1 M KCl without (dotted line) and with (solid line) pretreatment of contact in 0.5 mM ferrocenemethanol for 1, 5, 10 and 20 min. Inset: Cyclic voltammogram of unmodified CPE in 0.5 mM ferrocenemethanol (supporting electrolyte: 0.1 M KCl). Scan rate: 50 mV s^{-1}.....145

Figure 6.2 Cyclic voltammograms of the unmodified nanocarbon paste electrode (previously pretreated for 20min) at 0, 1, 2, 4, 6, 8 and 10 min in 0.1 M KCl. Scan rate: 50 mV s^{-1}.....146

Figure 6.3 Cyclic voltammograms of modified nano-carbon paste electrode at 1, 2, 4, 6, 8 and 10 min in 0.1 M KCl for different concentrations of ferrocenemethanol in oil of (a) 20 mM, (b) 10 mM, (c) 5 mM, (d) 50 mM. Scan rate: 50 mV s^{-1}. 147

Figure 6.4 (a) Cyclic voltammograms after 3-hour immersion of modified nanocarbon paste electrode in 0.1 M KCl at scan rates of 50 to 800 mV s^{-1}; (b) Plot of peak current against square root of scan rate for peak P2a.....149

Figure 6.5 Cyclic voltammograms of modified nanocarbon paste in 0.1 M KCl with (solid line) and without (dashed line) solution stirring. Scan rate: 50 mV s^{-1}. Concentration of ferrocenemethanol in oil: 20 mM. 150

Figure 6.6 Cyclic voltammograms in 0.1 M KCl of modified nanocarbon paste containing 50%, 55%, 60% and 65% carbon (w/w). Scan rate: 50 mV s^{-1}. Concentration of ferrocenemethanol in oil: 10 mM. 152

Figure 6.7 Cyclic voltammograms of modified nano-carbon paste electrode in 0.1 M of (a) KNO_3, (b) KSCN, (c) KPF_6, (d) $KAsF_6$. Scan rate: 50 mV s^{-1}. Concentration of ferrocenemethanol in oil: 10 mM. 154

Figure 7.1 Cyclic voltammograms of carbon paste electrode with (a) paraffin oil and (b) $[C_8py][PF_6]$ as binder at 0 and 10 min of immersion in 0.05 mM EE2 in phosphate buffer pH 7. Scan rate: 100 mV s^{-1}. 168

Figure 7.2 Cyclic voltammograms of graphite:$[C_8py][PF_6]$ electrode after immersion for 0 min, 30 min, 60 min, 90 min and 120 min in 5.0 μM EE2 in phosphate buffer pH 7 with stirring. Scan rate: 100 mV s^{-1}. Inset: Graph showing peak current at times from 0 to 120 min. 169

Figure 7.3 Cyclic voltammograms of graphite:$[C_8py][PF_6]$ composite electrode in 5.0 μM (i) EE2, (ii) estradiol and (iii) 4-nonylphenol in phosphate buffer pH 7. Scan rate: 100 mV s^{-1}. Inset: corresponding structures of compounds studied. 170

Figure 7.4 Chemical structures of the ionic liquids studied.....171

Figure 7.5 Peak currents for voltammetric scans in 5.0 μM EE2 in phosphate buffer pH 7 on graphite paste electrode made with different ionic liquids (■ $[C_8py][PF_6]$, □ $[C_6py][PF_6]$, ● $[C_4mim][PF_6]$, ▲ $[C_4py][NTf_2]$) as binder at different times of 60 min, 90 min and 120 min of solution stirring. Scan rate: 100 mV s^{-1}.....172

Figure 7.6 Cyclic voltammograms of carbon-$[C_8py][PF_6]$ electrode with (i) 10%, (ii) 30%, (iii) 50%, (iv) 70% and (v) 90% graphite (w/w) in 5.0 μM EE2 in phosphate buffer pH 7. Scan rate: 100 mV s^{-1}. Inset: Plot of peak currents as a function of different percentages of graphite. 173

Figure 7.7 Cyclic voltammograms of carbon-$[C_8py][PF_6]$ electrode with (i) 2.5%, (ii) 5%, (iii) 7.5%, (iv) 10% and (v) 20% MWCNTs (w/w) in 5.0 μM EE2 in phosphate buffer pH 7. Scan rate: 100 mV s^{-1}. Inset: Plot of peak currents as a function of different percentages of MWCNTs. 174

Figure 7.8 (a) Linear sweep voltammograms at EE2 concentrations of 0.0, 0.08, 0.2, 0.4, 0.6, 0.8, 1.0 and 2.0 μM. Scan rate: 100 mV s^{-1}; (b) Calibration curve for MWCNTs-$[C_8py][PF_6]$ composite electrode (5:95 w/w) in EE2 in phosphate buffer pH 7 at concentrations from 0.08 μM to 2 μM. 176

Figure 7.9 (a) Linear sweep voltammograms at EE2 concentrations of 0.0, 0.05, 0.1, 0.2, 0.5, 0.8, 1.0 and 2.0 μM. Scan rate: 100 mV s^{-1}; (b) Calibration curve for MWCNTs-$[C_8py][PF_6]$-modified graphite SPE in EE2 in phosphate buffer pH 7 at concentrations from 0.05 μM to 2 μM. 178

List of Tables

Table 1.1 Selected properties of glassy carbon and graphite 14

Table 3.1 Literature for electroanalysis of endocrine disruptors at different electrodes. 57

Table 3.2 Average empirical values of β and diffusion coefficients.....69

Table 4.1 Some examples of modification of boron-doped diamond (BDD) via dropcasting.....96

Table 5.1 Cyclic voltammetric data for $Ru(NH_3)_6^{3+/2+}$ at 100 mV s^{-1} for different electrodes 127

Table 5.2 Cyclic voltammetric data for $Fe(CN)_6^{3-/4-}$ at 100 mV s^{-1} for different electrodes 131

Table 5.3 Cyclic voltammetric data for $IrCl_6^{2-/3-}$ at 100 mV s^{-1} for different electrodes. 132

Table 5.4 Cyclic voltammetric data for ferrocenemethnol at 100 mV s^{-1} for different electrodes. 134

Table 6.1 Average values of midpoint potential (E_{mid}) of peak P2 for different supporting electrolyte. 155

Table 6.2 Gibbs energy of transfer of some ferrocenium compounds 156

Table 7.1 Some simple applications of ionic liquid-carbon nanotube composites for non-enzymatic electroanalysis. GC: glassy carbon. 164

Table 7.2 Literature for electroanalysis of endocrine disruptors at different electrodes. 179

Chapter 1

Introduction

1.1 General overview of electrochemical applications

The essence of electrochemistry lies in the studying of the relation between the passage of electrical charge and chemical processes. Electrochemistry finds widespread applications in modern life and the first part of this introduction provides a brief illustration of some practical uses of electrochemistry, specifically in the areas of electroanalysis, electrosynthesis and electrochemical power generation and transformation.

1.1.1 Electroanalysis

Electroanalysis involves the application of electrochemical methods to the determination of chemical quantities and finds various uses such as environmental monitoring, biomedical sensing and industrial process control. The variety of electroanalytical techniques can be usefully classified into two main types, namely potentiometric and amperometric [1].

In potentiometric methods, the potential established across a membrane is measured under equilibrium conditions. These potentials at effectively zero current reflect the composition of the redox active species present in the system of interest. The most commonly encountered potentiometric probe can be found in the measurement of pH

using glass electrodes. Such methods are also widely used for the quantitation of other ionic species such as calcium, potassium or fluoride ions [1].

Amperometric or controlled-potential techniques measure the current passed as a result of an applied potential at an electrode and include different techniques such as various forms of voltammetry, polarography and amperometry. In these methods, electrons are transferred across the electrode|solution interface and the rates of oxidation or reduction allow the analysis of electroactive species. Various advantages of such techniques include selectivity towards electroactive species, very low detection limits, high sensitivity and a wide range of possible electrodes. These have led to the development of a variety of electrochemical sensing technologies for applications in diverse laboratory and field measurements such as for environmental, clinical and industrial uses [2].

1.1.2 Electrosynthesis

Another major application of electrochemistry is in the area of electrosynthesis, which contributes to the making of some products of great economic value. In these processes, electrodes at sufficiently positive potentials are able to act as a reductant while at sufficiently negative potentials they can function as an oxidant. The electrolysis of some molten salts or its aqueous solution enables the industrial production of certain metals such as aluminium, lithium, sodium, potassium, magnesium and calcium, some of which are almost exclusively made by such means [3].

An additional example of an important industrial operation based on electrochemical technology is the chloralkali process, which involves the electrolysis of brine, that is, a

concentrated aqueous solution of sodium chloride. The principal products manufactured from this process are chlorine gas, hydrogen gas and sodium hydroxide solution [3].

On a much smaller scale than the above methods is the Baizer-Monsanto process for the reductive hydrodimerisation of acrylonitrile to adiponitrile at a cadmium electrode as described by the net equation of the reaction [4]:

$$2\ CH_2{=}CHCN + 2\ e^- + 2\ H^+ \rightarrow NCCH_2CH_2CH_2CH_2CN$$

The product, adiponitrile is a key intermediate in the synthesis of the polymer nylon.

1.1.3 Electrochemical Power

Electricity is a hallmark of modernity of human life and the supply of electrical power in the form of galvanic devices such as fuel cells and batteries is essential to support the functioning of many modern technological applications. In contrast to a combustion engine, the direct conversion of chemical energy to electrical energy in a fuel cell is not limited by the Carnot cycle thereby allowing a higher efficiency to be achieved [5].

With increasing concerns about the global climate as well as diminishing fossil fuel sources, there is growing demand for clean energy as an alternative to traditional hydrocarbon routes. Fuel cells hold great potential for such applications as they can be more efficient in energy conversion and generate lower amounts of greenhouse gas emissions. Typical cell designs that have gained attention include polymer electrolyte membrane and direct methanol fuel cells, which produce water as the by-product of reaction [6,7].

Electrocatalytic materials are essential to the operation of fuel cells for the improvement of faradaic efficiency as well as for the lowering of the overpotentials of the electrode reactions, especially in low-temperature devices. The most active catalyst for this purpose is platinum, however its high costs has prompted research into the improvement of catalyst utilisation and the development of cheaper alternates [8,9].

Other than fuel cells, electrochemical power can also be provided in the forms of batteries and supercapacitors. In batteries, the source of chemical energy is stored within the system itself, in contrast to the fuel cell where the reactants are supplied from external sources. As for supercapacitors, the working mechanism is mainly based on the capacitative properties of the electrochemical double layer [3].

1.2 Carbon materials

Carbon is an important material for many electrochemical applications due to its attractive properties such as high surface area, good electrical and thermal conductivities, chemical stability and low cost [10]. Moreover carbon materials are readily available and can exist in various forms such as powders, fibres, foams, tubes and films. A few examples of their uses in electrochemistry include glassy carbon and carbon paste electrodes for electroanalysis [1,11], graphite as the traditional anode material in the chloralkali industry [3] and high surface area carbon powders as supports for platinum-based electrocatalysts at the electrodes of fuel cells [12].

The ways that carbon atoms can be arranged are dependent on the type of bonding present at the carbon, which generally can be categorised as either sp^3 or sp^2 hydridisation. The wealth of possible carbon architectures is built upon the different

arrangements of its atoms. Various carbon allotropes exist: diamond represents the physical form showing sp^3-type bonding whilst sp^2-type bonding is typified by graphite. Amorphous carbon refers to carbon that exhibits much lower levels of crystallinity than that shown in diamond or graphite, and can have varying proportions of sp^3 and sp^2 bonds.

The diversity of carbon materials has blossomed in relatively recent times with the discovery and development of new and interesting forms of carbon including carbon nanotubes [13], electrically conductive diamond [14] and graphene [15]. Further research is therefore essential to better understand and develop these more advanced carbon materials, especially in the area of electrochemistry given the proven utility of conventional carbon electrodes.

The notable carbon forms that are encountered in this thesis are introduced below and these include diamond, graphite, amourphous carbons (nanocarbon and glassy carbon) and carbon nanotubes.

1.2.1 Diamond

The diamond crystal is cubic and has a tetrahedral arrangement of carbon atoms with sp3 hydridised bonding between them, with a bond length of 1.54 Å, as depicted by the structure in **Figure 1.1** [16]. The extensive three-dimensional strong covalent bonding in diamond makes it the hardest known natural substance and renders it useful in commercial applications such as abrasive grit and cutting tools.

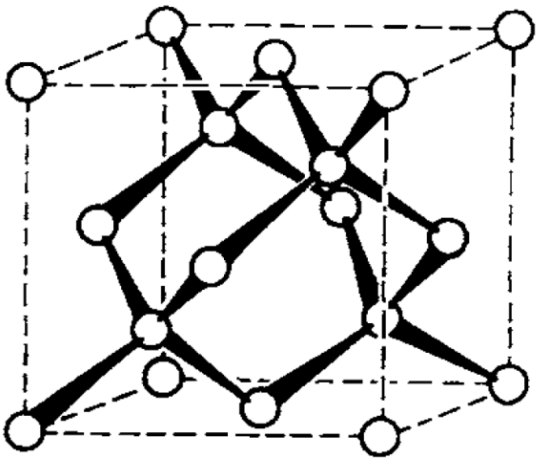

Figure 1.1 Structure of diamond [16].

While pure crystalline diamond is an excellent thermal conductor, it has a large bandgap of 5.45 eV [17], resulting in it being one of nature's best electrical insulator and therefore unsuitable as an electrode material. However, the conductivity of diamond can be improved to levels sufficient for electrochemical applications by the intentional incorporation of impurities, for instance boron or nitrogen. Boron is the most widely used dopant source for making conductive diamond. This imparts p-type semiconducting character, since boron is electron deficient relative to carbon. The boron doping level is often in the range of ~10^{20} atoms/cm^3, or roughly the replacement of one carbon atom per thousand [18].

High quality polycrystalline boron-doped diamond (BDD) thin film is routinely fabricated by the method of plasma-assisted chemical vapour deposition (CVD) [17].

The plasma source is either microwave radiation [19-21] or hot filaments [22]. In both methods, the gas phase is typically made up of hydrogen as the carrier gas, methane [19] or acetone/methane mixture [20] as the carbon source and other gases such as B_2O_3 as the dopant supply. The hydrogen also serves additional functions during the operation [23]:

- Removal of hydrogen from the methyl groups on the surface of the growing diamond film so as to expose fresh sites for deposition
- Production of the reactive methyl radical species by abstraction of hydrogen from the carbon source gas
- Passivation of the dangling bonds to decrease sp^3 to sp^2 reconstruction
- Gasification of any sp^2 non diamond impurity

As a result of the hydrogen atmosphere during CVD growth, the as-grown thin film boron-doped diamond possesses a surface that is largely hydrogen terminated. The accessibility of CVD growth techniques means that thin film boron-doped diamond electrodes can be available at relatively low cost, certainly nowhere near its gemstone counterpart. Polycrystalline BDD material produced by this procedure usually contains individual randomly oriented microcrystallites with size on the order of several micrometres, as shown by the SEM micrograph in **Figure 1.2.**

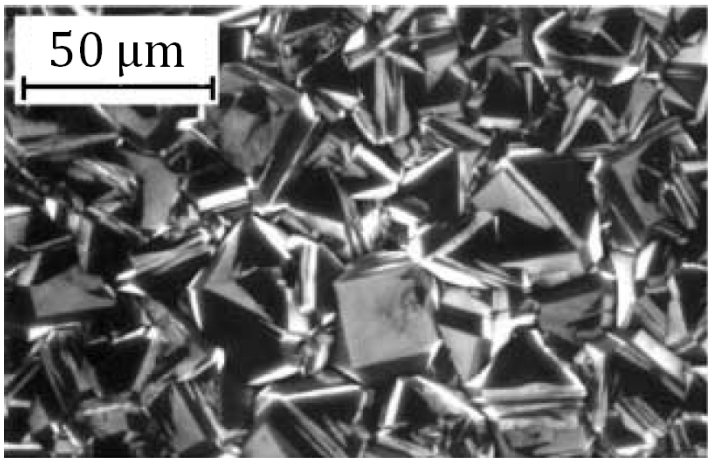

Figure 1.2 SEM micrograph of CVD-grown polycrystalline boron-doped diamond [24].

Boron-doped diamond exhibits several distinct properties that set it apart from conventional electrode materials.

- The high corrosion resistance and mechanical stability of BDD electrodes allow their use in more challenging conditions such as chemically aggressive environments [25], high power ultrasound [26] and very high anodic potentials [27].
- It possesses an extremely wide working potential window in aqueous media, which extends from ~ −1.35 V to +2.3 V (SHE) on high quality conductive diamond [28,29]. A comparison of the potential window with a typical metal (platinum) electrode is provided in **Figure 1.3.**
- Its low background current is an order of magnitude lower than that of glassy carbon [30].
- It is relatively resistant to surface fouling compared to other carbon electrodes and so can be used over longer periods without repeated regenerative treatments [28,31,32].

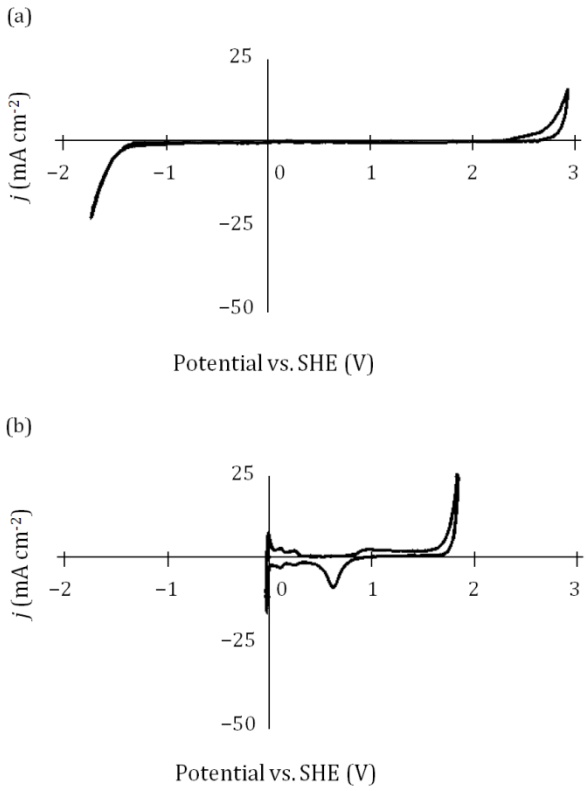

Figure 1.3 Cyclic voltammograms of (a) high-quality boron-doped diamond and (b) platinum electrodes in 0.5 M H_2SO_4. Scan rate: 200 mV s^{-1}. SHE: Standard hydrogen electrode [33].

These advantageous properties of BDD have attracted much interest in research on its electrochemical applications. One such important area is the use of BDD electrodes for electroanalysis [31]. The fairly low capacitative current of conductive diamond enhances the signal to background ratio, which is associated with the limit of detection, and is beneficial for the detection of low levels of target analytes. The large potential range between the oxygen and hydrogen evolution enables electroanalysis outside the potential window offered by other conventional electrodes. Moreover the excellent strength of diamond allows it to be combined with ultrasound to improve mass transfer of reactants [31,34]. A range of analytes have been studied on BDD electrodes and some examples are given below.

- organics
  - ⇨ chlorophenols [35], catecholamines [36], dopamine [37], pharmaceuticals [38], nucleic acids [39]
- inorganics
  - ⇨ azide [40], hydrazine [41], hydrogen peroxide [42], iodine, iodide [43], nitrate [44]
- metal ions
  - ⇨ arsenic [45], mercury [46], cadmium, lead [47,48], manganese [49]

With high applied anodic potentials, reactive oxygen species can be generated at the electrode surface of conductive diamond and this has led to numerous studies on the destructive oxidation of various compounds on BDD electrodes with a view to the treatment of wastewater. These substances include phenols [27], carboxylic acids [50], pharmaceuticals [51,52], dyes [53,54], surfactants [55], herbicides [56] and pesticides [57].

It can be seen that BDD diamond is endowed with certain properties superior to conventional electrode materials and this surely merits further attention towards its electrochemical research, which is an aim of this thesis.

1.2.2 Graphite

Graphite is composed of layers of carbon atoms arranged in hexagonal rings, as shown by the model in **Figure 1.4** and each layer can be referred to as a graphene sheet. The carbon atoms have sp2-hydridised bonding with the carbon-carbon bond length being 1.42 Å in the hexagonal rings while the spacing between graphene layers is 3.354 Å

[10]. Strong covalent bonds exist between the carbon atoms within a graphene layer, however weak van der Waals forces between the layers allow the carbon planes to easily slide past one another. This makes graphite a soft material which in its powdered form can be used as lubricants in commercial applications.

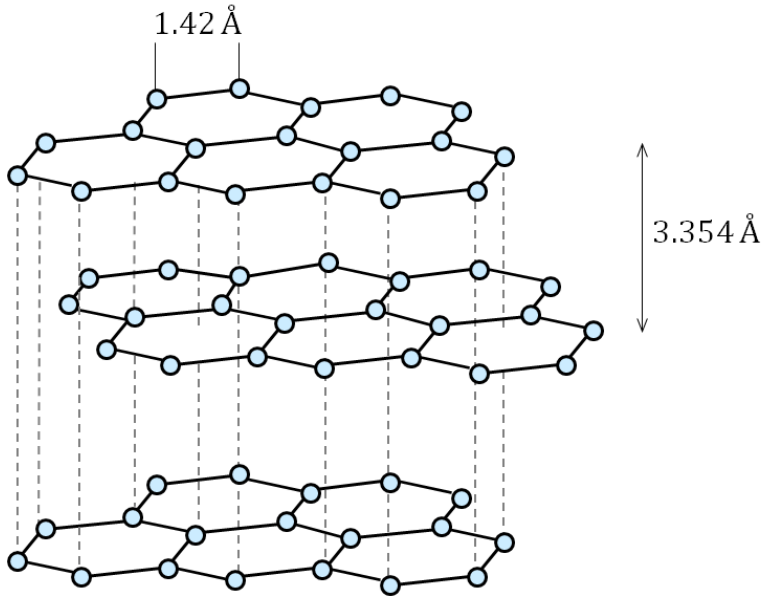

Figure 1.4 Structure of graphite

Due to the strength of covalent bonds within carbon planes, graphite is relatively chemically inert and thus suitable as an electrode material. Moreover it generally has a wider potential range in the same electrolyte compared to platinum, making it a useful electrode for electrochemistry at more positive and negative potentials [10]. It is also a widely used carbon phase in carbon composite electrodes including carbon paste electrode and impregnated-graphite electrode [11].

The graphitic microstructure forms the basis for a number of carbon microstructures having lower levels of crystallinity. Two such examples of amorphous carbon, namely nanocarbon and glassy carbon, are described next.

1.2.3 Nanocarbon (carbon black)

Nanocarbon (so-called carbon black) is widely used for rubber reinforcement and as pigmentation agents. It is mainly produced by the incomplete combustion of gaseous or liquid hydrocarbons [58]. The structure of nanocarbon particles is quasi-graphitic, with a lower three-dimensional order in the direction perpendicular to the graphene plane as well as a larger interplanar spacing (~3.5 to 3.6 Å) than that of graphite (3.354 Å) [10].

The surface area of nanocarbon commonly ranges from <10 to >500 m^2/g, corresponding to particle sizes of >80 to < 10 nm in diameter [10]. In addition to its size, the surface chemical composition exerts a certain influence on the adsorptive properties of nanocarbon [59].

With useful properties such as a high surface area and electrical conductivity, nanocarbon has been employed in electrochemistry mainly in the area of energy storage and conversion devices, for instance as a catalyst support material in fuel cells and as a conductive additive in batteries [60]. It is only quite recently that there is emerging interest concerning the use of nanocarbon for electrochemical sensing applications, such as in the detection of hydrogen peroxide [61], hydrazine [62], nicotine [63] and bisphenol A [64].

While the annual production of nanocarbon is on the order of millions of tonnes (~99% for use in the rubber and ink industries) [16], the level of electroanalytical attention given to this material could conceivably be regarded to pale in comparison to its immense industrial volume [65]. Given the very low cost (~$1/kg [65]) and ready accessibility of this carbon material, this thesis aims to explore aspects of its utility in electroanalysis.

1.2.4 Glassy carbon

Another form of amorphous carbon is glassy carbon, also often known as vitreous carbon, produced from heat treatment of polymeric resin at temperatures between 1000 and 3000°C usually under pressure [10]. It is a hard non-graphitising material with a black, glassy appearance and brittle nature similar to glasses, hence its name.

The model of glassy carbon proposed by Jenkins and Kawamura [66] is widely accepted as the structure for this carbon. As illustrated in **Figure 1.5**, the complex structure is made up of interwoven ribbons of graphitic structure. The intraplanar microcrystalline size, L_a, and the interplanar microcrystalline size, L_c, have values of ca. 50 and 15 Å, respectively [66,67].

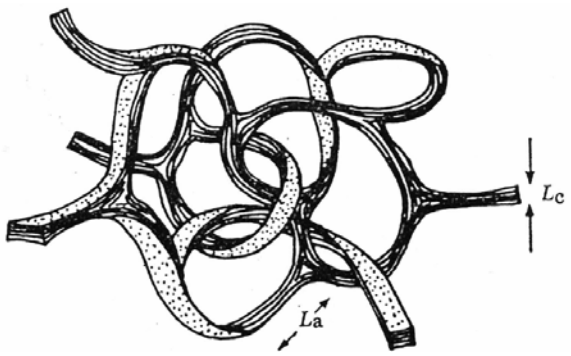

Figure 1.5 Jenkins-Kawamura model of glassy carbon [66]. L_a and L_c are the lengths for the intraplanar and interplanar graphitic domains.

Some selected physical properties of glassy carbon are compared with graphite in **Table 1.1**. The most notable feature of glassy carbon is its very low permeability to gases in comparison to graphite, even though the density of the former is lower. The significant volume of voids present in glassy carbon contributes to its porosity. However these voids are closed and therefore do not allow the passage of gaseous molecules through the material [10]. The high mechanical hardness of glassy carbon allows it to be easily polished when used as an electrode. Glassy carbon is highly resistant to chemical attack [67] and has a rather wide electrochemical window, making it one of the most commonly used carbon electrode material in electroanalytical studies [68,69].

Table 1.1 Selected properties of glassy carbon and graphite [70,71]

Physical property	**Glassy carbon**	**Graphite**
Bulk density (g cm^{-3})	1.3-1.55	1.6
Gas permeability (cm^2 s^{-1})	10^{-6}-10^{-12}	10^{-2}
Tensile strength (kg cm^{-2})	400-1000	420
Thermal conductivity (W m^{-1} K^{-1})	4-25	125-167
Elecctrical resistivity (Ω cm) × 10^4	10-50	7

1.2.5 Carbon nanotubes

Carbon nanotubes (CNTs) [72] exist in two main types of structures. One is of the single-walled (SWCNT) variety, which is formed of a single graphitic sheet rolled into a cylindrical tube, as illustrated in **Figure 1.6** for an armchair configuration. Another type is multi-walled (MWCNT), which consists of multiple concentric and closed SWCNTs. The diameters of carbon nanotubes are typically ~0.4 to >3 nm for SWCNTs and ~1.4 to >100 nm for MWCNTs [73,74]. The main methods of synthesis of carbon nanotubes are arc discharge, laser ablation, and chemical vapor deposition [72].

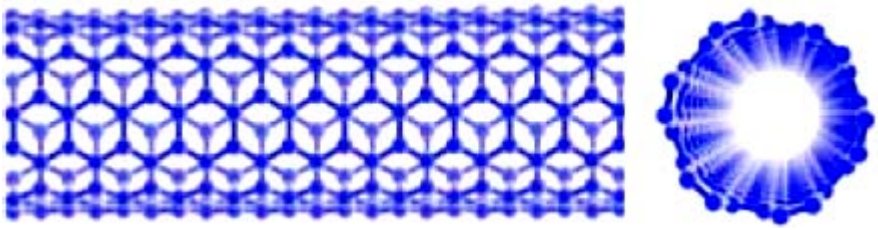

Figure 1.6 Schematic diagram of a structure for a single-walled carbon nanotube (armchair configuration) [74]. Projections normal to and along the tube axis are given left and right respectively.

The unique properties of carbon nanotubes have spurred intense research on this material. Numerous potential and practical applications of carbon nanotubes have been reported, such as for gas sensors [75], nanoelectronic devices [76], field emission electron sources [77], hydrogen storage [78] and nanoprobes in scanning tunnelling microscopy and atomic force microscopy [79].

By virtue of its advantageous characteristics such as high surface area, electronic conductivity and chemical stability, carbon nanotubes have attracted attention for electrochemical energy storage applications, especially in high power supercapacitors [80,81]. Carbon nanotubes have also been widely used for the construction of electrode construction for electroanalysis in several configurations [82]:

- Simple film on typically glassy carbon electrode to increase surface area, lower the overvoltage of reaction and/or alleviate surface fouling effects in the detection of various compounds such as β-nicotinamide adenine dinucleotide (NADH) [83], thyroxine [84], redox protein [85] and cytochrome c [86]

- Combined with other modifiers to enhance the electrode surface functionalities. These include metal nanoparticles [87], enzymes [88,89] and oligonucleotide [90].
- Nanotube paste electrode [91,92]
- Nanotube nanoelectrode [93], owing to the very high current density (up to 10^9 A cm^{-2} [94]) possible at this material.

1.3 Aims and scope of thesis

This thesis aims to study aspects of electrochemical properties at carbon-based electrodes, with a particular focus on boron-doped diamond (Chapters 3 and 4) and carbon composite (Chapters 5, 6 and 7) materials.

Chapter 2 explains the fundamental concepts underpinning the electrochemical processes encountered in this volume and the basic principles behind the relevant measurement techniques are described.

Chapter 3 investigates the voltammetry of some estrogenic compounds at modified and unmodified boron-doped diamond electrodes, with the aims of studying the basic reaction mechanisms as well as analysing these compounds. Another aim is to examine the use of nanocarbon as an electrode modifier towards the improvement of the limit of detection of the target analytes.

Chapter 4 explores the approach of a simple physical deposition method for the surface functionalisation of conductive diamond electrodes. The objective is to understand the

interaction between the BDD surface and the modifier component by investigating the effects on the electrocatalysis of oxygen reduction.

Chapter 5 extends the research on nanocarbon through the introduction of an alternative electrode configuration, specifically in the form of nanocarbon paste electrodes. This chapter aims to characterise these electrodes by a comparison with the more traditional graphitic formulation using well-defined redox probes.

Chapter 6 develops from chapter 5 and examines the interfacial behaviour at nanocarbon paste electrodes, leading to the determination of the energetics of molecular and ionic transfers between two dissimilar liquid phases.

Chapter 7 studies the role of ionic liquids as an alternative binder phase for the construction of carbon composite materials, with the aim of investigating the application of such materials to the modification of screen printed carbon electrodes for adsorptive stripping voltammetry.

References

[1] J. Wang, Analytical Electrochemistry, Wiley, New York, 2006.

[2] C.M.A. Brett, Pure Appl. Chem. 73 (2001) 1969.

[3] K. Oldham, J. Myland, A. Bond, Electrochemical Science and Technology: Fundamentals and Applications, Wiley, Chichester, 2011.

[4] A.J. Bard, G. Inzelt, F. Scholz, Electrochemical Dictionary, Springer, Berlin & Heidelberg, 2012.

[5] F. Beguin, E. Frackowiak, Carbons for Electrochemical Energy Storage and Conversion Systems, CRC Press, London, 2009.

[6] M. Winter, R.J. Brodd, Chem. Rev. 104 (2004) 4245.

[7] D.S. Falcão, V.B. Oliveira, C.M. Rangel, A.M.F.R. Pinto, Renew. Sust. Energ. Rev. 34 (2014) 58.

[8] A. Esmaeilifar, S. Rowshanzamir, M.H. Eikani, E. Ghazanfari, Energy 35 (2010) 3941.

[9] L. Qu, Y. Liu, J.B. Baek, L. Dai, ACS Nano 4 (2010) 1321.

[10] K. Kinoshita, Carbon: Electrochemical and Physicochemical Properties, Wiley, New York, 1988.

[11] I. Švancara, K. Vytřas, J. Barek, J. Zima, Crit. Rev. Anal. Chem. 31 (2001) 311.

[12] S. Sharma, B.G. Pollet, J. Power Sources 208 (2012) 96.

[13] S. Iijima, Nature 354 (1991) 56.

[14] K. Patel, K. Hashimoto, A. Fujishima, J. Photochem. Photobiol., A 65 (1992) 419.

[15] K.S. Novoselov, A.K. Geim, S.V. Morozov, D. Jiang, Y. Zhang, S.V. Dubonos, I.V. Grigorieva, A.A. Firsov, Science 306 (2004) 666.

[16] N.N. Greenwood, A. Earnshaw, Chemistry of the Elements, Elsevier Science, Amsterdam, 2012.

[17] A. Kraft, Int. J. Electrochem. Sci. 2 (2007) 355.

[18] R.L. McCreery, Chem. Rev. 108 (2008) 2646.

[19] M. Hiramatsu, C.H. Lau, A. Bennett, J.S. Foord, Thin Solid Films 407 (2002) 18.

[20] T. Yano, D.A. Tryk, K. Hashimoto, A. Fujishima, J. Electrochem. Soc. 145 (1998) 1870.

[21] M. Kamo, Y. Sato, S. Matsumoto, N. Setaka, J. Cryst. Growth 62 (1983) 642.

[22] M. Fryda, T. Matthée, S. Mulcahy, A. Hampel, L. Schäfer, I. Tröster, Diamond Relat. Mater. 12 (2003) 1950.

[23] C.G. Zoski, Handbook of Electrochemistry, Elsevier, Amsterdam, 2007.

[24] C.H. Goeting, F. Marken, A. Gutierrez-Sosa, R.G. Compton, J.S. Foord, New Diamond Front. Carbon Technol. 9 (1999) 207.

[25] F. Okino, H. Shibata, S. Kawasaki, H. Touhara, K. Momota, M. Nishitani-Gamo, I. Sakaguchi, T. Ando, Electrochem. Solid-State Lett. 2 (1999) 382.

[26] A.J. Saterlay, J.S. Foord, R.G. Compton, Electroanalysis 13 (2001) 1065.

[27] J. Iniesta, P.A. Michaud, M. Panizza, G. Cerisola, A. Aldaz, C. Comninellis, Electrochim. Acta 46 (2001) 3573.

[28] Y.V. Pleskov, Russ. J. Electrochem. 38 (2002) 1275.

[29] H.B. Martin, A. Argoitia, U. Landau, A.B. Anderson, J.C. Angus, J. Electrochem. Soc. 143 (1996) L133.

[30] J.W. Strojek, M.C. Granger, G.M. Swain, T. Dallas, M.W. Holtz, Anal. Chem. 68 (1996) 2031.

[31] R.G. Compton, J.S. Foord, F. Marken, Electroanalysis 15 (2003) 1349.

[32] R. Trouillon, D. O'Hare, Electrochim. Acta 55 (2010) 6586.

[33] G.M. Swain, A.B. Anderson, J.C. Angus, MRS Bulletin 23 (1998) 56.

[34] A.J. Saterlay, F. Marken, J.S. Foord, R.G. Compton, Talanta 53 (2000) 403.

[35] C. Prado, G.G. Murcott, F. Marken, J.S. Foord, R.G. Compton, Electroanalysis 14 (2002) 975.

[36] D. Shin, B.V. Sarada, D.A. Tryk, A. Fujishima, J. Wang, Anal. Chem. 75 (2003) 530.

[37] E. Popa, H. Notsu, T. Miwa, D.A. Tryk, A. Fujishima, Electrochem. Solid-State Lett. 2 (1999) 49.

[38] T.A. Ivandini, B.V. Sarada, C. Terashima, T.N. Rao, D.A. Tryk, H. Ishiguro, Y. Kubota, A. Fujishima, J. Electroanal. Chem. 521 (2002) 117.

[39] T.A. Ivandini, B.V. Sarada, T.N. Rao, A. Fujishima, Analyst 128 (2003) 924.

[40] A. Suzuki, T.A. Ivandini, A. Kamiya, S. Nomura, M. Yamanuki, K. Matsumoto, A. Fujishima, Y. Einaga, Sens. Actuators, B 120 (2007) 500.

[41] C. Batchelor-McAuley, C.E. Banks, A.O. Simm, T.G.J. Jones, R.G. Compton, Analyst 131 (2006) 106.

[42] T.A. Ivandini, R. Sato, Y. Makide, A. Fujishima, Y. Einaga, Diamond Relat. Mater. 14 (2005) 2133.

[43] S. Fierro, C. Comninellis, Y. Einaga, Talanta 103 (2013) 33.

[44] C.M. Welch, M.E. Hyde, C.E. Banks, R.G. Compton, Anal. Sci. 21 (2005) 1421.

[45] T.A. Ivandini, R. Sato, Y. Makide, A. Fujishima, Y. Einaga, Anal. Chem. 78 (2006) 6291.

[46] A. Manivannan, M.S. Seehra, A. Fujishima, Fuel Process. Technol. 85 (2004) 513.

[47] E.A. McGaw, G.M. Swain, Anal. Chim. Acta 575 (2006) 180.

[48] K.E. Toghill, L. Xiao, G.G. Wildgoose, R.G. Compton, Electroanalysis 21 (2009) 1113.

[49] A. J. Saterlay, J. S. Foord, R. G. Compton, Analyst 124 (1999) 1791.

[50] D. Gandini, E. Mahé, P.A. Michaud, W. Haenni, A. Perret, C. Comninellis, J. Appl. Electrochem. 30 (2000) 1345.

[51] E. Brillas, I. Sirés, C. Arias, P.L. Cabot, F. Centellas, R.M. Rodríguez, J.A. Garrido, Chemosphere 58 (2005) 399.

[52] E. Brillas, S. Garcia-Segura, M. Skoumal, C. Arias, Chemosphere 79 (2010) 605.

[53] C. Flox, S. Ammar, C. Arias, E. Brillas, A.V. Vargas-Zavala, R. Abdelhedi, Appl. Catal., B 67 (2006) 93.

[54] F.L. Migliorini, N.A. Braga, S.A. Alves, M.R.V. Lanza, M.R. Baldan, N.G. Ferreira, J. Hazard. Mater. 192 (2011) 1683.

[55] B. Louhichi, M.F. Ahmadi, N. Bensalah, A. Gadri, M.A. Rodrigo, J. Hazard. Mater. 158 (2008) 430.

[56] E. Brillas, B. Boye, I. Sirés, J.A. Garrido, R.M. Rodríguez, C. Arias, P.-L. Cabot, C. Comninellis, Electrochim. Acta 49 (2004) 4487.

[57] Y. Samet, L. Agengui, R. Abdelhédi, Chem. Eng. J. 161 (2010) 167.

[58] J.B. Donnet, Carbon Black: Science and Technology, Second Edition, Taylor & Francis, London, 1993.

[59] H.P. Boehm, Carbon 32 (1994) 759.

[60] I.J. Sanders, T.L. Peeten, Carbon Black: Production, Properties, and Uses, Nova Science Publishers, New York, 2011.

[61] F. Arduini, F. Di Nardo, A. Amine, L. Micheli, G. Palleschi, D. Moscone, Electroanalysis 24 (2012) 743.

[62] J. Panchompoo, L. Aldous, C. Downing, A. Crossley, R.G. Compton, Electroanalysis 23 (2011) 1568.

[63] T.W.B. Lo, L. Aldous, R.G. Compton, Sens. Actuators, B 162 (2012) 361.

[64] M. Portaccio, D. Di Tuoro, F. Arduini, D. Moscone, M. Cammarota, D.G. Mita, M. Lepore, Electrochim. Acta 109 (2013) 340.

[65] L. Dai, Carbon Nanotechnology: Recent Developments in Chemistry, Physics, Materials Science and Device Applications, Elsevier Science, Amsterdam, 2006.

[66] G.M. Jenkins, K. Kawamura, Nature 231 (1971) 175.

[67] P.J.F. Harris, Philos. Mag. 84 (2004) 3159.

[68] W.E. Van der Linden, J.W. Dieker, Anal. Chim. Acta 119 (1980) 1.

[69] F. Scholz, Electroanalytical Methods: Guide to Experiments and Applications, Springer, Berlin & Heidelberg, 2009.

[70] D.W. McKee, Annu. Rev. Mater. Sci. 3 (1973) 195.

[71] P.L. Walker Jr, Carbon 10 (1972) 369.

[72] H. Dai, Acc. Chem. Res. 35 (2002) 1035.

[73] Z.K. Tang, L. Zhang, N. Wang, X.X. Zhang, G.H. Wen, G.D. Li, J.N. Wang, C.T. Chan, P. Sheng, Science 292 (2001) 2462.

[74] R.H. Baughman, A.A. Zakhidov, W.A. de Heer, Science 297 (2002) 787.

[75] D.R. Kauffman, A. Star, Angew. Chem. Int. Ed. 47 (2008) 6550.

[76] S. Saito, Science 278 (1997) 77.

[77] W.A. de Heer, A. Châtelain, D. Ugarte, Science 270 (1995) 1179.

[78] A.C. Dillon, K.M. Jones, T.A. Bekkedahl, C.H. Kiang, D.S. Bethune, M.J. Heben, Nature 386 (1997) 377.

[79] H. Dai, J.H. Hafner, A.G. Rinzler, D.T. Colbert, R.E. Smalley, Nature 384 (1996) 147.

[80] C. Niu, E.K. Sichel, R. Hoch, D. Moy, H. Tennent, Appl. Phys. Lett. 70 (1997) 1480.

[81] P. Simon, Y. Gogotsi, Nat. Mater. 7 (2008) 845.

[82] A. Merkoçi, M. Pumera, X. Llopis, B. Pérez, M. del Valle, S. Alegret, Trends Anal. Chem. 24 (2005) 826.

[83] M. Musameh, J. Wang, A. Merkoci, Y. Lin, Electrochem. Commun. 4 (2002) 743.

[84] W. Kangbing, J. Xiaobo, F. Junjie, H. Shengshui, Nanotechnology 15 (2004) 287.

[85] J.J. Gooding, R. Wibowo, Liu, W. Yang, D. Losic, S. Orbons, F.J. Mearns, J.G. Shapter, D.B. Hibbert, J. Am. Chem. Soc. 125 (2003) 9006.

[86] J. Wang, M. Li, Z. Shi, N. Li, Z. Gu, Anal. Chem. 74 (2002) 1993.

[87] G.G. Wildgoose, C.E. Banks, R.G. Compton, Small 2 (2006) 182.

[88] Y. Lin, F. Lu, Y. Tu, Z. Ren, Nano Lett. 4 (2004) 191.

[89] K. Balasubramanian, M. Burghard, Anal. Bioanal. Chem. 385 (2006) 452.

[90] H. Cai, X.N. Cao, Y. Jiang, P.G. He, Y.Z. Fang, Anal. Bioanal. Chem. 375 (2003) 287.

[91] M.a.D. Rubianes, G.A. Rivas, Electrochem. Commun. 5 (2003) 689.

[92] M.D. Rubianes, G.A. Rivas, Electroanalysis 17 (2005) 73.

[93] J.K. Campbell, L. Sun, R.M. Crooks, J. Am. Chem. Soc. 121 (1999) 3779.

[94] Z. Yao, C.L. Kane, C. Dekker, Phys. Rev. Lett. 84 (2000) 2941.

Chapter 2

Experimental Methods and Background

2.1 Introduction

This chapter aims to provide a general overview of the background theory and techniques which are pertinent to the experimental work in this thesis. Fundamental concepts in electrochemistry are explained, including charge transfer kinetics, mass transfer and the interfacial structure, so as to provide a basic understanding for the study of electrode processes. Electrochemical methods used in the following chapters, in particular cyclic voltammetry and square wave voltammetry, are covered. The current convention used here is that of the IUPAC in which positive potentials are to the right of the origin and anodic currents are taken as positive [1]. The surface characterisation technique of scanning electron microscopy will also be presented.

2.2 Equilibrium electrochemistry

Electrochemistry is concerned with the study of the transfer of charge across the interface between an electronic conductor (an *electrode*) and an ionic conductor (an *electrolyte*). Such electrode processes are heterogeneous in nature. A simple electrode reaction can be illustrated by the following process

$$\mathrm{O(aq)} + \mathrm{e^-(electrode)} \rightleftarrows \mathrm{R(aq)} \qquad (2.1)$$

in which O represents an oxidised species in solution, which gains an electron from an electrode to form R, the reduced species. This can be prepared by the immersion of a suitable electrode (e.g. platinum wire or an inert metal) into an aqueous solution containing the redox active species, as shown in **Figure 2.1**.

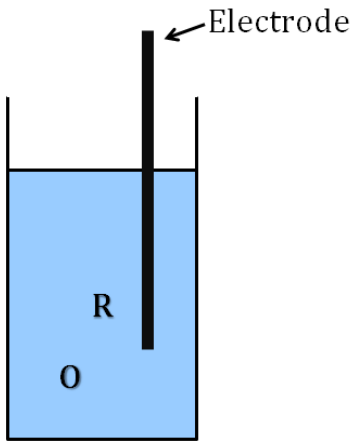

Figure 2.1 An electrode immersed in an aqueous solution containing the redox active species O and R.

As the reaction involves the transfer of electrons, it can be expected that a net electrical charge develops on each of the two phases. Depending on the position of equilibrium, the electrode can have a net positive or negative charge, with the solution phase having the corresponding opposite charge of equal magnitude. This charge separation gives rise to a potential difference across the electrode|solution interface and forms the basis for the electrode potential established at the electronic conductor. If Φ_S and Φ_E represent the potentials for the solution and the electrode respectively, then this potential drop across the electrode/solution interface $\Delta\Phi_{E/S}$ is given by

$$\Delta\Phi_{E/S} = \Phi_E - \Phi_S \qquad (2.2)$$

The difference in potential can be considered in terms of the electronic energy levels within the electrode and the solution species which will be illustrated by reduction of the species O [2,3]. As shown in **Figure 2.2**, before the electron transfer the valence band of the electrode is filled to the Fermi level and the species O has an unfilled molecular orbital available to be gain electrons. As the Fermi level is higher in energy than the vacant orbital, it is energetically favourable for electrons to flow from the electrode to the species O converting them to species R. This energy difference is the driving force for the charge transfer.

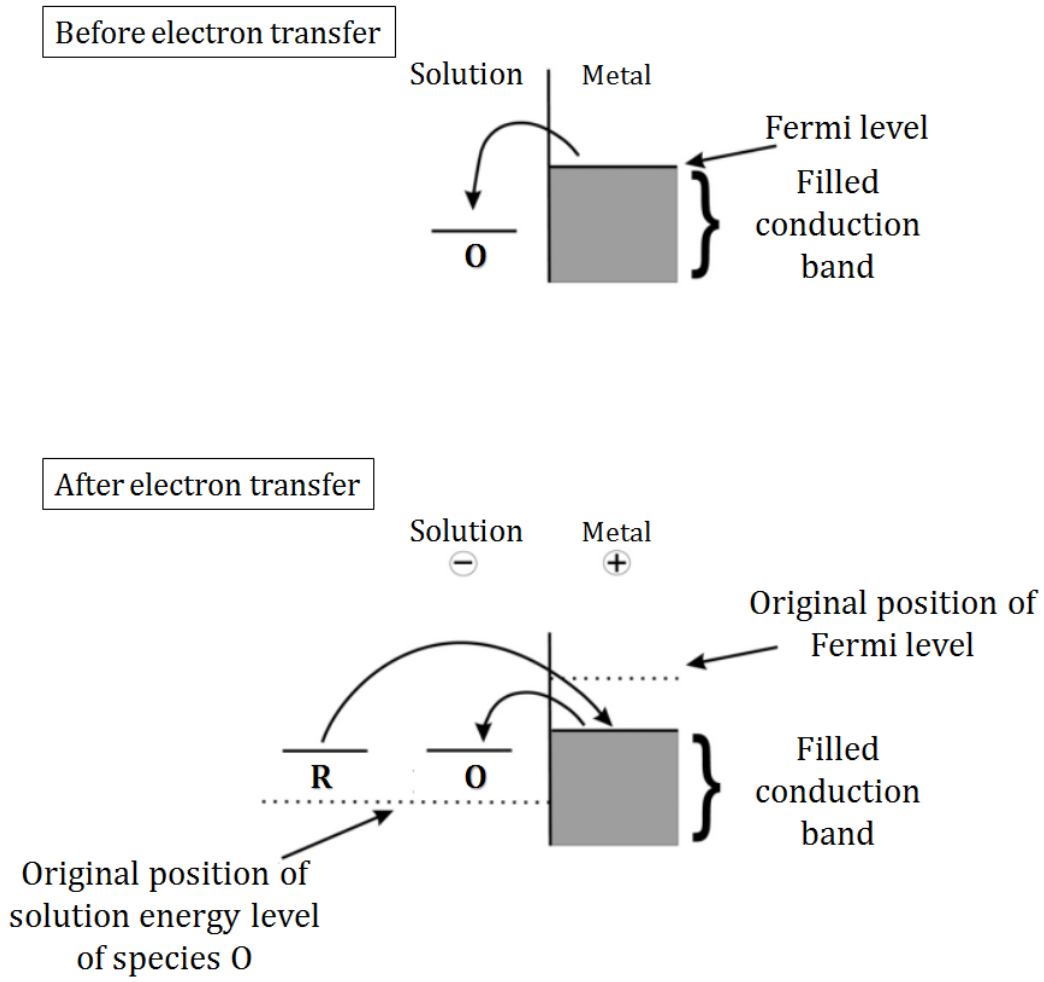

Figure 2.2 Diagram of the energy of electrons in the solution species and in the electrode. Adapted from [3]

As the electron transfer progresses, positive charge builds up on the electrode and a corresponding negative charge results in the solution phase. The energy levels are altered until eventually the Fermi level lies in between the energy levels of the two electroactive species such that the rate at which electrons leave the electrode and reduce O becomes equal to the rate at which electrons enter the electrode from the R species which gets oxidised. This corresponds to the system reaching equilibrium and possessing a characteristic potential established at the electrode|solution interface.

The measurement of potential in practice is typically carried out with a high impedance voltmeter. As the measurement of the potential difference is not possible at a single interface, a second reference electrode must be included for such a measurement to be made feasible [4].

When the activities of the relevant electroactive species are known, the equilibrium potential can be predicted by the Nernst equation:

$$E = E^0 + \frac{RT}{F}\, ln \frac{a_O}{a_R} \tag{2.3}$$

where R is the universal gas constant (8.314 J K^{-1} mol^{-1}), T is the absolute temperature, F is the Faraday constant (96485 C mol^{-1}), a_O and a_R are the activities of the species O and R respectively. E^0 is known as the standard electrode potential and it is measured by the standard hydrogen electrode (*vide infra*) as reference, with all species having unit activity.

In experimental electrochemistry, it is commonly the case that the concentration is a more important quantity rather than the activity hence equation 2.3 can be written in terms of concentration to give

$$E = E^{0\prime} + \frac{RT}{F}\, ln\frac{[O]}{[R]} \tag{2.4}$$

where $E^{0\prime}$ is known as the formal potential. The activity of a species *x* in solution is related to its concentration by the expression

$$a = \gamma[x] \tag{2.5}$$

where γ is the activity coefficient.

$E^{0\prime}$ is related to E^0 by the following equation:

$$E^{0\prime} = E^0 + \frac{RT}{F}\, ln\frac{\gamma_O}{\gamma_R} \tag{2.6}$$

2.3 Non-equilibrium electrochemistry

While equilibrium electrochemistry, in which there is no net flow of charge, is important, the case whereby a net electrical current passes through the electrochemical cell is often of greater relevance in practice. Electrochemical systems in which there is a net flow of charge in a given direction can be broadly classified as either galvanic or electrolytic processes depending on the Gibbs energy. A galvanic reaction is a spontaneous electron transfer reaction ($\Delta G < 0$) while an electrolytic process ($\Delta G > 0$) necessitates an external applied potential different from its equilibrium value in order to drive the reaction. This thesis is primarily concerned with the study of electrochemical reactions of the latter type.

For an electron-transfer reaction to occur, it is necessary for the electroactive species to be within molecular distances of the electrode surface. Therefore, a simple electrode reaction must involve at least three steps:

- the supply of reactant to the electrode surface;
- the transfer of charge across the electrode|solution interface
- the removal of the product from the surface.

This multistep process is typified by the scheme in **Figure 2.3**. The overall rate of electrode reaction will be determined by the slowest of these steps. A particular reaction might therefore be limited either by the electron transfer kinetics or by the rate at which material is carried to (or from) the electrode via mass transport [5,6]. More complex electrode reactions can involve additional surface or chemical processes that precede or follow the electron transfer event.

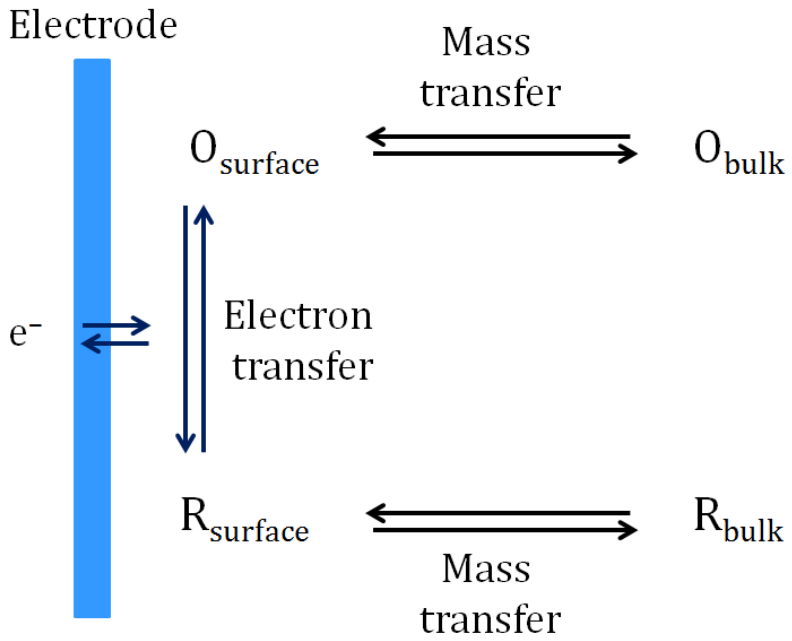

Figure 2.3 Schematic representation of some processes involved in a simple one-electron transfer electrode reaction.

When a potential positive to the equilibrium potential is applied to an electrode immersed in a solution containing O and R, the system will shift to a new equilibrium where the concentrations of O and R are those set out by the Nernst equation at this potential, provided the electron transfer kinetics is fast. At a potential of $E + \Delta E$, the equality of the Nernst equation can be met by the ratio of [O]/[R] increasing. This necessitates the conversion of R into O such that an anodic current occurs. For a potential negative to the equilibrium potential, the same argument will lead to a net cathodic current being observed.

2.4 Electrode kinetics

In addition to thermodynamic considerations, the rate at which O and R are interconverted is also of interest. In accordance with homogeneous kinetics, the rates of oxidation and reduction can be expected to be the product of a rate constant and the concentration of the reactant at the site of electron transfer, that is, the electrode surface (denoted by the subscript 0). For the simple case of a one-electron reduction of O to R (equation 2.1) this can be expressed as follows:

$$Rate\ of\ reduction = k_c[O]_0 = \frac{i_c}{FA} \tag{2.7}$$

$$Rate\ of\ oxidation = k_a[R]_0 = \frac{i_a}{FA} \tag{2.8}$$

where k_c and k_a are the heterogeneous rate constants for the forward cathodic and the reverse anodic reactions respectively, i_c and i_a are the cathodic and the anodic currents respectively, and A is the electrode area.

The overall current for a redox reaction is given by the anodic and cathodic contributions:

$$i = i_a + i_c = FA\{k_a[R]_0 - k_c[O]_0\} \tag{2.9}$$

The rate of the heterogeneous electron transfer is dependent on the potential gradient at the electrode|solution interface and based on the principles of transition state theory the rate constants are generally related by

$$k_a = k^0 \exp\left(\frac{\beta F\eta}{RT}\right) \tag{2.10}$$

$$k_c = k^0 \exp\left(-\frac{\alpha F\eta}{RT}\right) \tag{2.11}$$

where k^0 is the standard electrochemical rate constant and α and β are known as the transfer coefficients [7,8] which normally lie in the range zero to unity. η is the overpotential and is defined as

$$\eta = E - E^{0\prime} \tag{2.12}$$

The overpotential can be regarded as the driving force for oxidation or reduction, depending on its sign.

The transfer coefficient is a dimensionless parameter which can be interpreted in terms of the nature of the transition state. For a value close to zero the transition state behaves more like the reactants whereas when it approaches unity the transition state resembles the products, at least with respect to the potential dependence of its standard Gibbs energy. The value of the transfer coefficient is typically close to 0.5 for many reactions, indicating the transition state to possess intermediate character [3,5].

Based on the above equations, the net current can be expressed in the form

$$i = FA\left\{k^0 \exp\left(\frac{\beta F\eta}{RT}\right)[R]_0 - k^0 \exp\left(-\frac{\alpha F\eta}{RT}\right)[O]_0\right\} \quad (2.13)$$

This is the Butler-Volmer equation [9-11] which describes how the observed current varies as a function of the overpotential and the transfer coefficients when mass transport limitations are absent. When k^0 is large, little or no overpotential is required to drive the electrochemical reaction and this is known as a reversible process. In contrast, a small value of k^0 necessitates a high overpotential and such an electrode process is termed irreversible.

When the overpotential becomes sufficiently large in the anodic direction such that only the oxidative component is significant and the Butler Volmer equation simplies to

$$i = FAk^0 \exp\left(\frac{\beta F\eta}{RT}\right)[R]_0 \quad (2.14)$$

And upon taking the natural logarithm on both sides of the equation becomes

$$\ln i = \frac{\beta F}{RT}\eta + constant \quad (2.15)$$

Similarly at overpotentials which drive the cathodic reaction, negligible anodic currents occur and the following equation is obtained

$$\ln|i| = -\frac{\alpha F}{RT}\eta + constant \quad (2.16)$$

Equations 2.15 and 2.16 allow the value of the transfer coefficients to be derived experimentally from the slope of a plot of ln i against (over)potential. This is known as Tafel analysis and is illustrated in **Figure 2.4**. When both the anodic and cathodic

processes can be measured and analysed using Tafel plots, the point of intersection of the extrapolation of the two Tafel lines provides an estimate of the quantity $i_{0,}$ known as the exchange current [5].

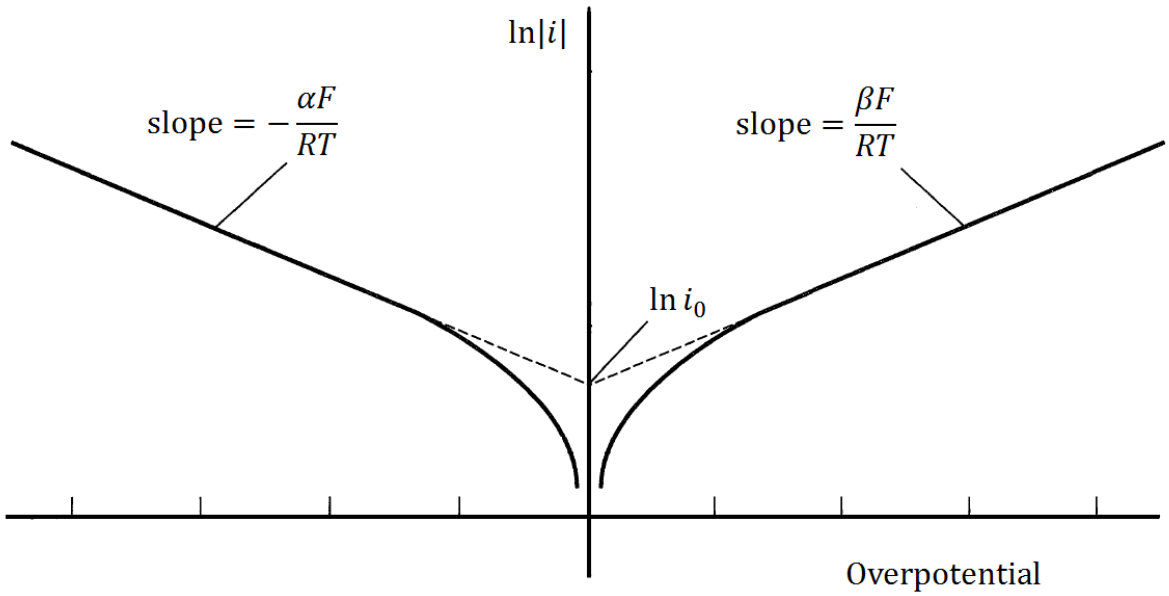

Figure 2.4 Tafel analysis.

2.5 Mass transfer

When the electrode kinetics is sufficiently fast, the reaction rate will be largely controlled by the transport of material to the electrode surface. Mass transfer refers to the movement of material from one location in solution to another and arises either from differences in electrical or chemical potential at the two locations or from movement of a volume element of solution [12]. The main modes of mass transfer that are significant depending on the experimental conditions include the following:

- Diffusion
- Convection
- Migration

2.5.1 Diffusion

Diffusion is the spontaneous movement of a species driven by a concentration gradient from a region of high to a region of low concentration so as to minimise the concentration difference. For the simple case of linear diffusion to a planar surface, it has been shown by Fick [13] that the number of moles of material diffusing through a unit area in one second, that is, the 'diffusional flux', *J*, for a species is given by Fick's first law

$$J = -D_A \frac{\partial [A]}{\partial x} \tag{2.17}$$

where [A] is the concentration of species A and D_A is a constant of proportionality which is known as the diffusion coefficient and is characteristic of the diffusing species. The diffusion coefficient provides a measure of the mobility of a molecule in a solvent over a certain time and as a rule of thumb the larger the molecule, the smaller the value of D [3].

Fick's second law expresses the variation of concentration at a particular point as a function of time and is given by

$$\frac{\partial [A]}{\partial t} = D_A \frac{\partial^2 [A]}{\partial x^2} \tag{2.18}$$

The solution to this differential equation, together with boundary conditions appropriate to the electrode reaction, allows the development of a precise theoretical description of electrochemical experiments.

2.5.2 Convection

Convection is the movement of a species as a result of external mechanical forces. Two forms of convection may be distinguished. The first is natural convection, which arises from sources such as random vibrations in the laboratory or the small density gradient resulting from both concentration and temperature changes local to the electrode associated with the chemical transformation at the surface. Natural convection is generally irreproducible and thus undesirable in electrochemical experiments. Its effects can usually be neglected by carrying out measurements on a relatively short timescale [3].

The second type is forced convection, which is the deliberate stirring or agitation of the solution by mechanical means. This is usually included as part of the experiment in order to dominate the mass transport in the system. Forced convection is normally designed to possess well-defined hydrodynamic behaviour so that a quantitative description of the electrode processes can be established.

2.5.3 Migration

Migration is the movement of charged species under the influence of an electric field. The potential drop across the electrode/solution interface is able to exert an electrostatic force on ions present in the region and such motion contributes to the mass transfer to and from the electrode surface. However migratory fluxes are not easily predictable and

the differing rate of mass transfer can lead to difficulties in the interpretation of experimental data.

To diminish the effects from migration, a chemically and electrochemically inert 'background electrolyte' is usually added to the solution at high concentrations, commonly around, or in excess of 0.1 M. This provides several important advantages. First, the large amount of electrolyte improves the solution conductivity making it less resistive to the passage of current through the electrochemical cell.

Secondly, the high levels of this supporting electrolyte significantly decrease the distance over which the electric potential drops from its value in the electrode (Φ_e) to that in bulk solution (Φ_s). The absence of potential gradients outside this narrow interfacial region hence prevents migration effects.

A third benefit is that the ionic strength of the solution stays practically constant during electrolysis due to the relatively high concentration background electrolyte in comparison to that of the reactants and products. As a result the activity coefficients of the reactants and products, which are influenced by ionic strength, are kept constant [5].

The combination of the three mass transfer modes introduces complexity in the interpretation of experimental data owing to some undesirable effects as explained above. It is therefore useful to eliminate at least one of the mass transport methods. In the experimental work of this thesis, the effects of convection are minimised by conducting experiments under still conditions (no stirring) while those due to migration are made negligible through the addition of a high concentration of supporting

electrolyte. This means that the mass transfer involved arises predominantly from diffusion.

2.6 Faradaic and non-faradaic processes

There are two kinds of processes which occur at electrodes. One type consists of reactions in which there is a flow of charge across the electrode-solution interface, i.e. oxidation and reduction. Such reactions are described by Faraday's Laws and so are called faradaic processes. The magnitude of the faradaic current is given by

$$i = \frac{dQ}{dt} = \frac{d(mnF)}{dt} = nF\frac{dm}{dt} \tag{2.19}$$

where Q is the amount of charge passed, t is the time, m is the number of moles of reactant consumed or product formed.

Under some conditions, a given electrode-solution interface will show no charge-transfer reactions occurring as a result of being thermodynamically or kinetically unfavourable. However, processes such as adsorption and desorption can occur, and the structure of the electrode-solution interface can change with varying potential or solution composition. These are called non-faradaic processes and give rise to the background current in electrochemical measurements [14].

2.6.1 Electrical double layer

The applied potential to an electrode leads to its surface possessing a certain charge which has electrostatic effects within the electrolyte solution. Oppositely charged species as well as dipoles are attracted to the electrode surface to maintain electrical

neutrality and the electrode-solution interface behaves as an electrical capacitor. This resulting structure is known as an electrical double layer and is illustrated by the model in **Figure 2.5**.

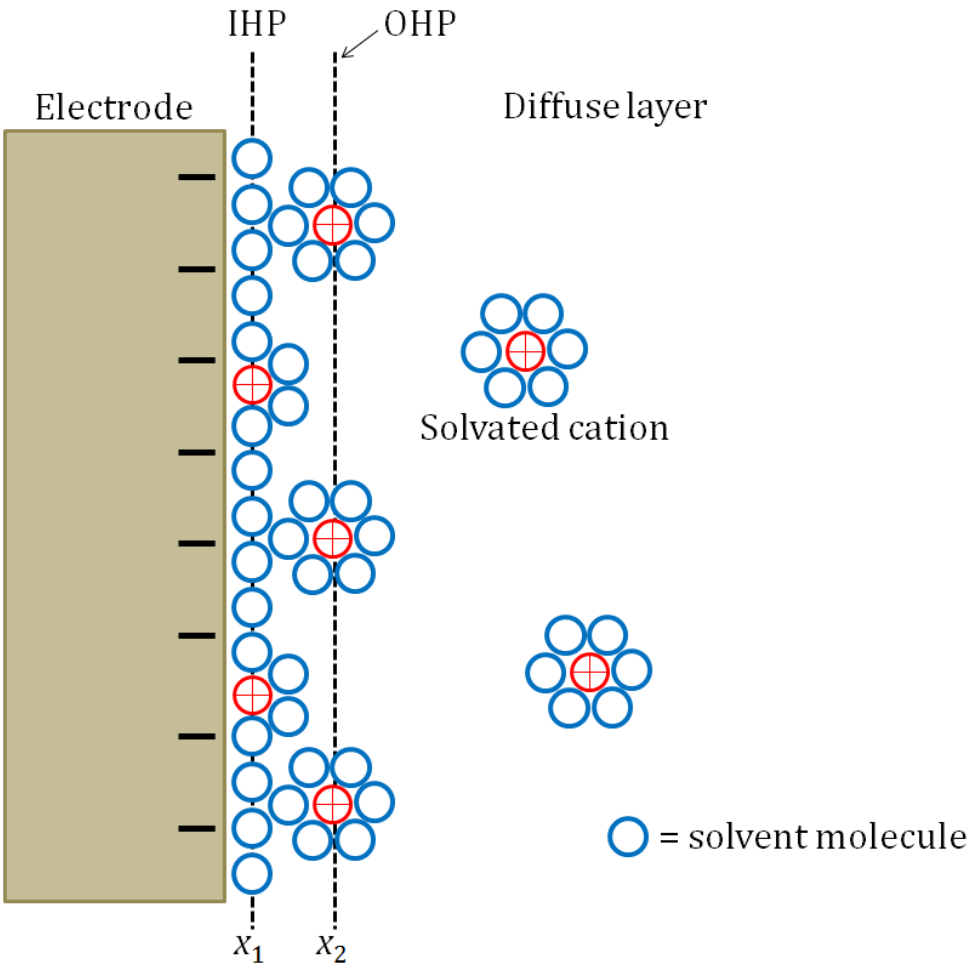

Figure 2.5 Schematic diagram of the electrical double layer. Adapted from [15]

On the solution side, the region closest to the electrode consists of solvent molecules and specifically adsorbed ions, which are at a distance of x_1 from the electrode surface. The plane drawn through the electrical centres of these ions is called the inner Helmholtz plane (IHP). The next layer comprises solvated ions, whose electrical centres form the boundary of the outer Helmholtz plane (OHP). As these ions are surrounded

by solvent molecules, they may not approach the electrode surface closer than a certain distance, x_2. Due to random thermal motion, some of the ions which neutralise the charge on the electrode surface are spread out in a diffuse layer beyond the OHP [12,16,17].

2.7 Electrochemical cell

In order to differentiate the electrodes used in an electrochemical cell, they can be designated based on their specific roles: the working electrode (WE), the reference electrode (RE), and the counter electrode (CE), also known as the auxiliary electrode. The working electrode is generally where the reaction of interest occurs. The function of the counter electrode is to pass the same current as that which is flowing through the working electrode. Thus the potentiostat sets the counter electrode to the necessary potential for passing this current.

Reference electrodes are necessary to provide a stable and accurate value of potential as a reference voltage [12,18]. The standard hydrogen electrode (S.H.E.) is the reference electrode for standard electrode potentials and by convention it is defined as having a potential of zero. It consists of a platinised platinum electrode immersed in an acid solution of unit activity over which hydrogen gas bubbles at 1 atm pressure as shown below.

$$Pt|H_2\ (gas,\ 1\ atm)|H^+\ (aqueous,\ a = 1)$$

Despite its fundamental status, it is not very convenient for routine work. Therefore in practice potentials are usually measured with other reference electrodes than the S.H.E.

One common reference electrode is the saturated calomel electrode which has a potential of 0.242 V (vs S.H.E.):

$$Hg|Hg_2Cl_2|KCl \text{ (saturated in water)}$$

Another widely used reference electrode is the silver-silver chloride electrode:

$$Ag|AgCl|KCl \text{ (saturated in water)}$$

with a potential of 0.197 V (vs S.H.E.).

2.7.1 Three-electrode cell design

As described earlier in section 2.2, a minimum of two electrodes is required in practice to measure the potential difference across both interfaces. In a two-electrode electrochemical cell, the electrode other than the working electrode has to serve as both a reference and a counter electrode. If an appreciable current is drawn through the reference electrode, the chemical composition within it is altered thereby changing the potential according to the Nernst equation. This means it will not be able to provide a stable reference point for measurements.

To overcome this change in reference electrode potential, the three-electrode electrochemical cell is often used, as depicted in **Figure 2.6**. In this cell design, the potential is determined across the working and reference electrodes by a high-impedance potentiostat while electrical charge is passed through the working and counter electrodes. As there is negligible current drawn through the reference electrode, its composition remains effectively the same and a constant potential value can be maintained.

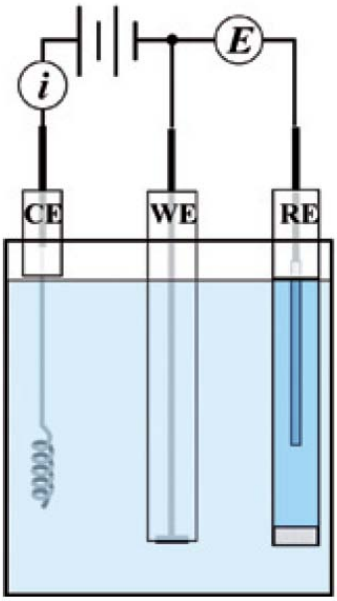

Figure 2.6 Schematic diagram of a three-electrode electrochemical cell. CE: counter electrode; WE: working electrode; RE: reference electrode. [15]

2.8 Electrochemical techniques

2.8.1 Cyclic voltammetry

Cyclic voltammetry (CV) is a potential sweep method which involves scanning a selected potential range and measuring the current response arising from the charge transfer and associated reactions which occur. CV is widely used in the study of electrode processes and is a powerful technique towards understanding electrochemical reaction mechanism and kinetics.

The basic cyclic voltammetry scheme is depicted in **Figure 2.7**. The related technique of linear sweep voltammetry corresponds to only the first section of the triangular waveform.

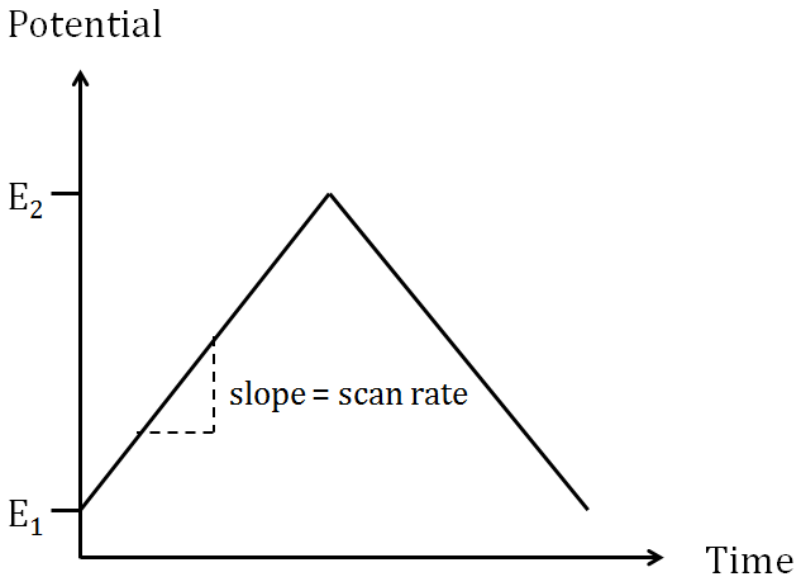

Figure 2.7 Potential waveform in a cyclic voltammetry experiment

A cyclic voltammetric experiment is typically conducted in a stationary solution and hence diffusion is the main mode of mass transfer to the electrode surface. A general current response to the potential sweep is illustrated by the cyclic voltammogram in **Figure 2.8**. The current starts to increase as potentials are reached where the electrochemical rate constant becomes sufficiently large and it continues until a maximum after which the current falls off. The peak in the voltammogram reflects a balance between an increasing heterogeneous rate constant and a decrease in surface concentration.

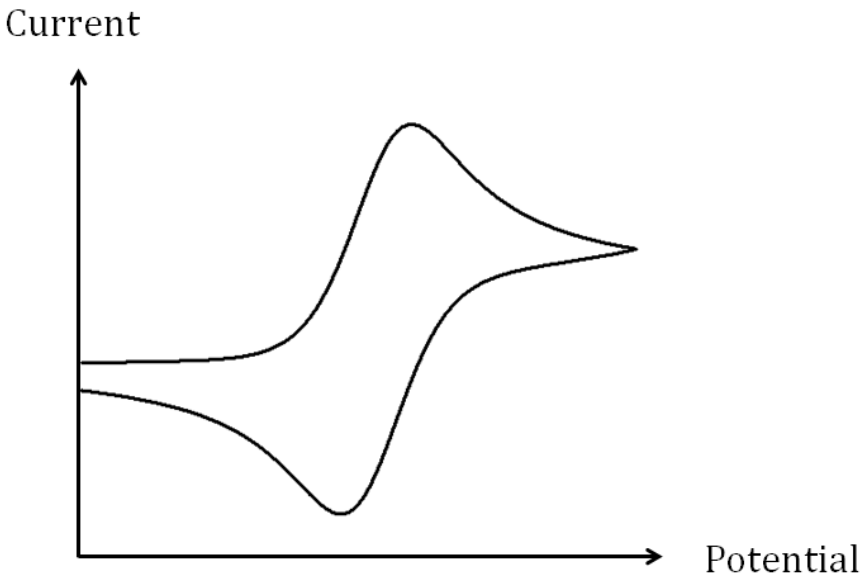

Figure 2.8 Cyclic voltammogram for a reversible electron transfer reaction

For reversible reactions, in which electrode kinetics is fast relative to the time-scale of the prevailing mass transport, the product of the initial oxidation or reduction is subsequently reduced or oxidised respectively when the scan direction is reversed. The peak current, i_p, in this case can be described by the Randles-Sevcik equation [19,20]:

$$i_p = 0.446nFA[R]_{\text{bulk}}\sqrt{\frac{nF\upsilon D}{RT}} \tag{2.20}$$

where n is the number of electrons transferred, υ is the scan rate, $[R]_{bulk}$ is the concentration of the species R in the bulk solution and the rest of the symbols are as given earlier in the text.

It can be noted from the equation that the peak current is directly proportional to the bulk concentration and the square root of scan rate. The latter property constitutes a diagnostic for the mechanism of mass transfer for the electrode reaction under study.

Another characteristic feature of the voltammetric response of a reversible reaction is its peak-to-peak separation which is given by

$$\Delta E_p = E_{p,a} - E_{p,c} \cong \frac{57}{n}\text{mV} \quad \text{at 298 K} \tag{2.21}$$

The separation of the peaks is an indicator of the reversibility of an electrode reaction. From the above equation, the peak-to-peak separation should be a constant and is independent of scan rate. When the reaction deviates from reversibility, the value of ΔE_p increases from the value of 57/n mV and becomes dependent on the scan rate.

For completely irreversible reactions, only the oxidation or reduction corresponding to the initial sweep direction can be observed and there is no reverse peak. The Randles-Sevcik equation [3] in this case is

$$i_p = 0.496\sqrt{(n' + \alpha_{n'})}nFA[R]_{\text{bulk}}\sqrt{\frac{F\nu D}{RT}} \tag{2.22}$$

where n' is the number of electrons transferred before the rate limiting step and $\alpha_{n'}$ is the electron transfer coefficient of the rate determining step. The majority of redox systems fall between the two limiting cases and show quasi-reversible behaviour.

In the case of adsorbed species, the shape of the cyclic voltammogram changes since they do not have to diffuse to the electrode surface. The peak current for such a reaction is proportional to υ, which allows it to be distinguished from the instance of diffusional control.

2.8.2 Square wave voltammetry

Square wave voltammetry (SWV) is a pulse technique based on a series of potential steps of varying heights and in forward or reverse directions [21]. The square wave voltammetric waveform consists of a square wave superimposed on a base potential staircase as demonstrated in **Figure 2.9**. The square wave is defined by a pulse height, or square wave amplitude, ΔE_P, the staircase height, ΔE_S, the pulse time, t_P, and the cycle period, t_S. [3,22] Alternatively, the pulse time can be represented in terms of the square wave frequence, $f = 1/2\ t_P$. The staircase changes by ΔE_S at the beginning of each cycle so that the scan rate is

$$\frac{\Delta E_S}{2t_P} = f\Delta E_S \tag{2.23}$$

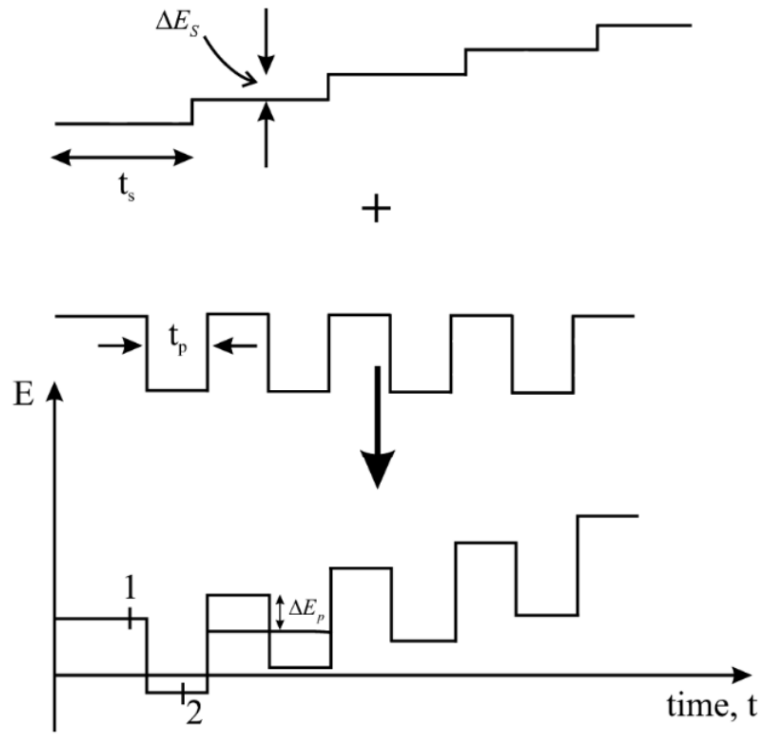

Figure 2.9 Potential waveform and measurement scheme for square wave voltammetry [3].

The current is determined at two points in each cycle, once at the end of the forward pulse (at t_1) and once at the end of the reverse pulse (at t_2). The difference of the two measurements is plotted against the base staircase potential, as shown in **Figure 2.10**.

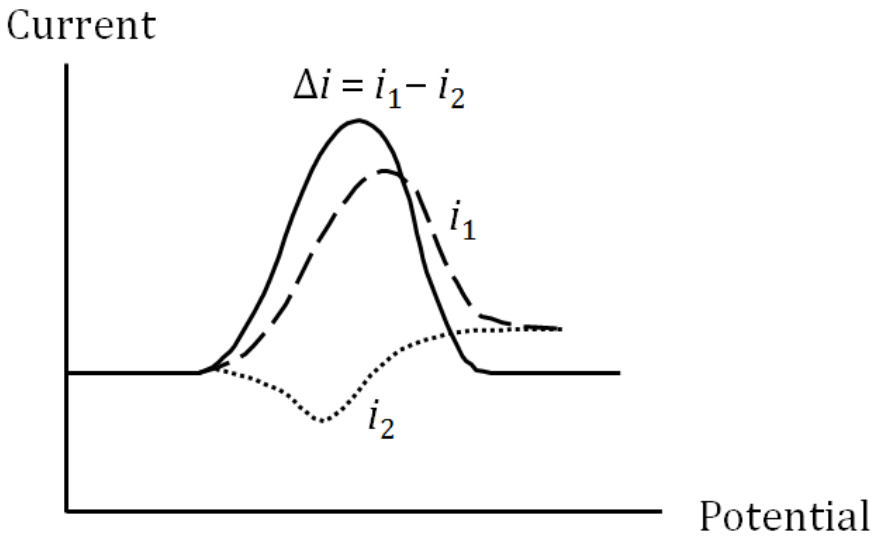

Figure 2.10 Schematic square wave voltammetric profile

The major advantage of SWV is the effective elimination of the capacitive contribution to the current. This is due to the subtraction of one current from the other and also because over the small potential range between forward and reverse pulses the interfacial capacitance is approximately constant. The sensitivity in this method is enhanced since the net current is greater than either the forward or reverse components [23].

2.9 Electrochemical instrumentation

The electrochemical measurements in the subsequent chapters of this thesis were conducted using a μ-AUTOLAB III potentiostat (Eco-Chemie, Netherlands) which is

connected to a computer running GPES (General Purpose Electrochemical System) software version 4.9. The electrochemical cell was set up with a standard three-electrode configuration comprising a working electrode of interest, a platinum coil counter electrode, and a Ag/AgCl (1M KCl) reference electrode against which working electrode potentials are referred. All experiments were carried out at room temperature unless stated otherwise. Specific experimental conditions and details regarding the working electrodes of study are described later in their respective experimental sections.

2.10 Scanning electron microscopy

Scanning electron microscopy (SEM) is a widely used technique in materials characterisation for the observation of the surfaces of specimens. A schematic diagram showing the principles of the SEM is given in **Figure 2.11**. A high voltage source generates a beam of high energy electrons which is accelerated and focused onto the surface of the sample. The electron beam is rastered across a specific area to probe its topography. Due to the inelastic collision with the incident beam, there is a resulting emission of secondary electrons which are collected and processed to produce the SEM image.

The outstanding advantage of the SEM is its ability to provide an image resolution of typically around 10 nm, which is much superior to the optical microscope [24]. The relatively large depth of focus means that SEM images have a three dimensional appearance. In addition to electronic emission, electromagnetic radiation can be produced. This arises from the relaxation to lower energy states of high energy electrons after the excitation of inner shell electrons by the incident electron beam. Such photons are of characteristic wavelength and relate to the difference in energy levels

between the respective shells for a given element. This allows the identification of the spatial chemical composition on the specimen surface in what is known as energy dispersive X-ray analysis (EDX) [25].

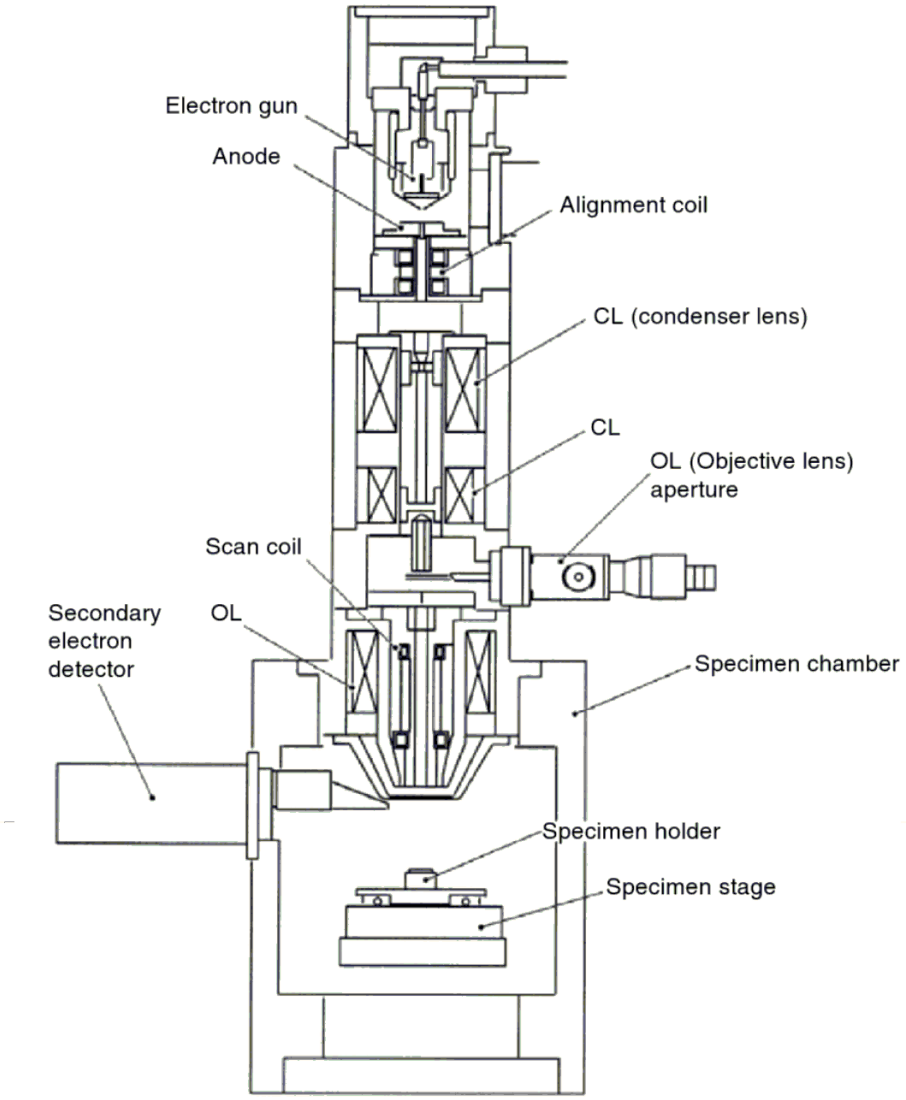

Figure 2.11 Schematic illustration of a scanning electron microscope [26]

References

[1] IUPAC Analytical Chemistry Division Commission on Electroanalytical Chemistry, Pure Appl. Chem. 45 (1976) 131.

[2] R.G. Compton, G.H.W. Sanders, Electrode Potentials, Oxford University Press, Oxford, 1996.

[3] R.G. Compton, C.E. Banks, Understanding Voltammetry, Imperial College Press, London, 2011.

[4] S. Trasatti, Pure Appl. Chem. 58 (1986) 955.

[5] A.C. Fisher, Electrode Dynamics, Oxford University Press, Oxford, 1996.

[6] D. Pletcher, A First Course in Electrode Processes, Royal Society of Chemistry, Cambridge, 2009.

[7] R. Guidelli, R.G. Compton, J.M. Feliu, E. Gileadi, J. Lipkowski, W. Schmickler, S. Trasatti, Pure Appl. Chem. 86 (2014) 259.

[8] R. Guidelli, R.G. Compton, J.M. Feliu, E. Gileadi, J. Lipkowski, W. Schmickler, S. Trasatti, Pure Appl. Chem. 86 (2014) 245.

[9] J.A.V. Butler, Transactions of the Faraday Society 19 (1924) 729.

[10] J.A.V. Butler, Transactions of the Faraday Society 19 (1924) 734.

[11] T. Erdey-Gruz, M. Volmer, Z. Physik. Chem. A 150 (1930) 203.

[12] A.J. Bard, L.R. Faulkner, Electrochemical Methods: Fundamentals and Applications, Wiley, New York, 2000.

[13] A. Fick, Philosophical Magazine Series 4 10 (1855) 30.

[14] E. Gileadi, Physical Electrochemistry, Wiley, Weinheim, 2011.

[15] C.G. Zoski, Handbook of Electrochemistry, Elsevier, Amsterdam, 2007.

[16] P.H. Rieger, Electrochemistry, Chapman & Hall, New York, 1994.

[17] D.C. Grahame, Chem. Rev. 41 (1947) 441.

[18] H. Kahlert, in: F. Scholz (Ed.), Electroanalytical Methods, Springer Berlin & Heidelberg, 2002

[19] J.E.B. Randles, Transactions of the Faraday Society 44 (1948) 327.

[20] A. Ševčík, Collect. Czech. Chem. Commun. (1948) 349.

[21] J.G. Osteryoung, R.A. Osteryoung, Anal. Chem. 57 (1985) 101A.

[22] J. Wang, Analytical Electrochemistry, Wiley, New York, 2006.

[23] C.M.A. Brett, A.M.O. Brett, Electroanalysis, Oxford University Press, Oxford, 1998.

[24] R. Egerton, Physical Principles of Electron Microscopy: An Introduction to TEM, SEM, and AEM, Springer US, 2006.

[25] J. Goldstein, D.E. Newbury, D.C. Joy, C.E. Lyman, P. Echlin, E. Lifshin, L. Sawyer, J.R. Michael, Scanning Electron Microscopy and X-ray Microanalysis: Third Edition, Springer US, 2013.

[26] W. Zhou, Z.L. Wang, Scanning Microscopy for Nanotechnology: Techniques and Applications, Springer, New York, 2007.

Chapter 3

The Voltammetry and Electroanalysis of Some Estrogenic Compounds at Modified Diamond Electrodes

In this chapter, the voltammetry of some estrogenic compounds (estradiol, nonylphenol, bisphenol A, ethynylestradiol, estrone, estriol) in aqueous solution at boron doped diamond electrodes is presented. For oxidised (hydrophilic) electrodes electrochemically irreversible kinetics were observed for the diffusing molecules allowing the inference of diffusion coefficients and charge transfer coefficients. In contrast for hydrogen terminated (hydrophobic) surfaces significant adsorption was observed. A limit of detection of 1-100 μM for the estrogenic compounds was found using the oxidised BDD electrode. Surface modification of the oxidised BDD with nanocarbon (so-called Carbon Black) allowed pre-concentration of the target by adsorption onto the nanocarbon prior to analysis and a corresponding reduction of the limit of detection by ca three orders of magnitude to 5-100 nM. The work presented in this chapter has been published in *Electroanalysis* [1].

3.1 Introduction

Certain phenolic compounds which are found as pollutants in environmental waters [2] are members of a class of chemicals known as endocrine disruptors, representing

naturally occurring or man-made substances which interfere with the function of hormones in the human body. **Figure 3.1** shows examples of some estrogenic and endocrine disrupting compounds, which can persist after water purification treatments and which even at low concentrations can exert potential biological effects [3,4].

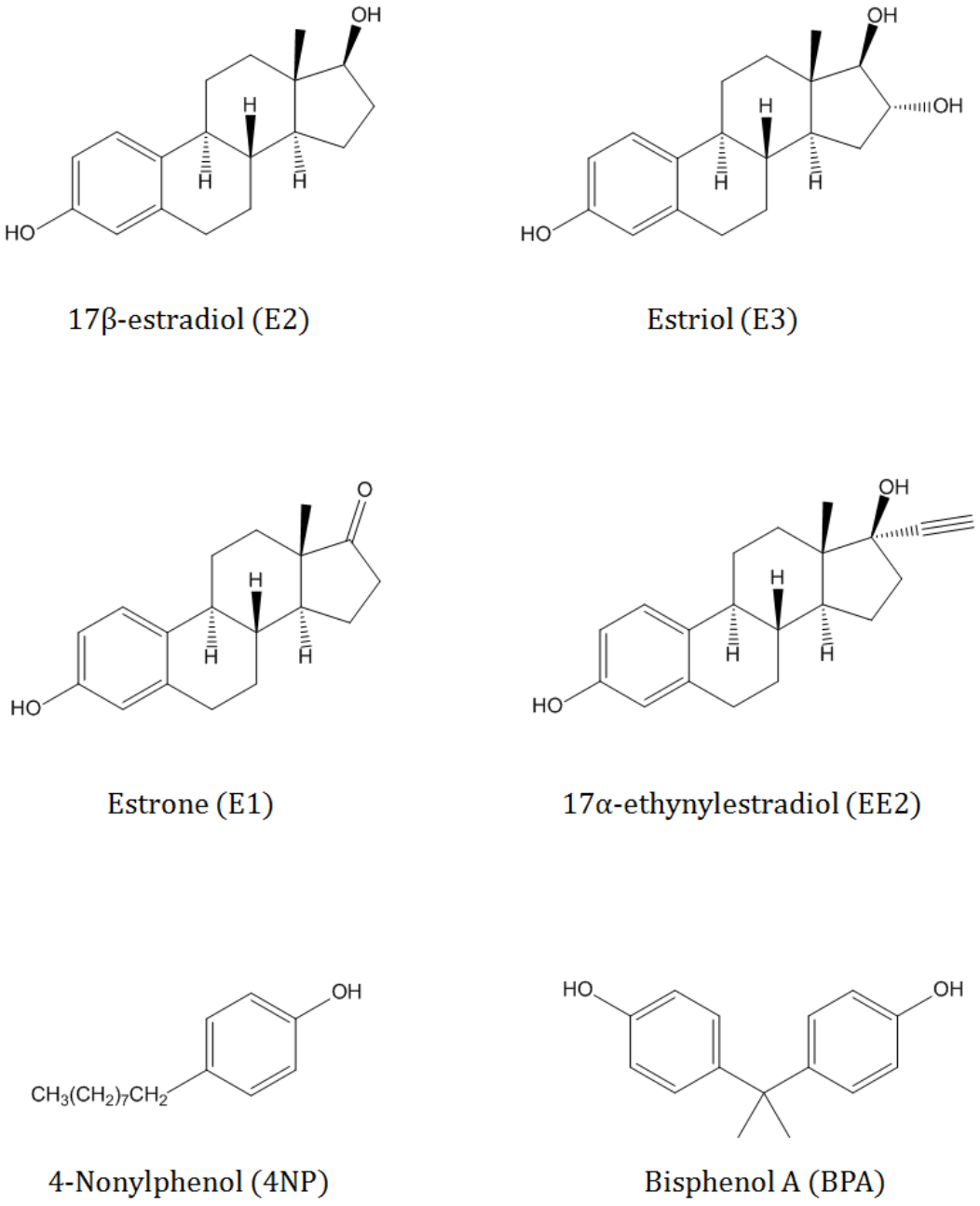

Figure 3.1 Examples of estrogens and some endocrine disruptors.

Current knowledge about the exposure of human and wildlife to endocrine disruptors is limited [4] and a main focus of agencies such as the World Health Organisation (WHO) and European Commision (EC) concerns the identification and assessment of these compounds [5]. A priority list of substances has been developed by the EC to be investigated for their possible endocrine disrupting properties which includes alkylphenols, benzophenones, and bisphenols [5].

Treated sewage effluent has been reported to exert certain estrogenic effects on fish [6] and concentrated animal feed operations have also received attention as potentially important sources for the release of estrogens into the environment [7]. These effluents contained 17β-estradiol, estrone, estriol and 17α-ethynylestradiol at reported concentrations from 0.2 to 17400 ng/L [7,8], depending on the source. Nonylphenols have been measured in municipal wastewater, rivers, surface waters and industrial discharge at 0.2 to 1617 µg/L [9-11]. The concentrations of bisphenol A was reported to be present in raw water and drinking water in the lower ng/L range [3], as well as in river water at 2–230 ng/L [12].

The levels of estrogens and endocrine disruptors found in the environment range from sub-ng/L to mg/L, that is, from concentrations of picomolar to micromolar. Analytical methods which can cover such a wide span of concentrations will be desirable for the detection of this emerging class of potential pollutants. Quantification of these compounds are usually carried out using various chromatographic techniques [13-15], enzyme-linked immunosorbent assay (ELISA) [16], radioimmunoassay [17] and electrophoresis [18]. Despite their regular use, these techniques are not without drawbacks, which can often include relatively high costs, derivatisation requirements,

extensive sample preparation and analysis times, with the use of considerable amounts of organic chemicals for sample elution being environmentally undesirable.

Electrochemical methods can be an attractive alternative analytical technique due to lower costs, simpler operation, wide dynamic range and fast analysis times [19]. The electrodes which are commonly employed to detect endocrine disruptors typically comprise a carbon support, such as glassy carbon, modified with carbon nanotubes to increase surface area, surfactants to control electrode fouling and catalytic metal centres to impart electrocatalytic activity [20-29]. Representative data for these modified electrodes used are shown in **Table 3.1**, including the linear dynamic range and limit of detection with regard to particular endocrine disruptors. Typically the electrodes function by the target molecule adsorbing on the high surface area electrode modifier, after which it is detected by electrochemical oxidation using some form of adsorptive voltammetry. Although promising results can be obtained, the difficulty in reproducible preparation of these modified electrodes along with the inherent cost of CNTs, up to 600 US$ per g depending on specification [30], must be considered something of a disadvantage.

Boron-doped diamond [31-34] electrodes, which are now available at low economic cost (< 10 US$ cm^{-2}) produced by chemical vapour deposition, represent an interesting new alternative carbon-based electrode material for use in this area and which is beginning to find useful authentic application in electroanalysis [35-40]. As mentioned earlier in Chapter 1, the electrode shows advantageous electrochemical properties including low pseudocapacitive background currents, a wide operating potential window and often relatively lower adsorptivity, compared to traditional carbon

materials [40-44]. The use of BDD for electroanalysis of endocrine disruptors has been very limited however, apart from a few reports such as one concerning the detection of estriol which showed irreversible electrochemical behavior and a linear dynamic range of 0.2-20 μM [45], and another work describing the amperometric detection of bisphenols coupled with capillary electrophoresis and off-line solid phase extraction, with a linear dynamic range of 1-400 μM [46].

One aim of the present chapter is therefore to explore in detail the properties of BDD as a carbon-based electrode for the detection of a range of endocrine disruptors. It is demonstrated in particular that the precise control of surface chemical termination, which can be achieved at diamond interfaces, enables the electrode to be tuned to exhibit diffusional or adsorptive voltammetry as desired in this particular application.

A second aim of the chapter is to investigate if more economic forms of carbon other than CNTs can be used as electrode modifiers to improve the limit of detection of the BDD electrodes. Nanocarbon (so-called Carbon Black) is a material which is commonly used for reinforcement in rubber products and as pigments [47], as introduced in Chapter 1. It is electrically conductive with a structure consisting of graphene-like layers which combine to form spherical particles [48]. Nano-carbon has been shown to be effective as an electrode modifier for glassy carbon in the detection of nicotine by adsorptive stripping voltammetry [49]. In the present work it is also demonstrated that nano-carbon black can serve as an ultra low cost electrode modifier for the electrochemical detection of endocrine disruptors.

Table 3.1 Literature for electroanalysis of endocrine disruptors at different electrodes.

The following abbreviations are used: not reported (NR), multi-walled carbon nanotubes (MWCNT), single-walled carbon nanotubes (SWCNT), boron-doped diamond (BDD), glassy carbon electrode (GCE), Congo Red (CR), β-cyclodextrin (CD), Ni(II)tetrakis(4-sulfonatophenyl) porphyrin (NiTPPS), quantum dots (QD), poly(amidoamine) (PAMAM), dihexadecyl hydrogen phosphate (DHP), 2,3-dimethylphenol (DMP), 4-terbutylphenol (TBP), Britton-Robinson buffer (BR), square wave voltammetry (SWV), chronoamperometry (CA), hydrodynamic amperometry (HyAm).

Electrode Modification	**Endocrine disruptor**	**Electrolyte (pH)**	**Technique**	**Linear dynamic range (µM)**	**LOD (µM)**	**Ref**
MWCNT-ionic liquid/GCE	E2	PBS (pH 7)	CV	0.01–1, 1–7.5	0.005	19
Ni(cyclam)/MWCNT/GCE	E2	NaOH	SWV	0.5–40	0.06	20
Pt nanoparticles/ MWCNT/GCE	E2, E1, E3	PBS (pH 7)	SWV	0.5–15; 2.0–50; 1.0–75	0.18; 0.84; 0.62	21
MWCNT-Nafion/GCE	E2	PBS (pH 7)	SWV	0.25–10	0.01	22
MWCNT-CR/GCE	E2	PBS (pH 8)	LSV	NR	NR	23
SWCNT-CD/GCE	BPA	PBS (pH 8)	CA	0.011–18.5	0.001	24

NiTPPS/MWCNT/GCE	BPA, nonylphenol, EE2	NaOH	HyAm	0.05–50; 0.1–40; 0.2–60	0.015; 0.26; 0.12	25
PAMAM/CoTe QD/GCE	BPA	PBS (pH 8)	CA	0.013–9.893	0.001	26
MWCNT/GCE	BPA, DMP, EE2, TBP	PBS (pH 7)	HyAm	0.3–100; 0.5–100; 1.0–100; 1.0–100	0.098; 0.171; 0.340; 0.308	27
MWCNT-DHP/GCE	trifluralin	BR (pH 5)	LSV	0.005–6.0	0.002	28
BDD	E3	NaOH (pH 12)	SWV	0.2–20	0.17	44

3.2 Experimental

3.2.1 Chemicals and Materials

17β-Estradiol, estriol, estrone, bisphenol A, 17α-ethynylestradiol and 4-nonylphenol were obtained from Sigma-Aldrich. All chemicals used were of analytical grade and all aqueous solutions were prepared using ultra pure water (~18.2 MΩ cm at 25°C). Standard solutions of each compound (1.0 mmol dm^{-3}) were prepared in methanol and diluted with phosphate buffer solutions (0.10 mol dm^{-3}) to obtain the appropriate concentrations. Commercial nanocarbon (diameter 27 ± 10 nm, Monarch 430®, Cabot Corporation) was used for surface modification, as received without any special pretreatment. Its SEM and XPS characterisations are described in Lo et al [49] and in Panchompoo et al [50] respectively.

3.2.2 Apparatus

Electrochemical experiments were conducted at room temperature using a standard three-electrode configuration, as described in Chapter 2. The set-up consists of a platinum coil counter electrode and a Ag/AgCl (1 M KCl) reference electrode, along with the working electrode, which is a boron-doped diamond electrode in this chapter. Hydrogen plasma treatment of the electrode surface was carried out with a microwave plasma system.

3.2.3 Preparation and Modification of Electrode

Boron-doped polycrystalline diamond (Element Six Co.) with a B doping concentration of ~5×10^{20} cm^{-3} was used as the working electrode, which was mounted in a home-built PTFE holder with an area of 0.44 cm^2 being exposed to the electrolyte. In the majority of the experiments, an oxidised BDD electrode was prepared and cleaned by

potential cycling in 0.1 mol dm^{-3} nitric acid between potentials of−1.5 V and +2.5 V between experiments. This is known to produce a BDD surface, which has a significant concentration of oxygen functional groups bound to it, including hydroxyl, carbonyl and carboxylic acid functionalities, and consequently a hydrophilic character [51,52].

To produce a hydrophobic hydrogen terminated surface, the electrode was exposed to a hydrogen plasma at 60 mbar pressure, 1.5 kW microwave power at a temperature of 600°C for 30 minutes. After this treatment, the substrate heater was switched off and the sample was left exposed to the hydrogen plasma which was gradually reduced in power until the plasma extinguished and the sample cooled to room temperature under flowing hydrogen. This yielded an electrode surface which XPS confirmed was largely free of adsorbed hydrocarbons or sp2 material which can adsorb if the “cool-down” period is not carefully controlled.

To modify the electrode with nano-carbon, 2 mg of nano-carbon was ultrasonicated in 1 cm^3 of acetonitrile and different volumes of this suspension were pipetted onto the surface of the oxidised BDD electrode, which was then left to dry in air. The electrodes were mechanically stable when immersed in still solutions, or when gently rinsed under flowing water. The nanocarbon modified BDD electrode is labelled as NC/BDD.

3.3 Results and Discussion

3.3.1 Electrochemical Studies Using an Oxidised Diamond Electrode

Cyclic voltammetry was used initially to assess the main features concerning the electrochemical interaction of the endocrine disruptors of interest at a clean, oxidised

BDD interface commencing with an anodic scan from 0.0 V. **Figure 3.2** shows the overlaid cyclic voltammograms of estradiol (E2), estriol (E3), estrone (E1), ethynylestradiol (EE2), 4-nonylphenol (4NP) and bisphenol A (BPA) in a phosphate buffer at pH 12.0. Each of the forward sweeps at a scan rate of 50 mV s^{-1} shows an anodic peak corresponding to the oxidation of the phenolic hydroxyl groups in the compounds [53], with a general mechanism as shown in **Figure 3.3**.

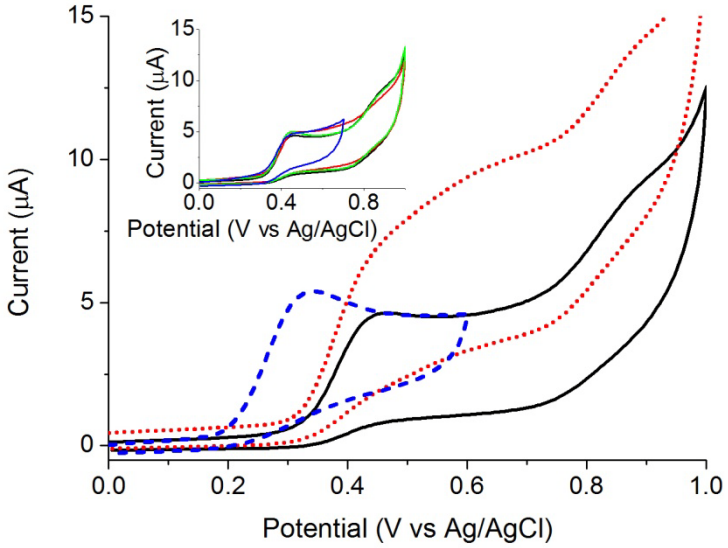

Figure 3.2 Cyclic voltammograms of estradiol (solid), 4-nonylphenol (dash) and bisphenol A (dot), Inset: estradiol (black), estriol (red), estrone (blue) and ethynylestradiol (green). 0.10 mM each in phosphate buffer pH 12.0, scan rate: 50 mV s^{-1}.

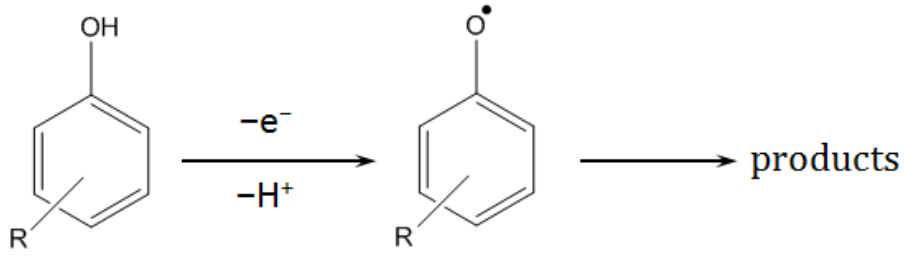

Figure 3.3 General reaction mechanism for the electrochemical oxidation of phenolic compounds.

The anodic peak potentials for E2, E3, E1 and EE2 are all observed at almost the same potential of about +0.45 V, which can be attributed to the similar steroidal structures of these natural and synthetic hormones (**Figure 3.1**). Therefore, it can be inferred that voltammetric methods at oxidised BDD electrodes can only determine the total estrogen content in a sample, rather than distinguish between all of the individual species. However the peak current of 4NP occurs at a lower potential of +0.34 V, thereby allowing it, at least in principle, to be distinguished from the estrogens when they are present at the same time.

No reduction wave can be observed for any of the chemicals used, indicating that the *overall* oxidation reaction is irreversible under the conditions of these experiments, and oxidation currents extend from the onset region up to the water oxidation region. This is because the first oxidation wave, corresponding to oxidation of the phenolic groups (**Figure 3.3**), is followed by more extensive chemically irreversible oxidation of the carbon backbone at higher potentials [53,54]. This tends to lead to the formation of strongly bound carbon species at the electrode surface [54]. In addition, the electro-oxidation of phenolic groups themselves result in the generation of phenoxy radicals which are highly reactive and can undergo a polymerisation reaction, leading to the formation of a polymer film [42].

Although BDD as an electrode material is generally less susceptible to adsorption compared to other materials such as glassy carbon [31,33,38,43,44], the resulting deposits formed from these pathways are strongly adherent and non-electroactive, thus passivating the surface. Strong molecular adsorption has been reported on BDD for the

case of quinizarin [55]. This is typified by the successive scan cycles of estradiol in **Figure 3.4**, which show a reduction in peak currents as the number of scans is increased.

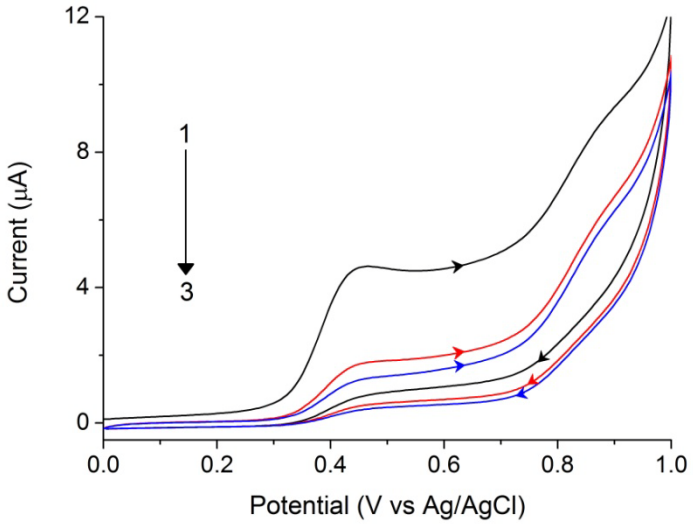

Figure 3.4 Cyclic voltammograms (three consecutive scans: #1 black, #2 red, #3 blue) of 0.10 mM estradiol in phosphate buffer pH 12.0, scan rate: 50 mV s^{-1}.

Experiments in which the solution was stirred, confirmed that the current reduction arose almost entirely from a diminished electrode activity, rather than a depletion in the concentration of estradiol at the electrode surface. This surface passivation was also reflected in an increase in the peak-to-peak separation in CV of the ferri/ferro–cyanide couple which increased from 219 mV for the clean BDD electrode (see below section 3.4) to 498 mV for the electrode after 3 scans in the estradiol solution. However, the restoration of the BDD electrode can be easily achieved by cycling the electrode potential through the limits of water stability in dilute nitric acid until a stable scan is obtained as described in the experimental section.

The tendency to “foul” the electrodes was similar for the different chemical species studied, with the exception of BPA, which produced more extensive fouling. Indeed, whereas the other chemicals studied produced a reasonably well-defined first oxidation wave, under the same conditions, the voltammetric peak due to BPA is poorly-defined (**Figure 3.2**) , due to the greater extent of surface passivation. This is possibly due to more extensive polymerisation owing to the presence of an additional phenol group in the starting material.

After the initial assessment described above, more detailed voltammetric assessments were made to gain mechanistic insights concerning the electrochemistry observed. The effect of the scan rate on the anodic peak current of the first oxidation process was investigated over the range of 0.01 to 1.0 V s^{-1} and representative voltammograms are shown in **Figure 3.5** for estradiol and nonylphenol. The anodic peak currents increase when the scan rate is increased. Plots of anodic peak current versus the square root of the scan rate in **Figure 3.5** (inset) exhibited a linear dependence, which indicates that the initial oxidation process of the phenolic groups occurs through diffusion of the electroactive species from solution to the electrode surface [56]. Similar diffusional behaviour was observed for EE2, E1, E3 and BPA in the same supporting electrolyte.

(a)

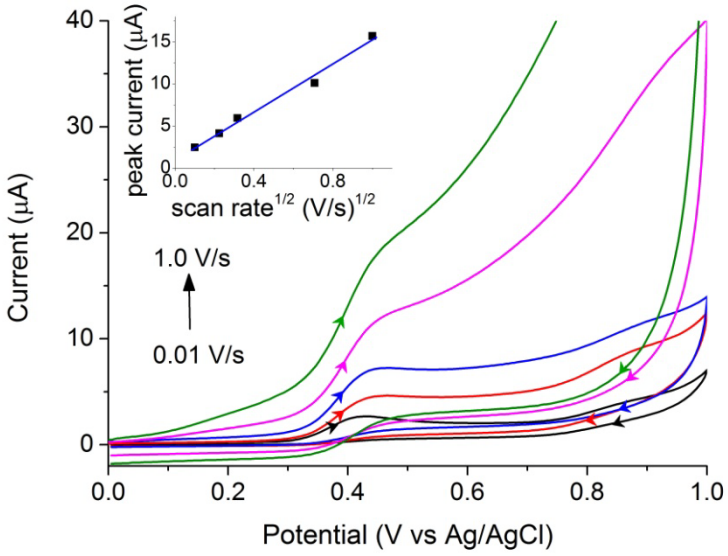

(b)

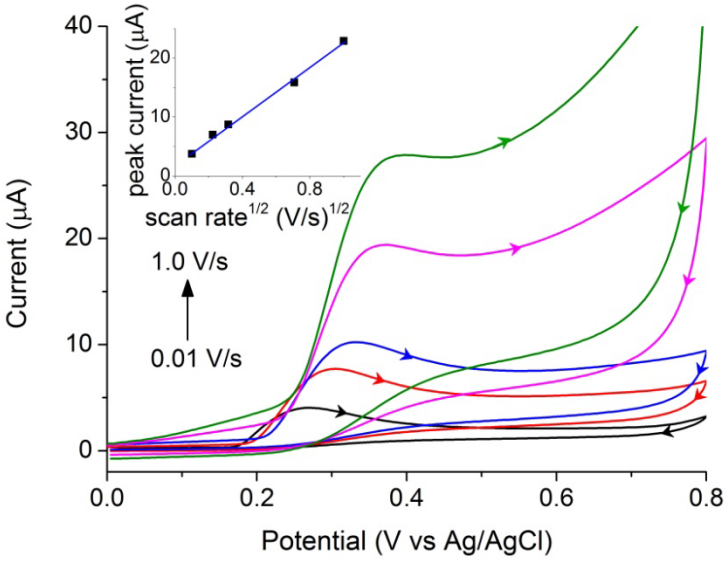

Figure 3.5 Cyclic voltammograms on oxidised BDD electrode of 0.10 mM of (a) estradiol; (b) 4-nonylphenol in phosphate buffer (pH 12.0) at scan rates of 0.01 to 1.0 V s^{-1}. Insets: Plots of anodic peak current versus the square root of scan rate.

As mentioned in the Introduction, the electrochemistry of these chemicals studied here at most electrode surfaces occurs via oxidation of adsorbed species, so this is a major mechanistic difference at BDD electrodes, arising from the chemical inertness of the diamond surface, which consequently is relatively resistant to adsorption.

The variation of the anodic peak potential and peak currents with pH was also examined to gain further mechanistic insight. In **Figure 3.6** data is presented for estradiol, showing a shift of the first oxidation peak to less positive potentials with an increase in pH. Slopes larger than 59 mV per pH unit were observed, consistent with the electrochemical irreversibility of the phenolate oxidation after deprotonation [56].

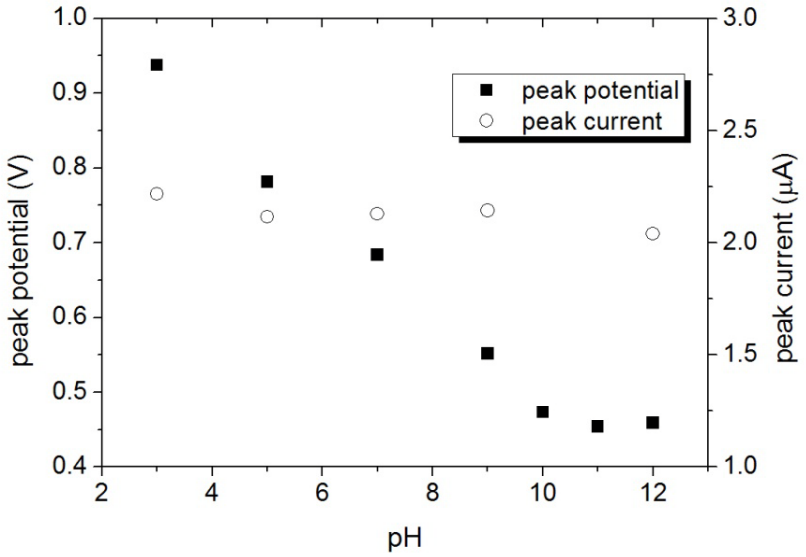

Figure 3.6 Influence of pH on anodic peak potential and current of 0.10 mM estradiol in phosphate buffer. Scan rate: 50 mV s^{-1}.

Above pH 10, the oxidation potential becomes independent of pH since according to the pK_a, for estradiol (10.46) [57], the phenolic species will exist mainly in their anionic phenolate form in this pH range, so no protons are transferred in the oxidation step. The peak current remained fairly constant from pH 3 to 12, indicating that both the neutral and phenolate forms of estradiol exhibit comparable electron transfer characteristics at the BDD electrode.

Tafel plots were derived from the ascending portion of the voltammetric peak corresponding to charge transfer control, as shown in **Figure 3.7** for estradiol for scan rates from 0.01 to 0.10 V s^{-1}. From the gradients of the linear fit, apparent electron transfer coefficients, β, of the rate-determining step were obtained, as the average of three Tafel slopes at different scan rates. The diffusion coefficients, D, was then calculated by using the transport limited *n*-electron transfer irreversible reaction described in equation (3.1)

$$i_p = 2.99 \times 10^5 n(n' + \beta)^{1/2} ACD^{1/2} \upsilon^{1/2} \quad (3.1)$$

where i_p is the peak current, *n'* is the number of electron transferred before the rate limiting step (taken to be zero here), *A* the electrode area, *C* the bulk concentration and υ the scan rate. The value of *n* was taken to be one.

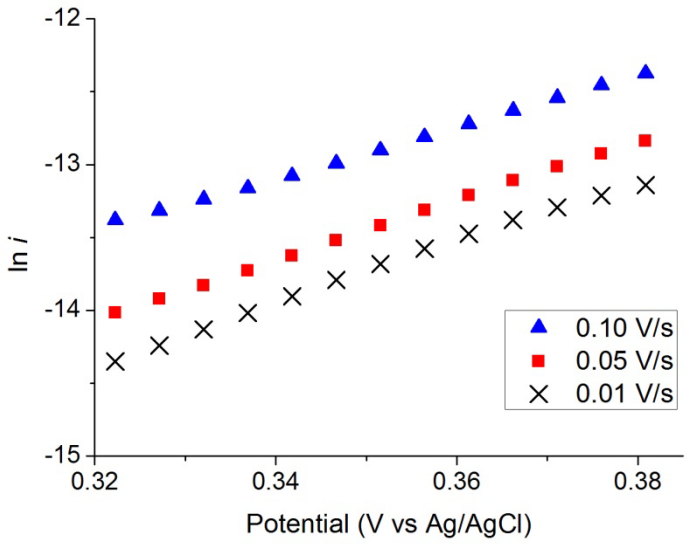

Figure 3.7 Tafel plots of 0.10 mM estradiol in phosphate buffer pH 12.0 at scan rates of 0.01 to 0.10 V s^{-1}.

These quantities are listed in **Table 3.2**, assuming a one-electron process in the calculation of D for all compounds, except a two-electron transfer for bisphenol A since this has 2 phenolic residues. Although the values of D are not readily available experimentally from the literature, the diffusivity of molecules in liquid phase can be estimated using the Wilke-Chang equation [58]:

$$D = 7.4 \times 10^{-8} \frac{(\chi M)^{1/2} T}{\eta V^{0.6}} \qquad (2)$$

where M is the relative molar mass of the solvent (water in this case), η is its viscosity, χ is an association parameter (taken to be 2.6 for water) and V is the molar volume at the normal boiling point of the solute estimated by the summation of atomic contributions of LeBas [59].

Table 3.2 Average empirical values of β and diffusion coefficients.

	β	D /10^{-5} cm^2 s^{-1}	Molar volume [a] /cm^3 mol^{-1}	D (Wilke-Chang) /10^{-5} cm^2 s^{-1}
Estriol	0.43	0.58	320.9	0.49
Estradiol	0.51	0.49	313.5	0.50
Estrone	0.48	0.67	306.1	0.51
Ethynylestradiol	0.52	0.51	343.1	0.47
Bisphenol A	0.55	0.30	266.0	0.55
4-Nonylphenol	0.77	0.43	303.2	0.51

[a] values at the normal boiling point estimated by the atomic contributions of LeBas method

The diffusion coefficients obtained from this study compare relatively well with those predicted by the empirical Wilke-Chang equation, which is widely used for its ease of application and general accuracy (about 10% average error among 251 solute-solvent systems [58]). Good agreement is observed, with the exception of BPA, again suggesting that diffusional electrochemistry is occurring. As discussed above, BPA seems to 'poison' the electrode very rapidly, producing voltammograms which show a less prominent initial oxidation wave in comparison with the other chemicals studied. It is therefore likely that this chemical produces less reliable quantitative voltammetric data.

Overall it can be concluded from the cyclic voltammetry data, including the scan rate and pH dependence along with the Tafel analysis that, with the possible exception of BPA, the electrochemistry of the compounds studied are characterised by "irreversible" electron transfer kinetics coupled to diffusional mass transport characteristics. In particular, because of the inert nature of the BDD electrode, adsorption which

dominates the electrochemistry on most other carbon based electrodes does not take place.

3.3.2 Electroanalytical Studies Using an Oxidised Diamond Electrode

Although adsorption controlled electrochemistry as normally observed for the endocrine disruptors studied, can be highly sensitive especially if high surface area film electrodes such CNTs are employed, because of the pre-concentration of the analyte within the film, it does also have disadvantages. For example the linear dynamic range can be limited since the surface of the electrode saturates with adsorbed analyte, and reproducibility requires precise preparation of the surface active coating and control of mass transport during the accumulation phase. In contrast the observation of diffusional electrochemistry at the BDD electrode offers the route to highly reproducible detection using an electrode which can easily be prepared. Experiments were therefore carried out to assess the analytical capabilities of BDD using estradiol, the most potent amongst the estrogenic hormones, as the example.

Square wave voltammetry, as mentioned in Chapter 2, is a pulsed voltammetric technique which provides advantages such as the ability to discriminate against broad background contributions to the measured current, thereby allowing a lower limit of detection to be attained. Being a more sensitive method towards distinguishing the faradaic current compared to CV, square wave voltammetry was used to examine the electrode response as a function of estradiol concentration.

To realise the excellent sensitivity of this pulse technique, optimisation of the parameters of square wave voltammetry is an important step. This involves the study of the dependence of pulse amplitude, frequency and scan increment on the signal response. Measured data is shown in **Figure 3.8**, which gives example data of how the accessible parameters influence peak height and peak resolution. From the data in **Figure 3.8** and similar data optimised parameters for subsequent analytical work were chosen: pulse amplitude of 40 mV; frequency of 20 Hz ; and scan increment of 2 mV.

Figure 3.9a shows the square wave voltammograms obtained for estradiol in a supporting electrolyte of phosphate buffer at pH 12.0 as a function of estradiol concentration. pH 12.0 was selected in part because the use of high pH lowers the oxidation potential and hence the possibility of interference from other reductants in "real" samples. Also the voltammetric peaks seemed better defined at higher pH. The corresponding standard curve was constructed using the anodic peak current (with background current subtracted) versus the estradiol concentration (**Figure 3.9**b). With the optimised parameters, the well-defined peak currents on the oxidised BDD electrode showed a linear increase from 5.0 to 100.0 μM, with a correlation coefficient of 0.9998 and a slope of 28 ± 0.2 A cm^3 mol^{-1}. The recent tendency for the derivation of the limit of detection (LOD) is to base its calculation from calibration plots on three times the standard deviation of the y-residuals [60]. Using this graphical approach, the LOD is thus 3σ divided by the slope of the line of best fit and the calculated value of LOD for estradiol is 1.6 μM. Another approach for the LOD is to estimate its value using the ratio of three times the background noise to slope [61], giving a value of 0.86 μM in this case, which agrees well with the alternative value.

(a) (b)

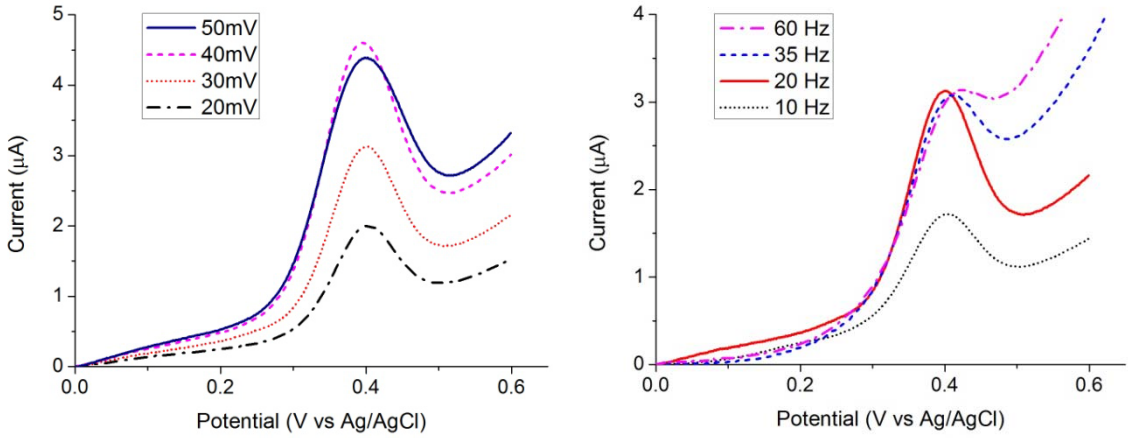

(c)

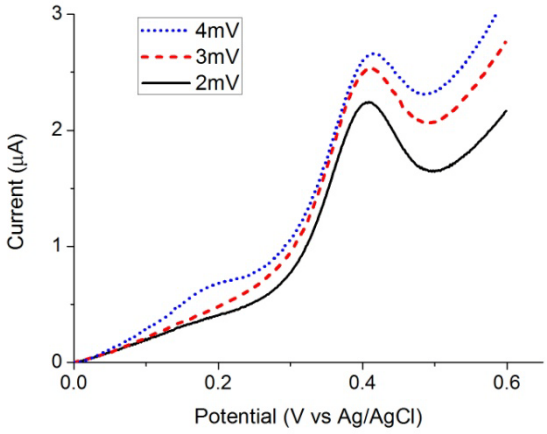

Figure 3.8 Square wave voltammograms on oxidised BDD electrode of estradiol in phosphate buffer pH 12.0 at different (a) pulse amplitudes of 20 to 50 mV; (b) frequency of 10 to 60 Hz; (c) scan increments of 2 to 4 mV. Concentration of estradiol for: 0.10 mM.

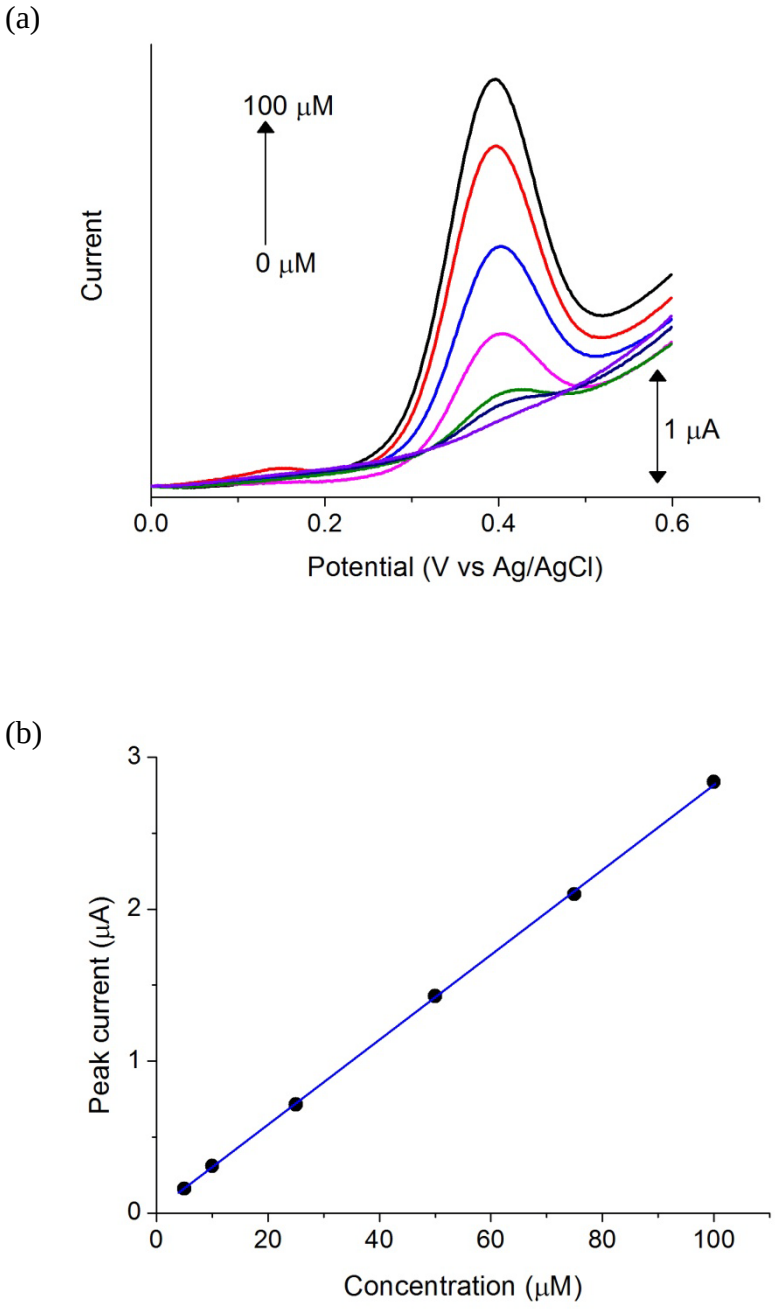

Figure 3.9 (a) Square wave voltammograms on oxidised BDD electrode of estradiol in phosphate buffer pH 12.0 at different concentrations of 0.0, 5.0, 10.0, 25.0, 50.0, 75.0 and 100.0 μM estradiol. (b) Calibration curve of peak current against concentration.

Overall, it can be concluded that the linear dynamic range, which exceeds 100 μM (the highest concentration studied) compares favourably with many of the results on modified electrodes in **Table 3.1**, as expected from the operative mechanism based on diffusional electrochemistry. The limit of detection also is comparable to many of the results in the table, although significantly lower detection limits are observed in particular instances. This arises because of the pre-concentration of the analyte which occurs in the modifying layers. In conclusion, given the very simple highly reproducible preparation of the BDD electrode in comparison with the modified electrodes in **Table 3.1**, it would appear that BDD is the material of choice for the detection of endocrine disruptors in the higher concentration range > 1 μM.

3.3.3 Electrochemical Studies Using a Hydrogen Terminated Diamond Electrode

The lack of adsorption of the phenolic substances on the BDD electrode, leading to diffusional electrochemistry, arises from the inert nature of the diamond surface. This in turn stems from the fact that species which can form strong covalent bonds to carbon tend to become attached to the diamond lattice, leading to a very stable and consequently inert surface. The electrochemical cycling in nitric acid is known to lead to a surface to which various oxygen functionalities such as hydroxyl, ether, carbonyl and carboxylate are bonded, giving rise to hydrophilic properties [62]. These can be converted to the more reduced forms by cathodic polarisation of the electrode at potentials around –2 V [63]. Complete termination of the BDD surface with hydrogen is possible if the BDD surface is exposed to a gaseous environment rich in atomic hydrogen or cathodically treated at very extreme potentials [62]. Experiments were therefore carried out to explore how these differing surface terminations might change the electrochemistry observed.

The changes induced in the behaviour for estradiol as shown in **Figure 3.10** as a result of cathodic polarisation of the electrode at−2.5 V in both HNO_3 and H_2SO_4 were quite typical. A small shift of the anodic peak to less positive potentials (+0.39 V) as a result of the reduction in overpotential is seen as well as a small increase in the peak current. Anodic polarisation of the electrode at +2.5 V in nitric acid reversed this effect, confirming it arises from a reversible change of the electrode such as change on surface termination.

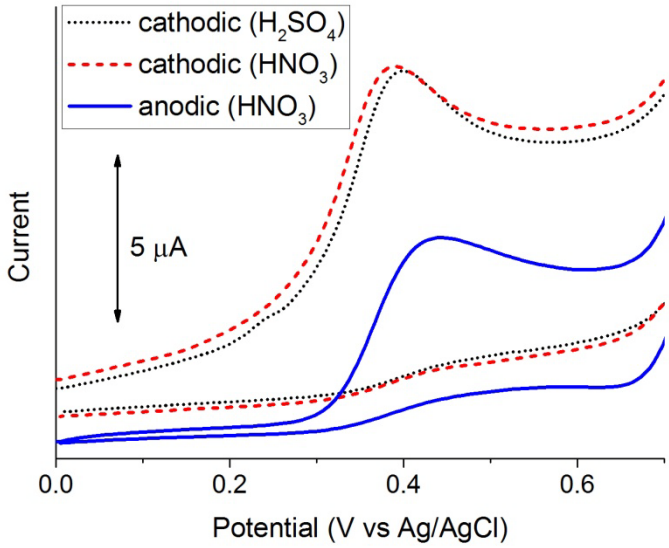

Figure 3.10 Cyclic voltammograms on BDD electrode in phosphate buffer pH 12 of 0.1 mM estradiol after cathodic pretreatment at−2.5 V in 0.5 M H_2SO_4 and 0.1 M HNO_3, and anodic treatment at +2.5 V in 0.1 M HNO_3. Scan rate: 50 mV s^{-1}.

The behaviour of the fully hydrogenated surface, as a result of exposure to a microwave hydrogen plasma is shown in **Figure 3.11**. After pretreatment, the cyclic voltammograms in **Figure 3.11**a all displayed significant shifts to less positive peak potentials for the oxidation of the compounds examined herein, with a significant increase in peak current.

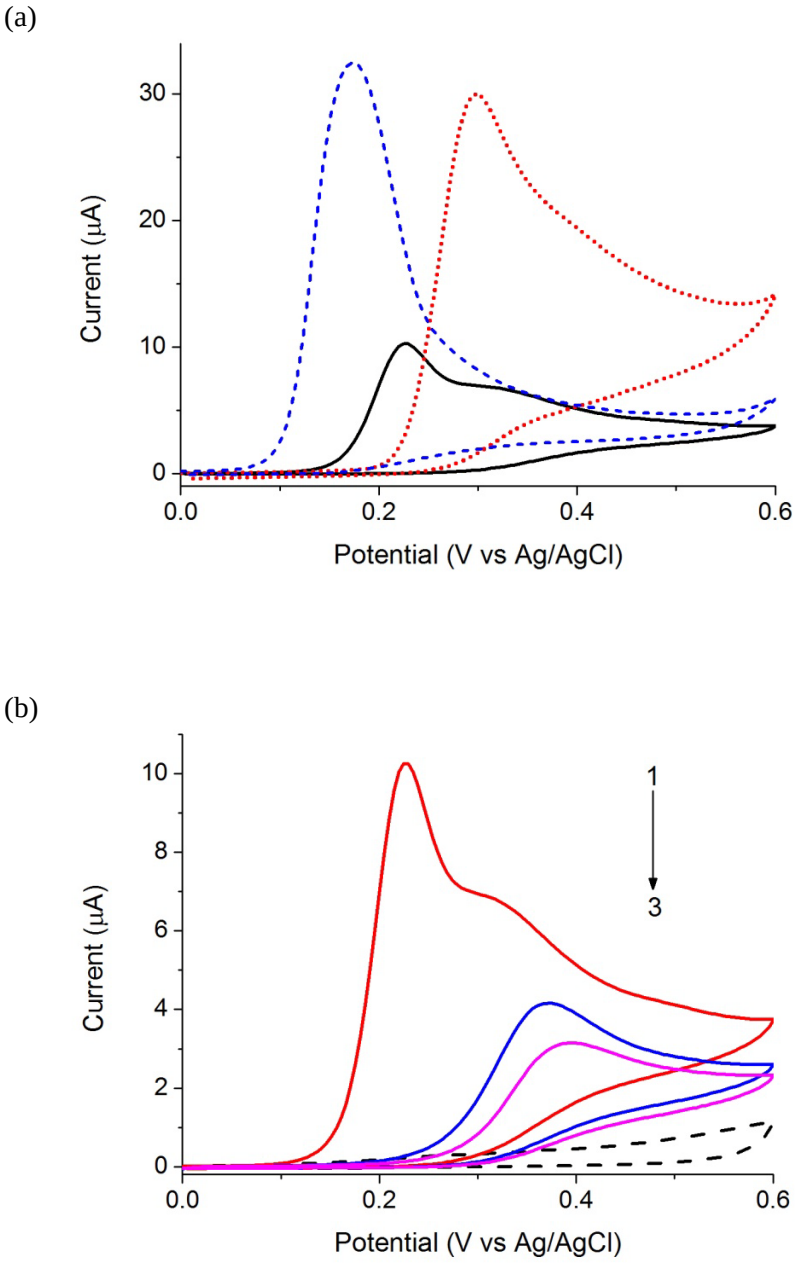

Figure 3.11 Cyclic voltammograms on BDD electrode in phosphate buffer pH 12 of: (a) estradiol (solid line), 4-nonylphenol (dashed line) and bisphenol A (dotted line) after hydrogen plasma pretreatment; (b) estradiol (three consecutive scans) with background scan (dashed line) after hydrogen plasma pretreatment. Concentration of each compound: 0.10 mM. Scan rate: 50 mV s^{-1}.

However the change is only characteristic of the clean hydrogenated surface since as can be seen in **Figure 3.11**b on subsequent electrochemical cycling, the cyclic voltammogram rapidly reverts to that of the untreated surface. As discussed above, this again probably arises because of the phenoxy radicals.

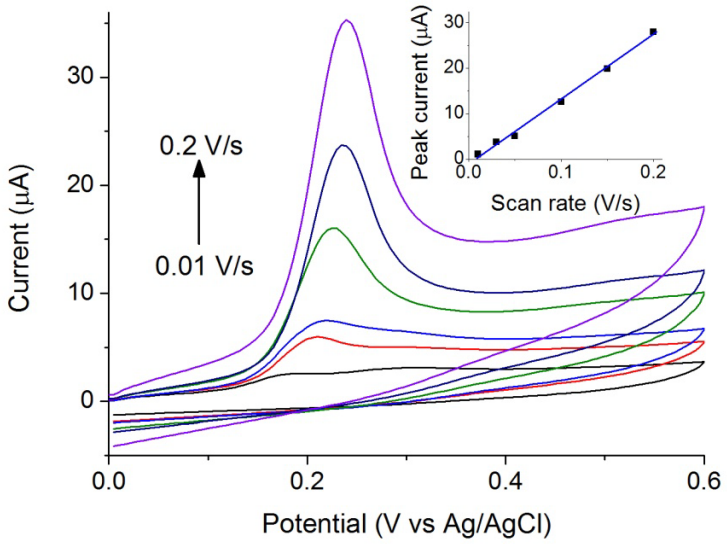

Figure 3.12 Cyclic voltammograms on BDD electrode in phosphate buffer pH 12 of 50.0 μM estradiol at scan rates of 0.01 to 0.20 V s^{-1} after hydrogen plasma pretreatment, inset: plot of anodic peak current versus scan rate.

For estradiol, the peak height after hydrogen plasma pretreatment is twice that of the clean oxygen-terminated BDD surface. Since the mechanism for the latter involves diffusional electrochemistry, this suggests that some change of mechanism is occurring which tends to concentrate the analyte in the region of the electrode. Indeed studies of the scan rate dependence which was investigated in **Figure 3.12** shows that the peak current increases linearly with the scan rate, showing that adsorption on the electrode becomes dominant [56]. Adsorption is likely to be due to the hydrophobic interaction

between the (hydrophobic) hydrogen-terminated BDD surface and the organic endocrine disruptors. Because of the increase in peak current, it is likely that the use of the hydrogenated surface could produce a modest increase in the detection limit, if other factors remain constant. However this seems to be outweighed both by the difficulty in producing the hydrogen termination, compared to the simple electrochemical cleaning used to prepare the oxidised surface, and also the fact that the changed properties are very readily lost even by a single electrochemical scan.

3.3.4 Electrode Modification with Nanocarbon

To achieve the highest sensitivity for electroanalysis, pre-concentration of the analyte within adsorbed layers of highly dispersed materials which modify the electrode surface is required using a technique known as adsorptive voltammetry [56]. In the present work, this was examined using nanocarbon as the electrode modifier. The electrochemical response of two common redox couples, ferrocenemethanol and potassium ferrocyanide, on both oxidised and NC/BDD electrode was first compared by cyclic voltammetry to ascertain changes to electrode properties introduced by the addition of nanocarbon and results are shown in **Figure 3.13**.

The redox reactions of both couples are judged to be diffusion-controlled from the linear response of the anodic peak current with the square root of the scan rate, as shown in **Figure 3.14**, indicating neither of these redox couples show a particular tendency to adsorb on nanocarbon. However both couples show a modest increase in the recorded peak current, as a result of the addition of nanocarbon.

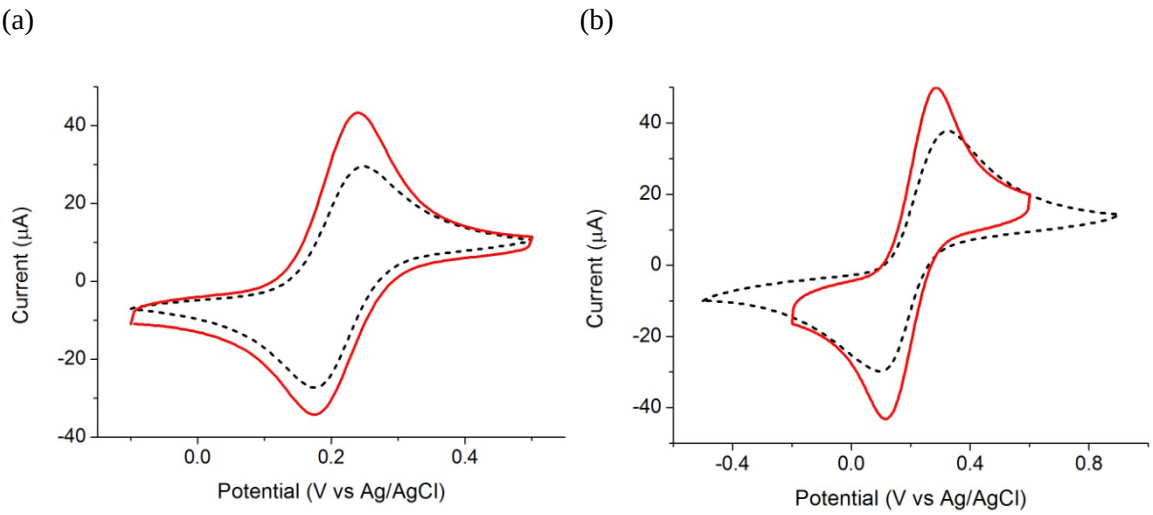

Figure 3.13 Redox couples in KCl solution on oxidised and nanocarbon-modified BDD electrodes: Cyclic voltammograms of (a) 0.50 mM ferrocenemethanol and (b) 1.0 mM ferrocyanide, oxidised (dashed line), NC/BDD (solid line), scan rate: 50.0 mV s^{-1}.

BDD electrodes often show peak currents in CV below that predicted by pure diffusion limitations, which has been attributed to the presence of electrochemically inactive areas were the B doping is inadequate [64], so possibly this feature is eliminated by addition of an electrically conducting film of nanocarbon. Thin layer diffusional effects may also likely operate within the nanocarbon film giving the illusion of enhanced reversibility [65-67]. A small increase in the pseudocapacitive background currents in CV were also observed in the presence of nanocarbon.

The peak-peak potential separation (ΔE_p) of ferrocenemethanol did not differ greatly at values of 40-60 mV on both the oxidised BDD as well as NC/BDD structure, which is close to the ideal 57 mV for a reversible system [56]. As for $[Fe(CN)_6]^{3-/4-}$, quasi-reversible kinetics was observed with a decrease of ΔE_p from 219 mV to 166 mV at 50

(a)

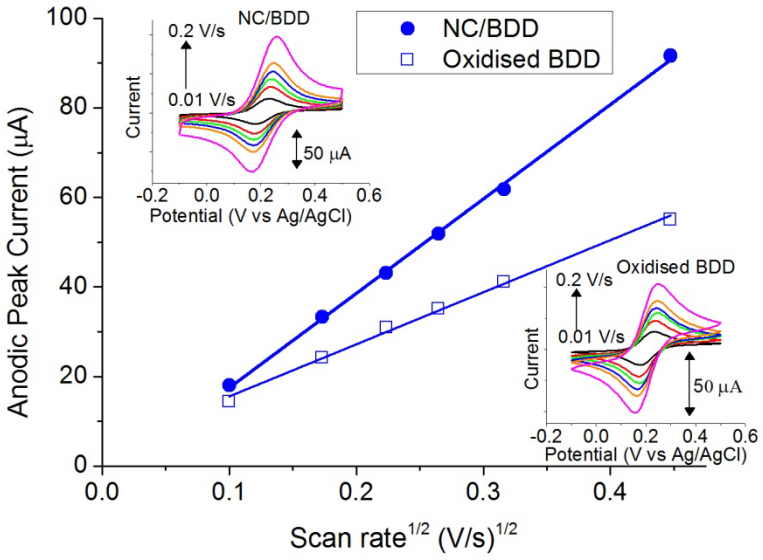

(b)

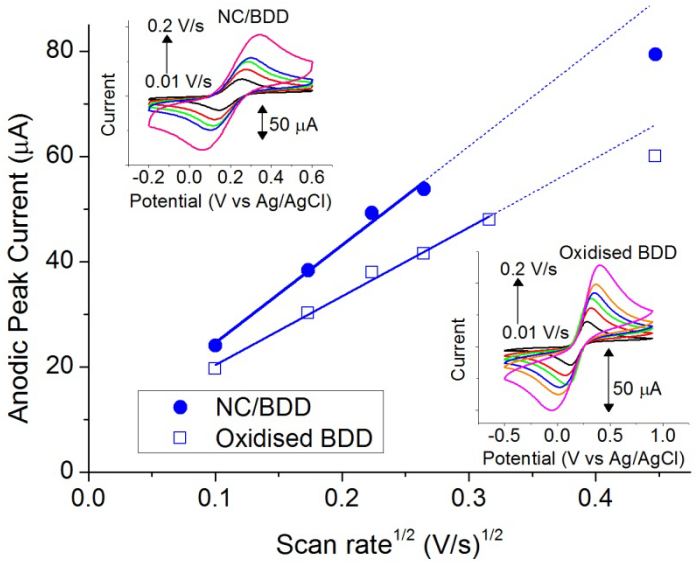

Figure 3.14 Redox couples in KCl solution on oxidised and nanocarbon-modified BDD electrodes: Plots of the peak current versus square root of scan rate for (a) 0.50 mM ferrocenemethanol and (b) 1.0 mM ferrocyanide, insets: cyclic voltammograms at scan rates from 10.0 to 200.0 mV s^{-1}.

mV s^{-1} scan rate after surface modification with nano-carbon, suggesting nanocarbon speeds up the electron transfer kinetics and/or that thin layer effects again operate. The results recorded for the endocrine disruptors are very different.

Results from estradiol are shown in **Figure 3.15**. From the cyclic voltammograms depicted in **Figure 3.15**, when compared to the unmodified BDD electrode, the oxidation of estradiol occurs at a less positive potential (+0.33 V), with a doubling of the peak current on NC/BDD for the same concentration of 0.10 mM in a phosphate buffer solution of pH 12.0. This increase in signal suggests pre-concentration of estradiol at the electrode surface, that is, the involvement of an adsorption process on the nanocarbon. This is confirmed by a plot of the peak current against scan rate values in **Figure 3.16** which shows a linear variation and passes through the origin, therefore indicating an adsorption-controlled oxidation on the NC/BDD.

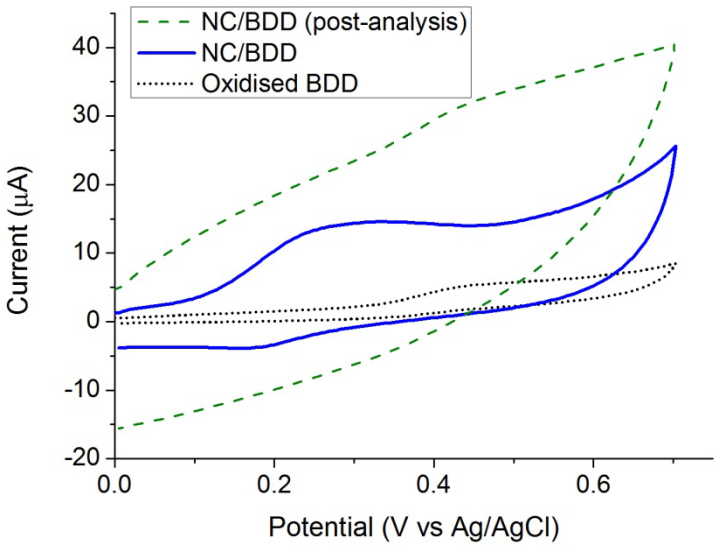

Figure 3.15 Cyclic voltammograms of 0.10 mM estradiol in phosphate buffer solution pH 12.0 on different electrode surfaces. Scan rate: 50.0 mV s^{-1}. Post-analysis: after use for analysis of estradiol.

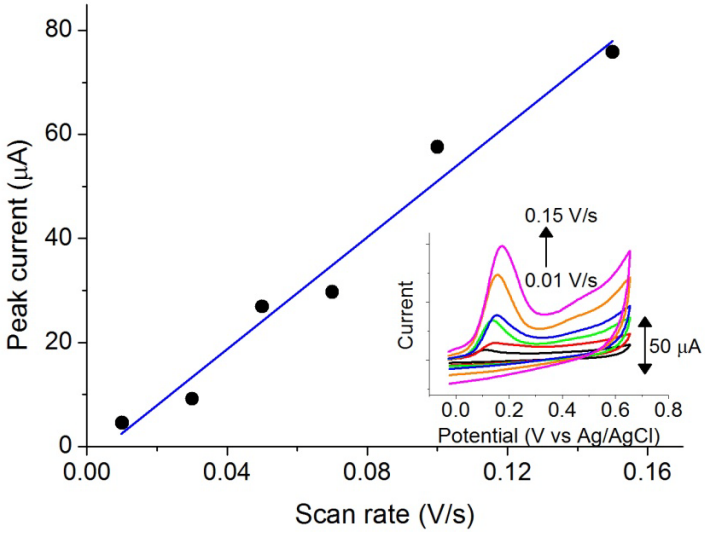

Figure 3.16 Peak current of estradiol in phosphate buffer pH 12.0 on NC/BDD for (a) 0.10 mM, versus scan rate, inset: cyclic voltammograms at scan rates from 10.0 to 150.0 mV s^{-1}.

Thus the high surface-area-to-volume ratio of the nanocarbon particles allows the accumulation of the analyte by adsorption and reduces the overpotential. After a scan is completed, subsequent scans look rather featureless, again suggesting that some passivation has occurred, due to reaction with the products of oxidation (**Figure 3.15**).

Since adsorption is occurring, the accumulation time is an important factor in the adsorption of analytes on the surface of the NC/BDD. After accumulation times from 0 to 120 s under stirring, cyclic voltammograms (under still conditions) were recorded and are shown in **Figure 3.17**. Lengthening the time from 0 to 30 s resulted in a 180% increase of the peak height, with further extension leading to diminishing gains, indicating that the adsorption achieves relatively rapid saturation. 120 s was thus chosen as the accumulation duration for efficiency. Preconcentration under an applied potential

over −0.5 to 0 V did not show improvement over open circuit accumulation therefore the latter mode was used.

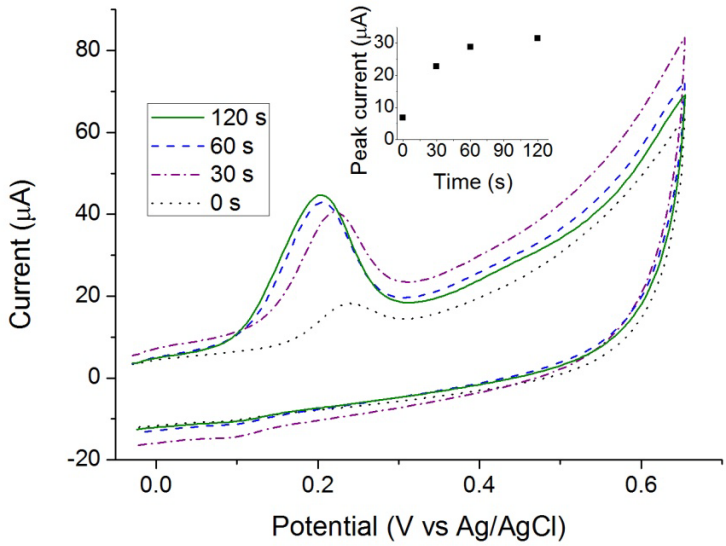

Figure 3.17 Cyclic voltammograms of 0.10 mM estradiol in phosphate buffer solution pH 12.0 on nanocarbon-modified BDD electrode at accumulation times of 0, 30, 60 and 120 s. Scan rate: 50.0 mV s^{-1}. Inset: Plot of peak current against accumulation times.

The amount of surface modifier, being another determining factor in the adsorptivity, was investigated by varying the volume of nanocarbon suspension cast on the clean BDD. As shown by the cyclic voltammograms in **Figure 3.18**, an increase in the peak current results from greater amounts of nanocarbon particles on the oxidised BDD electrode surface. However, the associated larger background is not favourable for analysis at low concentrations.

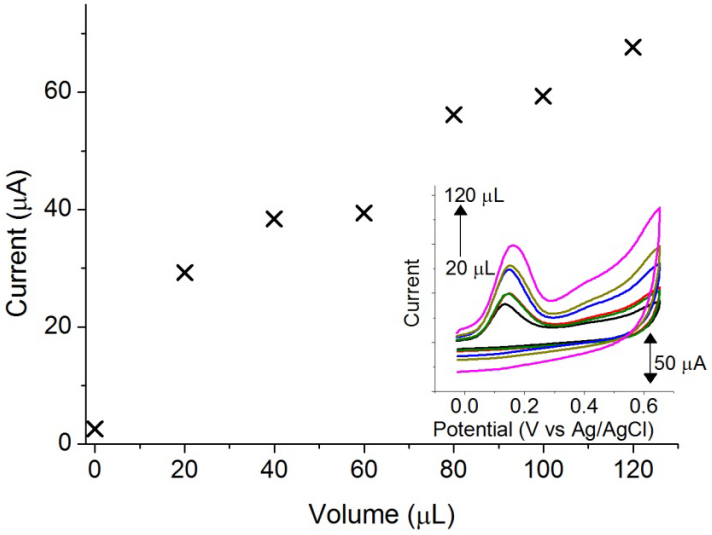

Figure 3.18 Peak currents of 0.10 mM estradiol in phosphate buffer pH 12.0 on NC/BDD with 0, 20, 40, 60, 80, 100 and 120 μL of nanocarbon for modification. Inset: cyclic voltammograms obtained with different amounts of nanocarbon. Scan rate: 50.0 mV s^{-1}.

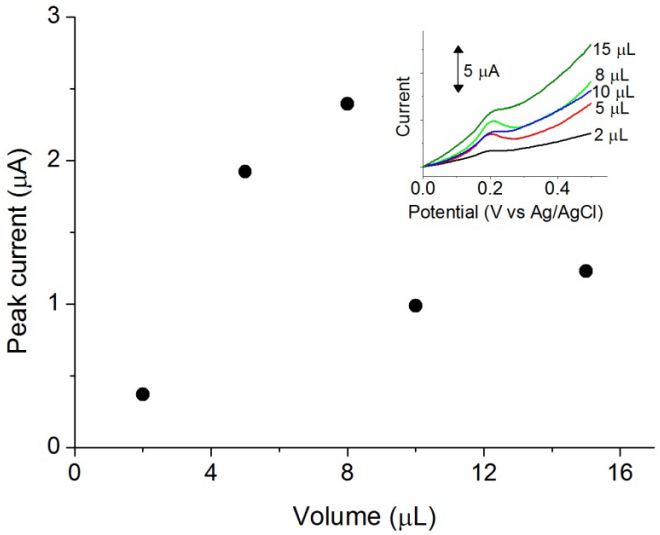

Figure 3.19 Peak currents of 100.0 nM estradiol in phosphate buffer pH 12.0 on NC/BDD with 2, 5, 8, 10 and 15 μL of nanocarbon for modification. Inset: square wave voltammograms obtained with different amounts of nanocarbon. Pulse amplitude: 40 mV; frequency: 20 Hz; scan increment: 2 mV.

Using the technique of square wave voltammetry, there is also an increase of the peak current with the amount of nanocarbon, reaching an optimum before declining (**Figure 3.19**). A loading of 8.0 μL of the 2 mg/ml nanocarbon suspension per cm^2 was chosen as giving around optimal results.

Figure 3.20a depicts the voltammetric response while **Figure 3.20**b shows the standard curve obtained using square wave adsorptive stripping voltammetry for estradiol in a supporting electrolyte of 0.1 M phosphate buffer at pH 12. The peak heights on the NC/BDD electrode exhibited linearity over the range of 5.0 to 100.0 nM and the data is suggestive of good electrode-to-electrode reproducibility. The correlation coefficient is 0.9996 and the slope is $(2.8 \pm 0.02) \times 10^4$ A cm^3 mol^{-1}.

The modification with nanocarbon particles resulted in an improvement of the sensitivity by three orders of magnitude over the oxidised BDD electrode. The limit of detection (LOD) was calculated with 3σ to slope to be 2.2 nM while the estimation of LOD using the ratio three times noise to slope is 2.1 nM. Similarly the LODs are estimated to be 3 nM, 9 nM and 70 nM for 4-nonylphenol, ethynylestradiol and bisphenol A respectively. The higher LOD value of bisphenol A stems from its lower sensitivity of detection. This could possibly arise from the surface passivation phenomenon as discussed for the oxidised BDD electrode.

The lower limit of linearity is as expected for an adsorptive process but the LOD compares well with state-of-the-art values of estradiol detection on other electrodes available from the literature (**Table 3.1**). In contrast with the quite sophisticated and relatively expensive modification with carbon nanotubes, the simple preparation with

the relatively inexpensive nanocarbon is able to achieve the same results when combined with the BDD electrode.

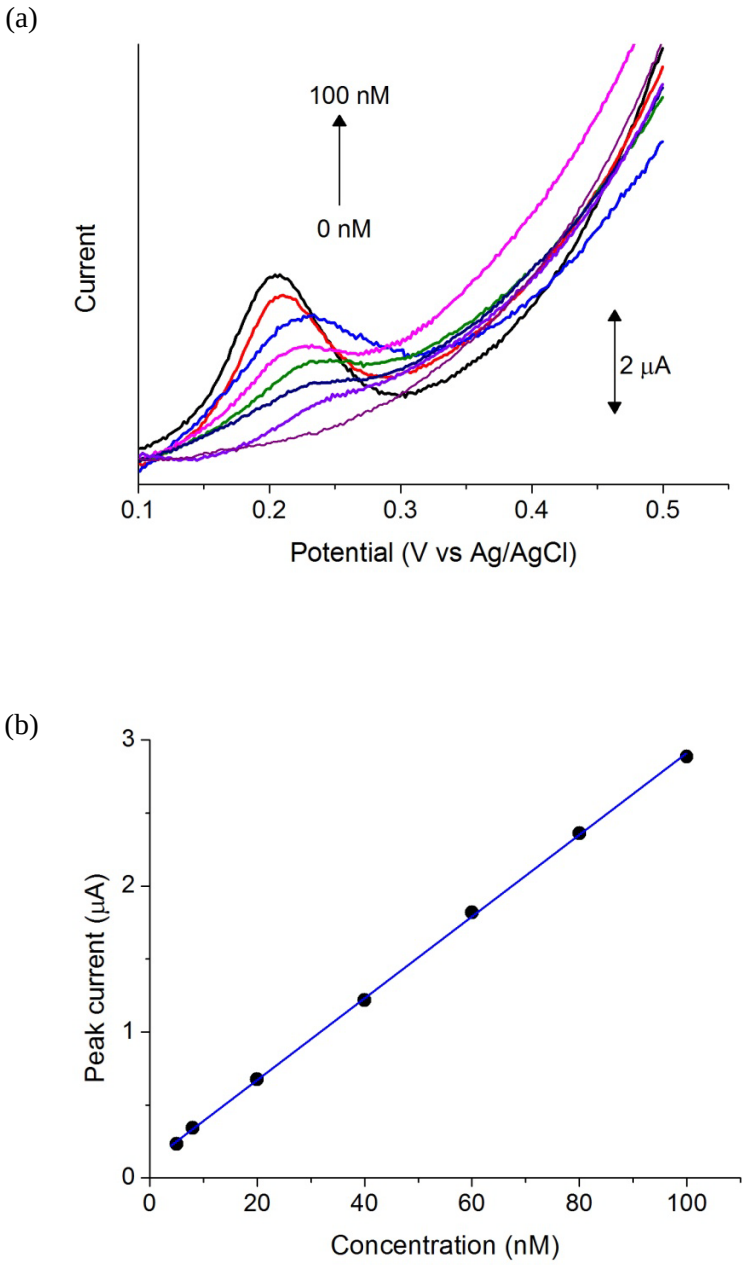

Figure 3.20 (a) Square wave voltammograms at different concentrations of 0.0, 5.0, 8.0, 20.0, 40.0, 60.0, 80.0 and 100.0 nM estradiol in 0.10 M phosphate buffer pH 12.0 on NC/BDD electrode. Pulse amplitude: 40 mV, frequency: 20 Hz, scan increment: 2 mV. (b) Calibration curve of peak current against concentration.

3.4 Conclusions

The electrochemical behaviour of estradiol and other endocrine disrupting compounds has been studied on the BDD electrode with different surface pretreatments, as well as on a nanocarbon-modified BDD electrode. On the clean as-prepared, hydrophilic oxidised BDD surface, the compounds studied exhibit diffusional electrochemistry since adsorption does not take place on this inert diamond surface. Reproducible electroanalysis can therefore be performed, with a linear dynamic range of 1- >100 μM and detection limits around 1 μM. 4-nonylphenol is oxidised at significantly lower potentials than the other endocrine disruptors, enabling its identification in suitable mixtures of these materials. Although the target analytes do not adsorb on the electrode surface, the products of electrochemical oxidation do even on this inert BDD electrode, which necessitates a simple cleaning procedure between analysis scans.

The electrochemistry observed is sensitive to the chemical termination of the BDD electrode. In particular strong adsorption is observed on the hydrophobic hydrogen terminated surface. Adsorption effects are also observed on the nanocarbon modified electrode leading to significant pre-concentration of the analyte in the modifying film. Highly sensitive detection is thus possible with a linear response in the range 5-100 nM and detection limits < 10 nM being observed for the compounds studied with the exception of BPA.

Overall it can be concluded that the oxidised BDD electrode is an excellent electrode material for electroanalysis in the high concentration range of these compounds 1-100 μM, whilst the nanocarbon modifed electrode offers state-of-the-art detection capabilities in the low concentration range 5-100 nM. Given the benefit in performance

provided by surface modification, the following chapter further explores this aspect of the BDD electrode in relation to electrocatalysis.

References

[1] P. Gan, R.G. Compton, J.S. Foord, Electroanalysis 25 (2013) 2423.

[2] C. Sonnenschein, A.M. Soto, J. Steroid Biochem. Mol. Biol. 65 (1998) 143.

[3] A. Wenzel, J. Müller, T. Ternes, Study on endocrine disrupters in drinking water, Schmallenberg and Wiesbaden, Germany, ENV.D.1/ETU/2000/0083, 2003.

[4] E.T. Damstra, S. Barlow, A. Bergman, R. Kavlock, G.V.D. Kraak, Global assessment of the state-of-the-science of endocrine eisruptors, WHO/PCS/EDC/02.2 2002.

[5] European Commission staff working document on the implementation of the "community strategy for endocrine disrupters" - a range of substances suspected of interfering with the hormone systems of humans and wildlife, Brussels Belgium, SEC/2007/1635, 2007.

[6] C.E. Purdom, P.A. Hardiman, V.V.J. Bye, N.C. Eno, C.R. Tyler, J.P. Sumpter, Chem. Ecol. 8 (1994) 275.

[7] S.R. Hutchins, M.V. White, F.M. Hudson, D.D. Fine, Environ. Sci. Technol. 41 (2007) 738.

[8] C. Desbrow, E.J. Routledge, G.C. Brighty, J.P. Sumpter, M. Waldock, Environ. Sci. Technol. 32 (1998) 1549.

[9] HELCOM, Draft guidance document on nonylphenol/ nonylphenolethoxylates, Helsinki Finland, HazSub 7/2002-3.3/2 2002.

[10] M.R. Servos, Water Qual. Res. J. Can 34 (1999) 123.

[11] L.T. Brooke, G. Thursby, Ambient aquatic life water quality criteria – nonylphenol, Washington DC, EPA-822-R-05-005 2005.

[12] T. Suzuki, Y. Nakagawa, I. Takano, K. Yaguchi, K. Yasuda, Environ. Sci. Technol. 38 (2004) 2389.

[13] S. Impens, K. De Wasch, M. Cornelis, H.F. De Brabander, J. Chromatogr. A 970 (2002) 235.

[14] J.B. Quintana, J. Carpinteiro, I. Rodríguez, R.A. Lorenzo, A.M. Carro, R. Cela, J. Chromatogr. A 1024 (2004) 177.

[15] C. Zwiener, F. Frimmel, Anal. Bioanal. Chem. 378 (2004) 862.

[16] C.-H. Huang, D.L. Sedlak, Environ. Toxicol. Chem. 20 (2001) 133.

[17] J.C. Wingfield, D.S. Farner, Steroids 26 (1975) 311.

[18] K.C. Chan, G.M. Muschik, H.J. Issaq, P.K. Siiteri, J. Chromatogr. A 690 (1995) 149.

[19] C.M.A. Brett, Pure Appl. Chem. 73 (2001) 1969.

[20] H. Tao, W. Wei, X. Zeng, X. Liu, X. Zhang, Y. Zhang, Microchim. Acta 166 (2009) 53.

[21] X. Liu, D.K.Y. Wong, Anal. Chim. Acta 594 (2007) 184.

[22] X. Lin, Y. Li, Biosens. Bioelectron. 22 (2006) 253.

[23] N. Terui, B. Fugetsu, S. Tanaka, Anal. Sci. 22 (2006) 895.

[24] C. Hu, C. Yang, S. Hu, Electrochem. Commun. 9 (2007) 128.

[25] Y. Gao, Y. Cao, D. Yang, X. Luo, Y. Tang, H. Li, J. Hazard. Mater. 199–200 (2012) 111.

[26] X. Liu, H. Feng, X. Liu, D.K.Y. Wong, Anal. Chim. Acta 689 (2011) 212.

[27] H. Yin, Y. Zhou, S. Ai, Q. Chen, X. Zhu, X. Liu, L. Zhu, J. Hazard. Mater. 174 (2010) 236.

[28] D. Vega, L. Agüí, A. González-Cortés, P. Yáñez-Sedeño, J.M. Pingarrón, Talanta 71 (2007) 1031.

[29] X. Wen, J. Fei, X. Chen, L. Yi, F. Ge, M. Huang, Environ. Pollut. 156 (2008) 1015.

[30] "Carbon Nanotubes" to be found under http://www.sigmaaldrich.com/materials-science/material-science-products.html?TablePage=16376687.

[31] R.G. Compton, J.S. Foord, F. Marken, Electroanalysis 15 (2003) 1349.

[32] J. Xu, M.C. Granger, Q. Chen, J.W. Strojek, T.E. Lister, G.M. Swain, Anal. Chem. 69 (1997) 591A.

[33] T.N. Rao, A. Fujishima, Diamond Relat. Mater. 9 (2000) 384.

[34] J. Angus, H. Martin, U. Landau, Y.E. Evstefeeva, B. Miller, N. Vinokur, New Diamond Front. Carbon Technol. 9 (1999) 175.

[35] J. Kruusma, C. Banks, R. Compton, Anal. Bioanal. Chem. 379 (2004) 700.

[36] C. Prado, S.J. Wilkins, F. Marken, R.G. Compton, Electroanalysis 14 (2002) 262.

[37] M.C. Granger, J. Xu, J.W. Strojek, G.M. Swain, Anal. Chim. Acta 397 (1999) 145.

[38] C. Terashima, T.N. Rao, B.V. Sarada, D.A. Tryk, A. Fujishima, Anal. Chem. 74 (2002) 895.

[39] M. Panizza, I. Duo, P.A. Michaud, G. Cerisola, C. Comninellis, Electrochem. Solid-State Lett. 3 (2000) 429.

[40] T.N. Rao, I. Yagi, T. Miwa, D.A. Tryk, A. Fujishima, Anal. Chem. 71 (1999) 2506.

[41] C.H. Goeting, F. Jones, J.S. Foord, J.C. Eklund, F. Marken, R.G. Compton, P.R. Chalker, C. Johnston, J. Electroanal. Chem. 442 (1998) 207.

[42] A. Fujishima, T.N. Rao, E. Popa, B.V. Sarada, I. Yagi, D.A. Tryk, J. Electroanal. Chem. 473 (1999) 179.

[43] J. Xu, Q. Chen, G.M. Swain, Anal. Chem. 70 (1998) 3146.

[44] G.W. Muna, N. Tasheva, G.M. Swain, Environ. Sci. Technol. 38 (2004) 3674.

[45] K.D. Santos, O.C. Braga, I.C. Vieira, A. Spinelli, Talanta 80 (2010) 1999.

[46] D.J. Browne, L. Zhou, J.H.T. Luong, J.D. Glennon, Electrophoresis 34 (2013) 2025.

[47] D. Borah, S. Satokawa, S. Kato, T. Kojima, Appl. Surf. Sci. 254 (2008) 3049.

[48] M. Wissler, J. Power Sources 156 (2006) 142.

[49] T.W.B. Lo, L. Aldous, R.G. Compton, Sens. Actuators, B 162 (2012) 361.

[50] J. Panchompoo, L. Aldous, M. Baker, M.I. Wallace, R.G. Compton, Analyst 137 (2012) 2054.

[51] M.C. Granger, G.M. Swain, J. Electrochem. Soc. 146 (1999) 4551.

[52] C.H. Goeting, F. Marken, A. Gutierrez-Sosa, R.G. Compton, J.S. Foord, New Diamond Front. Carbon Technol. 9 (1999) 207.

[53] L. Papouchado, R.W. Sandford, G. Petrie, R.N. Adams, J. Electroanal. Chem. Interfac. Electrochem. 65 (1975) 275.

[54] M. Gattrell, D.W. Kirk, J. Electrochem. Soc. 140 (1993) 903.

[55] I.B. Dimov, C. Batchelor-McAuley, L. Aldous, R.G. Compton, Phys. Chem. Chem. Phys. 14 (2012) 2375.

[56] R.G. Compton, C.E. Banks, Understanding Voltammetry, World Scientific, Singapore, 2007.

[57] A.R. Hurwitz, S.T. Liu, J. Pharm. Sci. 66 (1977) 624.

[58] C.R. Wilke, P. Chang, AlChE J. 1 (1955) 264.

[59] W.J. Lyman, W.F. Reehl, D.H. Rosenblatt, Handbook of Chemical Property Estimation Methods: Environmental Behavior of Organic Compounds, American Chemical Society, Washington DC, 1990.

[60] C.M.A. Brett, A.M.O. Brett, Electroanalysis, Oxford University Press, Oxford, 1998.

[61] D.C. Singer, A Laboratory Quality Handbook of Best Practices, ASQ Quality Press, Milwaukee, 2001.

[62] T.T. H. Notsu, A. Fujishima in Diamond Electrochemistry (Eds: A. Fujishima, Y. Einaga, T. N. Rao, D. A. Tryk), Elsevier Science, Amsterdam, 2005.

[63] R. Hoffmann, A. Kriele, H. Obloh, J. Hees, M. Wolfer, W. Smirnov, N. Yang, C.E. Nebel, Appl. Phys. Lett. 97 (2010) 052103.

[64] K. Honda, T. Noda, M. Yoshimura, K. Nakagawa, A. Fujishima, J. Phy. Chem. B 108 (2004) 16117.

[65] I. Streeter, G.G. Wildgoose, L. Shao, R.G. Compton, Sens. Actuators, B 133 (2008) 462.

[66] M.C. Henstridge, E.J.F. Dickinson, M. Aslanoglu, C. Batchelor-McAuley, R.G. Compton, Sens. Actuators, B 145 (2010) 417.

[67] M.J. Sims, N.V. Rees, E.J.F. Dickinson, R.G. Compton, Sens. Actuators, B 144 (2010) 153.

Chapter 4

Surface Modification of Boron-Doped Diamond with Microcrystalline Copper Phthalocyanine: Oxygen Reduction Catalysis

The surface modification of boron-doped diamond is studied in this chapter by using a simple and convenient dropcast technique to deposit copper phthalocyanine onto the electrode. Both unmodified and modified BDD electrodes of different surface terminations (namely hydrogen and oxygen) were compared via the electrochemical reduction of oxygen in aqueous solution. A significant lowering of the cathodic overpotential by ca 500 mV was observed after modification of hydrogen-terminated (hydrophobic) BDD while no voltammetric peak was seen on modified oxidised (hydrophilic) BDD, signifying greater interaction between copper phthalocyanine and the hydrogen-terminated BDD. Oxygen reduction was found to undergo a two-electron process on the modified hydrogen-terminated BDD, which was shown to be also active for the reduction of hydrogen peroxide. The lack of a further conversion of the peroxide was attributed to its rapid diffusion away from the triple phase boundary at which the reaction is expected to exclusively occur. The work presented in this chapter has been accepted for publication in *Chemistry Open*.

4.1 Introduction

Chemical vapour deposited boron-doped diamond [1,2] possesses some excellent electrochemical properties as already described in the previous chapters, which makes it an attractive carbon material for use in electrode reactions. As-grown thin film boron-doped diamond is largely hydrogen terminated and the “alkanelike” surface is thus hydrophobic [3,4]. Upon treatments such as anodic polarisation [3,5-7], potential cycling [8,9] and oxygen plasma [4], oxygen-containing groups can be introduced onto the BDD surface, consequently rendering it hydrophilic. The surface-chemical composition can therefore be altered to influence properties such as hydrophobicity and the electron transfer kinetics [4,10].

To impart additional functionality to the BDD, the surface of the substrate can be modified with electrocatalytic materials. The common approaches towards the attachment of such materials onto BDD electrodes include electrochemical deposition [11-15], photochemical reaction [16-20], electropolymerisation [21-23] and ion implantation [24,25]. These typically involve at least some level of instrumentation or covalent linkage.

The use of the relatively simple technique of dropcasting a coating onto BDD is rather limited however, but some examples from the literature are listed in **Table 4.1** [26-32]. These modifiers are predominantly particulate in nature. The limited use of such physical immobilisation is likely due to the general notion of BDD having greater chemical inertness relative to common carbon electrodes. Nevertheless, a few recent reports on BDD have described the observation of adsorptive behaviour of molecular compounds such as quinizarin [33], methyl viologen [34,35] and

anthraquinonedisulfonate [35] from solution. Therefore in this chapter the attachment of molecular modifiers in the form of microcrystals on BDD is explored using copper phthalocyanine (**Figure 4.1**) as an exemplar.

Table 4.1 Some examples of modification of boron-doped diamond (BDD) via dropcasting.

Modification method	**Modifier**	**BDD surface**	**Ref**
Dropcast	Pt/Sn nanoparticles	O-BDD [a]	[26]
Dropcast	Pt nanoparticles	O-BDD	[27]
Dropcast, calcination	IrO_2 nanoparticles	O-BDD	[27]
Dropcast	Nafion	-	[28]
Dropcast	Carbon black	O-BDD	[29]
Dropcast	Au/TiO_2 nanorod composites.	H-BDD [b]	[30]
Dropcast (with EDC)[c]	Heme undecapeptide; Horseradish peroxidase	O-BDD, H-BDD	[31]
Dropcast (with Nafion)	Pt–RuO_2/C composite	H-BDD	[32]

[a]O-BDD: oxygen-terminated BDD
[b]H-BDD: hydrogen-terminated BDD
[c]EDC: 1-ethyl-3-(3-dimethylaminopropyl)carbodiimide

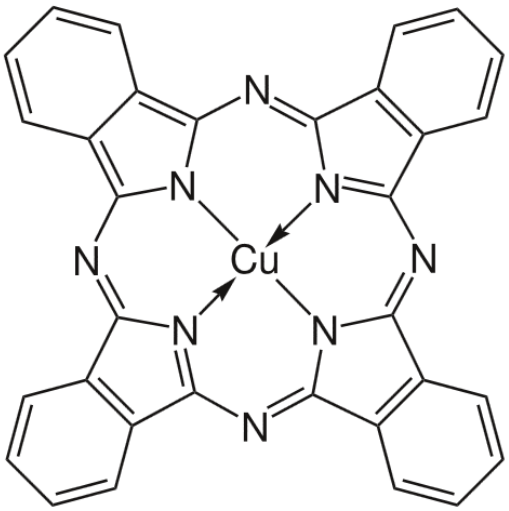

Figure 4.1 Chemical structure of copper phthalocyanine.

There have been only a few reports of the modification of BDD film electrodes with metallophthalocyanines. These were performed by vacuum deposition [36,37] or after photochemical modification with 4-vinylpyridine [38]. It is demonstrated in this work that a simple dropcast method can be effective for the immobilisation of metallophthalocyanine onto BDD as well. In particular, the influence of two different commonly used surface terminations, namely hydrogen and oxygen, on the interaction of metallophthalocyanine with BDD is compared. Moreover, it will be shown that the dropcasting leads to a random “array” of microcrystals of copper phthalocyanine on the BDD surface.

Metallophthalocyanines are well known as catalysts for homogeneous and heterogeneous chemical reactions [39-41], amongst which is the capability to lower the overpotential for the oxygen reduction reaction [42-46], hence this process is chosen to examine the metallophthalocyanine-BDD system in this work. Moreover the reduction of oxygen is of considerable technological importance for instance in the development of fuel cells [47,48]. In respect of oxygen reduction, BDD is especially useful for studying cathodic reactions without interference from water electrolysis owing to its large overpotential for hydrogen evolution [49,50] and its outstanding stability under reductive conditions.

4.2 Experimental

4.2.1 Chemicals and Materials

Copper(II) phthalocyanine (dye content >99%, Aldrich), acetonitrile (>99.7%, Rathburn), hydrogen peroxide (35wt%, Alfa Aesar), potassium dihydrogen phosphate (≥99.0%, Sigma Aldrich) and potassium hydrogen phosphate trihydrate (≥99.0%,

Sigma Aldrich) were used as received. All aqueous solutions were prepared using ultra pure water (~18.2 MΩ cm at 25°C). Oxygen and nitrogen were obtained from BOC gases. Gases were bubbled through for at least 15 minutes to saturate the solution and a nitrogen or oxygen atmosphere was kept over the solution during the experiment.

4.2.2 Apparatus

The set-up for the electrochemical experiments has been previously presented in Chapter 2. Surface morphology of the modified BDD electrodes was characterised by a Hitachi 520 SEM operating at an accelerating voltage of 20 kV.

4.2.3 Electrode Preparation

Hydrogen-terminated and oxidised (oxygen-terminated) boron-doped polycrystalline diamond was prepared and used as the working electrode as described in the experimental section of the previous chapter.

To modify the BDD electrode, 50 µL of copper phthalocyanine (1 mg in 1 mL acetonitrile) was pipetted onto the electrode surface in aliquots of 2-3 µL and allowed to dry in air between aliquots. This volume was found to give maximal voltammetric response, indicating the optimal coverage of the electrode. At least three “blank” voltammograms were run in oxygen saturated phosphate buffer solution pH 7 to equilibrate each freshly prepared electrode before further experiments were conducted. The electrode-to-electrode response was generally reproducible and stable at least over the length of the experiments. Modified electrodes were sonicated in acetone to remove the attached phthalocyanine.

4.3 Results and Discussion

In this section, oxygen reduction is first investigated at unmodified BDD electrodes to provide a starting point for studying the reaction. Next the cathodic process is examined at copper phthalocyanine modified BDD to compare the effects of differing surface terminations. Included is also a study of the behaviour of the modified hydrogen-terminated BDD towards the reduction of hydrogen peroxide.

4.3.1 Oxygen Reduction at Unmodified BDD Electrode

The electrochemical reduction of oxygen in aqueous solutions can proceed by the following two general pathways: either a direct four-electron route or a two-electron hydrogen peroxide mechanism [51-53]. Both pathways are described below for neutral conditions at pH 7.

Direct 4-electron pathway

$$O_2 + 2\ H_2O + 4e^- \rightleftharpoons 4\ OH^- \qquad (4.1)$$

Peroxide pathway

$$O_2 + 2\ H_2O + 2\ e^- \rightleftharpoons H_2O_2 + 2\ OH^- \qquad (4.2)$$

$$H_2O_2 + 2\ e^- \rightleftharpoons 2\ OH^- \qquad (4.3)$$

The direct 4-electron process is expected to exhibit a single voltammetric wave. For the peroxide route, there are two possibilities: (a) the potentials for the sequential electron transfers could be well separated, resulting in two distinct voltammetric waves or (b)

the reduction of peroxide could occur at or near the oxygen reduction potential, leading to a single voltammetric wave.

Cyclic voltammetry was first carried out on the unmodified boron-doped diamond with surface terminations of hydrogen and oxygen, in both O_2 and N_2 saturated phosphate buffer solution (PBS) at pH 7, to provide a basis for understanding the oxygen reduction at these electrodes. The cyclic voltammograms obtained are shown in **Figure 4.2**. In the N_2 saturated solution, both the hydrogen- and oxygen-terminated BDD gave very little response. However, in the O_2 saturated solution, the two types of surfaces gave rise to very different response. At the O-terminated surface there was no apparent peak whereas at the H-terminated surface, a large and irreversible voltammetric peak was observed with a peak potential at −1.09 V (vs Ag/AgCl), which can be attributed to

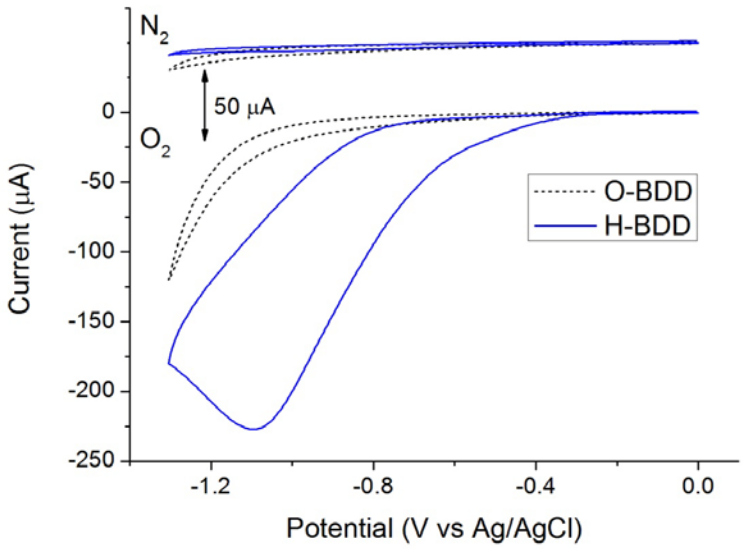

Figure 4.2 Cyclic voltammograms for hydrogen-terminated (H-BDD, solid line) and oxygen-terminated (O-BDD, dashed line) boron-doped diamond electrodes in N_2-saturated (above) and O_2-saturated (below) 0.1 M phosphate buffer pH 7. Scan rate: 100 mV s^{-1}. The potential was swept in a negative direction from 0 V.

the irreversible reduction of oxygen to hydrogen peroxide [54], as given by equation (4.2). The two-electron reduction of oxygen on the H-terminated BDD is typical of the peroxide pathway commonly seen on carbon electrodes [52,55].

The standard potential for the two-electron reduction of oxygen is +0.281 V (SHE) at pH 7 and the large overpotential on the H-terminated surface is consistent with the work of Yano et al [54] which found the oxygen reduction to be highly inhibited on as-grown BDD. This was attributed to a lack of adsorption sites for oxygen and/or reduced intermediates, a low density of states or a potential drop within a thin (~2 nm) surface layer.

As the reduction of oxygen involves the addition of hydrogen and the cathodic reaction is only observed on the H-terminated surface but not the O-terminated surface, there exists the possibility of the surface hydrogen providing the stoichiometric source. The surface density of carbon bonds on diamond and hence the maximum coverage of H is $\sim 10^{15}/cm^2$. Assuming an electron transfer for each H reacted, the charge required to exhaust the surface H in this case is $\sim 7\times10^{-5}$ C. The charge passed on the cathodic sweep for the H-terminated surface in O_2 saturated solution is 1.1×10^{-4} C therefore a single scan should exhaust the surface H if it is reacting.

Consecutive cyclic voltammetric scans were thus carried out and the voltammograms are shown in **Figure 4.3**. The second scan showed a reduction in the peak current, which can be attributed to the slow removal of reaction products from the reaction sites. After the solution was stirred by bubbling with oxygen, the subsequent voltammogram

showed a restoration of the peak current to that of the initial value. This confirms that the H-terminated BDD is indeed electrocatalytic compared to the O-terminated surface.

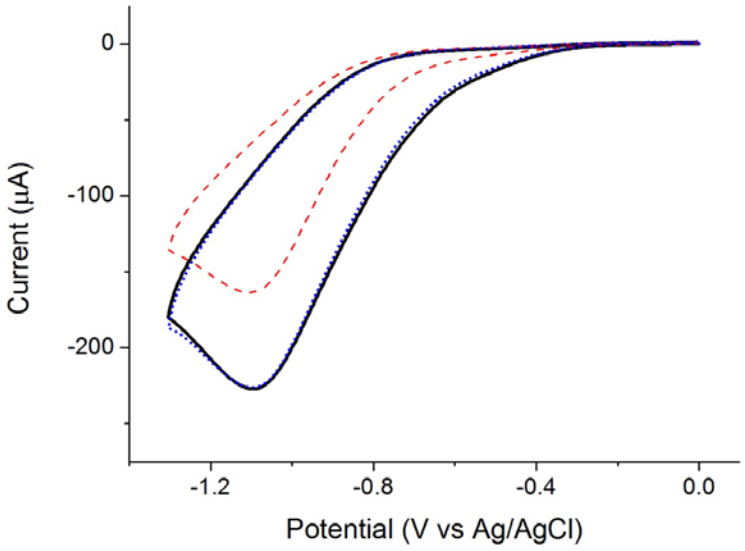

Figure 4.3 Cyclic voltammograms for H-terminated BDD electrode in O_2-saturated 0.1 M phosphate buffer pH 7 showing initial scan (solid line), second scan (dashed line) and subsequent scan after stirring (dotted line). Scan rate: 100 mV s^{-1}.

The voltammetric responses for oxygen reduction at the unmodified H-terminated BDD over a range of scan rates are shown in **Figure 4.4**. The inset depicts the linear variation of the peak current with the square root of the scan rate, indicating a mass transfer controlled reaction. The peak current for the transport limited *n*-electron transfer irreversible reaction is described in equation (4.4):

$$i_p = -0.496\sqrt{(n' + \alpha_{n'})}nFA[O_2]\sqrt{\frac{F\nu D}{RT}} \qquad (4.4)$$

where i_p is the peak current, n' is the number of electron transferred before the rate limiting step, $\alpha_{n'}$ is the electron transfer coefficient of the rate determining step, F is the

Faraday constant, *A* is the electrode area, $[O_2]$ is the oxygen concentration, υ is the scan rate, D is the diffusion coefficient, R is the gas constant and *T* is the absolute temperature.

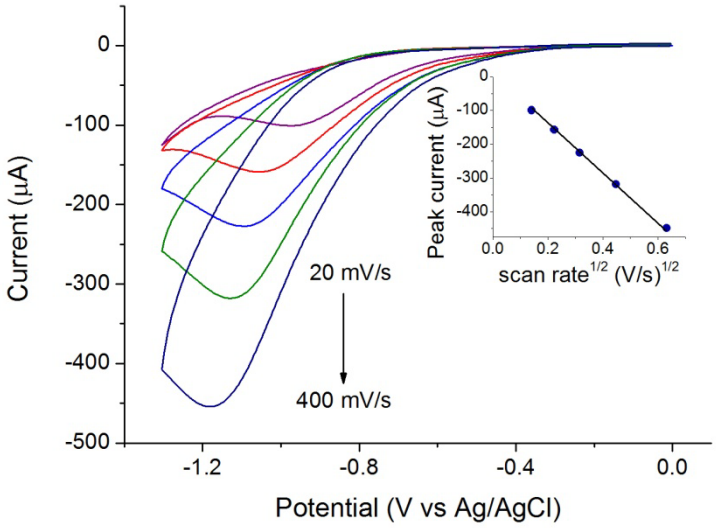

Figure 4.4 Cyclic voltammograms for H-terminated BDD in O_2-saturated 0.1 M phosphate buffer pH 7 at scan rates from 20 to 400 mV s^{-1}. Inset: Plot of peak current against square root of scan rate.

Tafel plots were derived from the descending section of the voltammetric peak corresponding to charge transfer control and these are shown in **Figure 4.5** for scan rates from 50 to 200 mV s^{-1}. From the gradients of the plots, an average value for $(\boldsymbol{n}' + \boldsymbol{\alpha}_{\boldsymbol{n}'})$ of 0.34 was obtained. The concentration of oxygen in a saturated solution is 1.3 mM [56] and the diffusion coefficient for oxygen is 2.1×10^{-5} cm^2 s^{-1} [57]. Using these values and the gradient of the best-fit line from the inset in **Figure 4.4**, the number of electrons transferred is calculated from equation (4.4) to be around 2, indicating the reduction of O_2 to H_2O_2, in agreement with the two-electron reduction of oxygen from rotating disk electrode measurements [54].

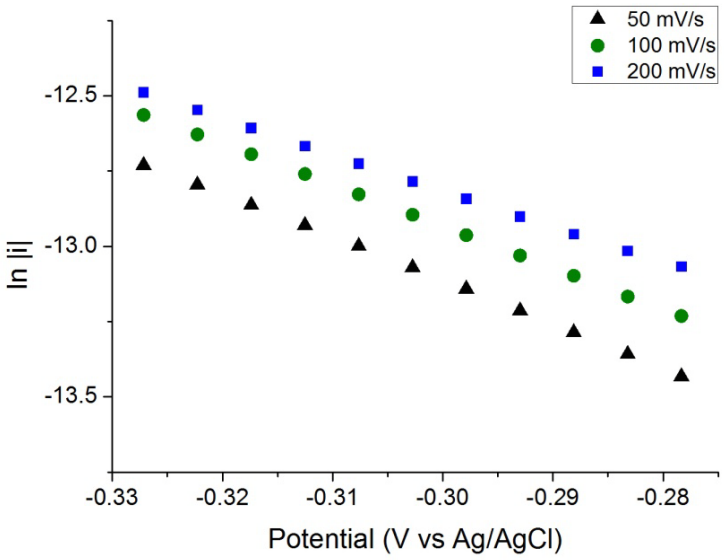

Figure 4.5 Tafel plots of cathodic current for H-terminated BDD in O_2-saturated 0.1 M phosphate buffer pH 7 at scan rates from 50 to 200 mV s^{-1}.

4.3.2 Effect of Surface Termination on the Interaction of Copper Phthalocyanine with BDD towards Oxygen Reduction

A simple dropcast technique was used to immobilise copper phthalocyanine onto the BDD electrode as described in the experimental section and the surface morphology of the modified H- and O-terminated electrodes were characterised by scanning electron microscopy (SEM). As revealed by the SEM micrographs in **Figure 4.6**, the structure of the modified electrodes both consisted of microcrystalline deposits of varying sizes up to ca 7 μm in length across the BDD surface.

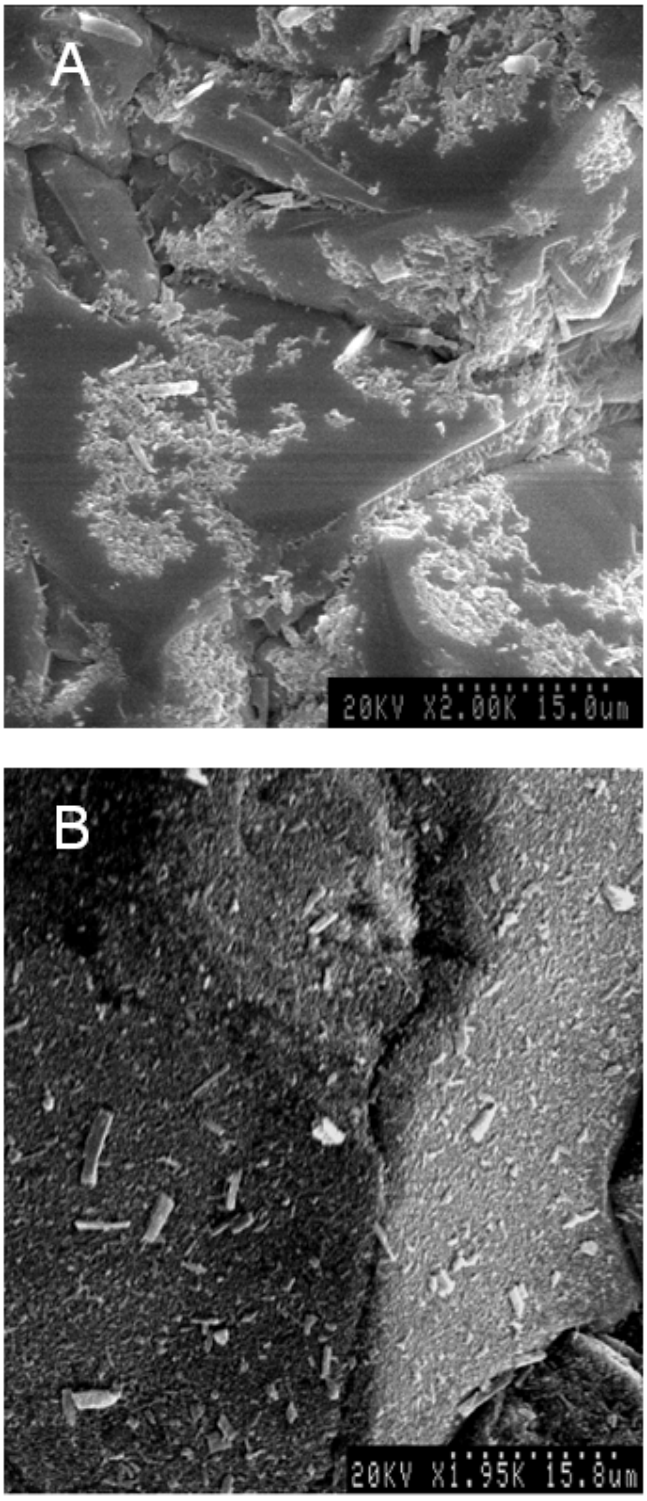

Figure 4.6 SEM micrographs of copper phthalocyanine modified (a) H-terminated, (b) O-terminated BDD.

The cyclic voltammograms on the modified H-terminated surface in both O_2- and N_2-saturated phosphate buffer solutions are shown in **Figure 4.7**. While the curve obtained in the N_2-saturated solution is relatively featureless, a large and irreversible cathodic peak was observed at−0.58 V (vs Ag/AgCl) in the O $_2$-saturated solution attributed to the reduction of oxygen. This represents a significant decrease in overpotential of over 500 mV compared to the unmodified H-terminated electrode and demonstrates the substantial electrocatalytic effect as a result of copper phthalocyanine modification. The behaviour for the modified O-terminated BDD is very different however, as shown in **Figure 4.8**. No apparent peak was observed for the voltammetric response in O_2-saturated solution.

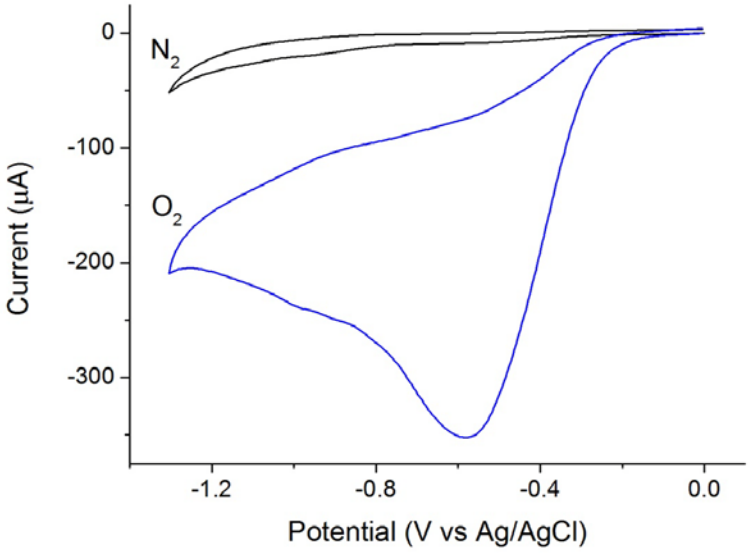

Figure 4.7 Cyclic voltammograms for copper phthalocyanine modified H-terminated BDD in N_2-saturated (above) and O_2-saturated (below) 0.1 M phosphate buffer pH 7. Scan rate: 100 mV s^{-1}.

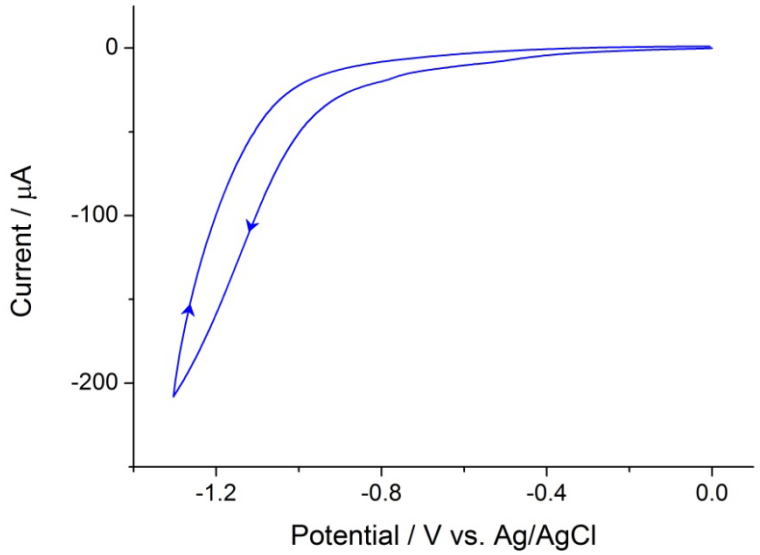

Figure 4.8 Cyclic voltammogram for copper phthalocyanine modified O-terminated BDD in O_2-saturated 0.1 M phosphate buffer pH 7. Scan rate: 100 mV s^{-1}.

Based on the results above, it is clear that the surface chemical termination has an effect on the interaction between copper phthalocyanine and BDD. Only on the H-terminated surface is there significant interaction with the metallophthalocyanine based on the observation of its positive impact on the electrocatalysis of oxygen reduction. This is likely due to the hydrophobic interaction between copper phthalocyanine and the (hydrophobic) H-terminated surface [34]. As for the oxidised BDD electrode, the hydrophilic surface is expected to have much weaker interaction with the nonpolar compound. From the absence of a voltammetric peak in an O_2-saturated solution, it can be inferred that the electrical connection of copper phthalocyanine microcrystallites to the O-terminated BDD is therefore inferior to the case of the H-termination.

Figure 4.9a displays the voltammetric data obtained at scan rates from 10 to 400 mV s^{-1} and the linear dependence of the peak current on the square root of the scan rate is

shown in **Figure 4.9**b, indicating the reduction of oxygen on the modified surface is a diffusion controlled process at the modified H-terminated surface.

(a)

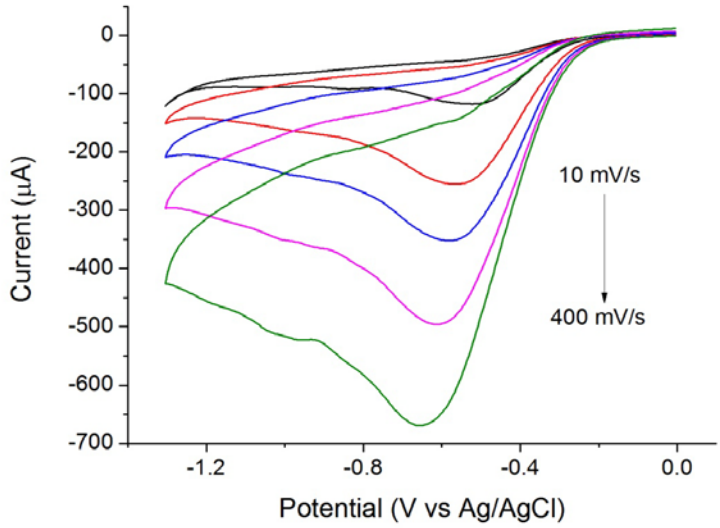

(b)

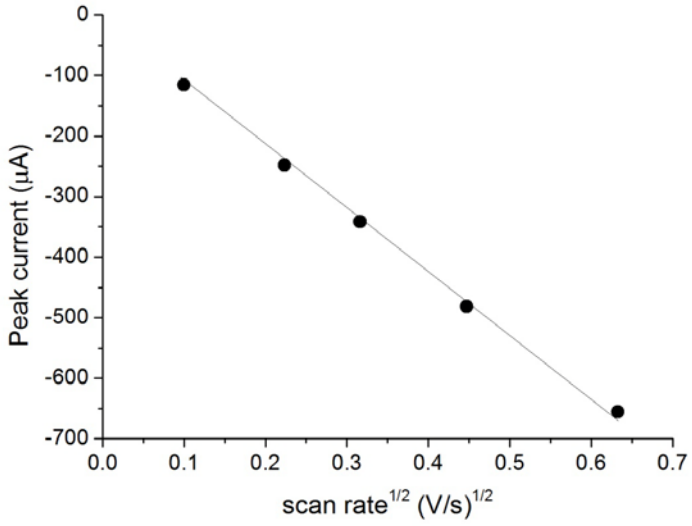

Figure 4.9 (a) Cyclic voltammograms for copper phthalocyanine modified H-terminated BDD in O_2-saturated 0.1 M phosphate buffer pH 7 at scan rates from 10 to 400 mV s^{-1}. (b) Plot of peak current against square root of scan rate.

Tafel analyses on the above data are shown in **Figure 4.10** and an average value for $(n' + \alpha_{n'})$ of 0.46 was derived from the gradients of the plots. Using the values of oxygen concentration in a saturated solution and the diffusion coefficient as quoted earlier, together with the gradient of the linear plot in **Figure 4.9**b, the number of electrons transferred is calculated using equation (4.4) to be 2, consistent with the reduction of O_2 to H_2O_2.

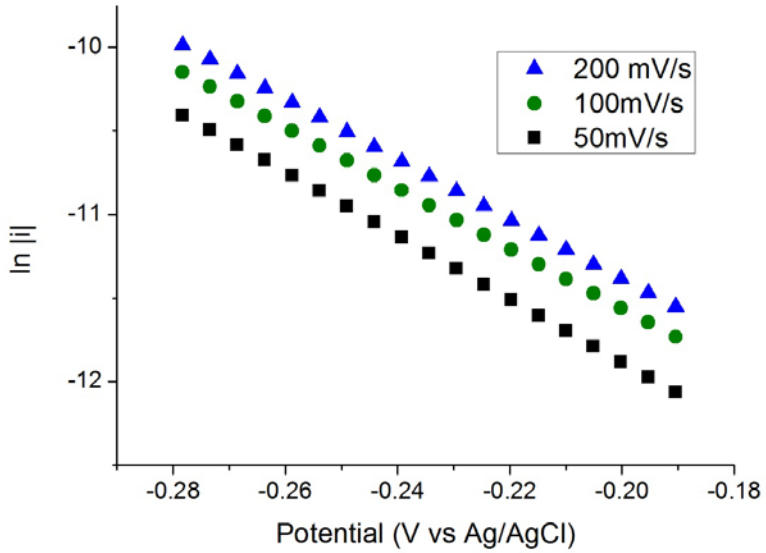

Figure 4.10 Tafel plots of cathodic current for copper phthalocyanine modified H-terminated BDD in O_2-saturated 0.1 M phosphate buffer pH 7 at scan rates from 50 to 200 mV s^{-1}.

4.3.3 Reduction of Hydrogen Peroxide at the Modified H-Terminated BDD

From the results above, the copper phthalocyanine modified H-terminated BDD exhibits a two-electron reduction in oxygen-saturated solution. It has been reported that oxygen can undergo a four-electron reduction at certain metallophthalocyanines [44-46]. Therefore the possibility of the electrochemical reduction of the hydrogen peroxide on the modified BDD surface was further investigated.

The unmodified H-terminated BDD surface was examined by cyclic voltammetry in a nitrogen-saturated solution and the measurement was featureless for the reduction of hydrogen peroxide. Standard addition of hydrogen peroxide was then conducted on the copper phthalocyanine modified H-terminated BDD in a N_2-saturated phosphate buffer solution to study the reaction without contribution from dioxygen. **Figure 4.11**a shows the cyclic voltammograms of hydrogen peroxide for concentrations of 0.0 to 2.0 mM, with a peak potential of−0.57 V (vs Ag/AgCl) at 0.1 mM. The magnitude of the peak current increases linearly with the hydrogen peroxide concentration, as shown in **Figure 4.11**b and the gradient of the calibration plot is -121.4 μA mM^{-1}.

Tafel analyses on the descending portion of the voltammetric curve yielded an average value of α to be 0.30. Together with the gradient of the calibration plot and the diffusion coefficient of hydrogen peroxide (8.3×10^{-6} cm^2 s^{-1}) [58], the number of electrons per molecule transferred can be calculated using equation (4.4), giving a value close to 2. This indicates that the reaction as described by equation (4.3) is taking place at the copper phthalocyanine modified H-terminated BDD.

The cathodic peak potential for the reduction of hydrogen peroxide is very similar to that for the reduction of oxygen and the reactions of both compounds have been demonstrated on the modified H-terminated BDD as above. Therefore this suggests that the reduction of oxygen should in principle be able to undergo an overall four-electron reaction via the stepwise mechanism with hydrogen peroxide as the intermediate, as described earlier. However it is clear that oxygen reduction progresses according to equation (4.2) with no further electrochemical reduction of hydrogen peroxide.

(a)

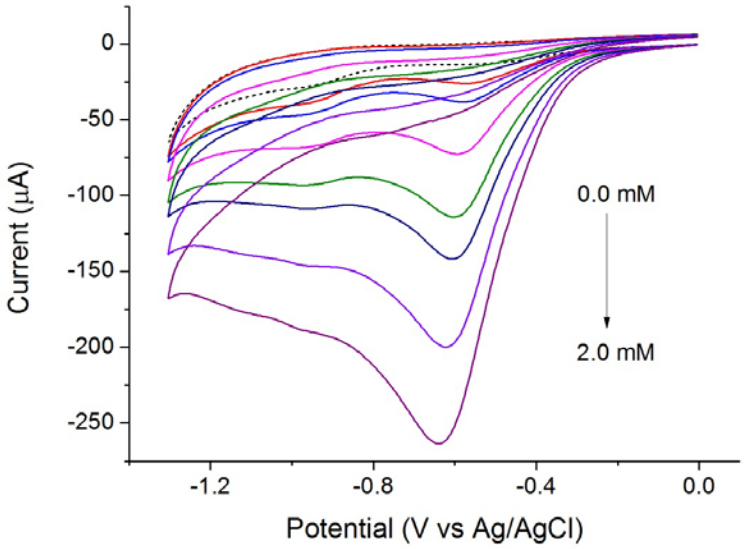

(b)

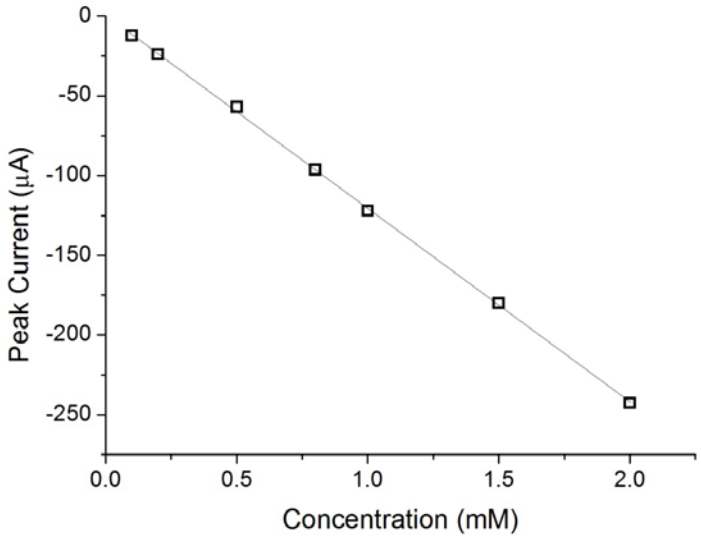

Figure 4.11 (a) Cyclic voltammograms for copper phthalocyanine modified H-terminated BDD in N_2-saturated 0.1 M phosphate buffer pH 7 containing 0.0 to 2.0 mM H_2O_2 (dashed line: 0.0 mM). Scan rate: 100 mV s^{-1}. (b) Plot of peak current against concentration of H_2O_2.

The key to this apparent conundrum likely lies in the structure of the surface deposition. As illustrated in **Figure 4.12**, the dropcast modification of molecular compounds could result in the formation of a continuous film or an array of microcrystallites on the electrode surface. In the former case, hydrogen peroxide is expected to further react via equation (4.3). However, the results above are suggestive of the case for the microcrystalline array, in which the charge transfer is thought to occur at the triple-phase boundary formed between the copper phthalocyanine microcrystallite, the boron-doped diamond, and the aqueous solution [59-63]. At the junction of contact of the three phases, the catalyst, electrons and reactants are all present in adequate proximity for reaction to occur.

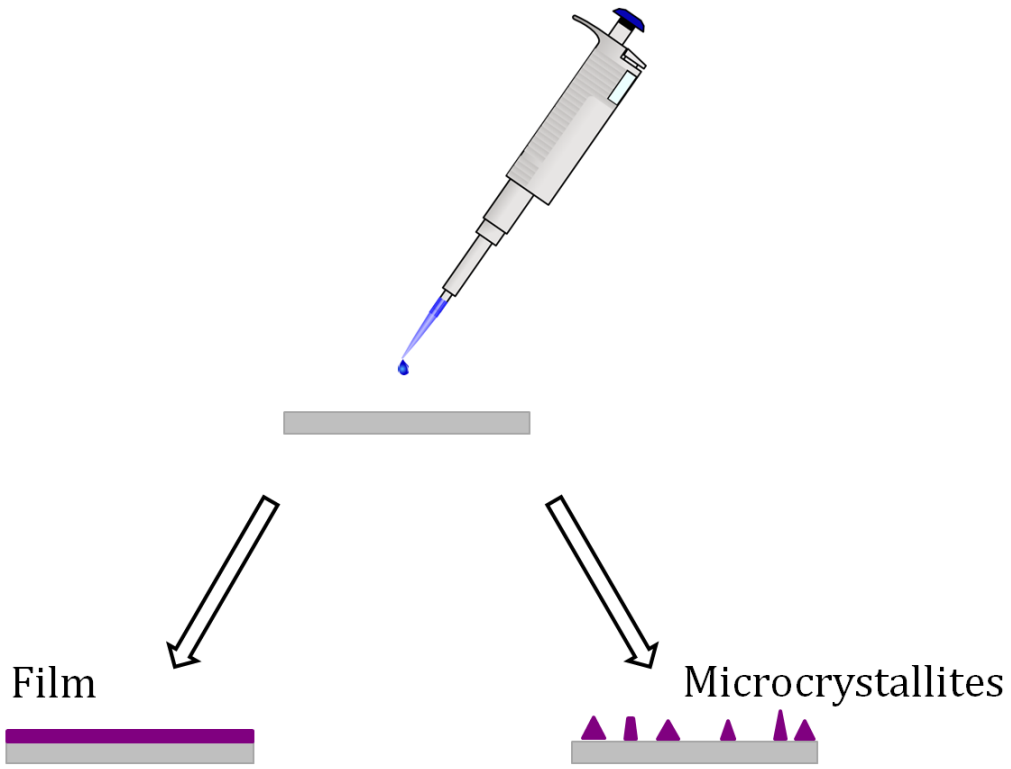

Figure 4.12 Schematic diagram of the possible surface formation via dropcast modification.

The fact that the reduction of oxygen is an overall two-electron process probably has to do with the microcrystallites behaving in effect as a random array of “microelectrodes” (**Figure 4.13**), allowing the hydrogen peroxide formed in this instance to diffuse radially into the bulk phase at a rapid rate before it can undergo further conversion according to equation (4.3). Indeed the presence of microcrystallites on the modified BDD surface has been evidenced earlier by SEM in **Figure 4.6** and this supports the inference of a triple boundary process. The consideration of the behaviour of the microcrystallites as an array of “microelectrodes” is dependent upon the sizes of the microcrystallites as well as the spacing between them, as these parameters have a bearing on the mass transport properties at the array [64].

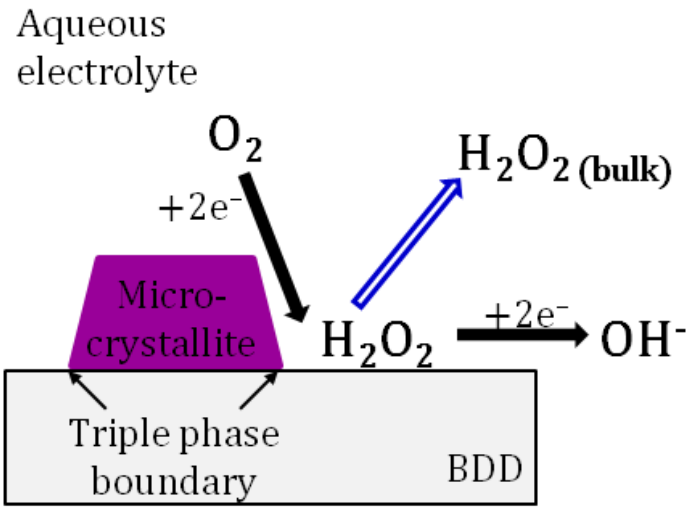

Figure 4.13 Schematic diagram showing possible outcomes of hydrogen peroxide during oxygen reduction at the triple phase boundary.

An alternative hypothesis for the cathodic signal in **Figure 4.11** could be that it arises from the oxygen resulting from the catalytic disproportionation of hydrogen peroxide in the presence of copper phthalocyanine as given in equation (4.5).

$$2\ H_2O_2 \longrightarrow O_2 + 2\ H_2O \qquad (4.5)$$

If the catalytic disproportionation is rapid, a voltammetric scan obtained after nitrogen has been passed through the solution to remove the generated oxygen should show a much diminished cathodic current. Another method would be to perform the experiment in the presence of excess sodium bisulfite which readily reacts with the generated oxygen thereby eliminating any contribution to the cathodic current from oxygen reduction.

However given that the transfer coefficient found for hydrogen peroxide reduction (α = 0.30) is different from that owing to oxygen reduction (α = 0.46) on the modified hydrogen-terminated electrode, this is suggestive of a distinct cathodic process occurring, rather than the reduction of oxygen from the disproportionation of hydrogen peroxide.

4.4 Conclusions

The dropcast coating of boron-doped diamond electrodes has been studied as a facile method for the surface modification of BDD with molecular materials. The electrochemical behaviour of unmodified and copper phthalocyanine modified BDD electrodes was examined via the reduction of oxygen, a reaction known to be catalysed by metallophthalocyanines. Such physical immobilisation was found to be sensitive to the BDD surface termination. Hydrogenated BDD modified in such a manner was able to significantly decrease the overpotential for the cathodic reaction by ca 500 mV when compared to the unmodified electrode. Oxidised BDD however displayed no such electrocatalysis even after modification by the copper macrocycle. These effects may be attributable to the greater interaction between the nonpolar molecular modifier and the "alkanelike" hydrogen terminated surface, through forces such as hydrophobic interactions.

On the modified H-terminated BDD, the electrochemical reduction of oxygen occurred through a diffusion control two-electron cathodic process via the peroxide pathway. In addition, the modified electrode showed activity for the electrochemical reduction of hydrogen peroxide at similar potentials as well. The role of microcrystallites is proposed to lead to the curtailment of the oxygen reduction at the peroxide stage due to the rapid diffusion of the reaction product away from the triple phase boundary at where the reaction is thought to occur. SEM characterisation of the surface morphology confirmed the presence of microcrystallites on the modified H-terminated BDD.

References

[1] Y. Einaga, J.S. Foord, G.M. Swain, MRS Bulletin 39 (2014) 525.

[2] H. Dong, S. Wang, J.J. Galligan, G.M. Swain, Front. Biosci. (Scholar edition) 3 (2011) 518.

[3] H. Notsu, I. Yagi, T. Tatsuma, D.A. Tryk, A. Fujishima, Electrochem. Solid-State Lett. 2 (1999) 522.

[4] I. Yagi, H. Notsu, T. Kondo, D.A. Tryk, A. Fujishima, J. Electroanal. Chem. 473 (1999) 173.

[5] E. Popa, H. Notsu, T. Miwa, D.A. Tryk, A. Fujishima, Electrochem. Solid-State Lett. 2 (1999) 49.

[6] H.B. Martin, A. Argoitia, U. Landau, A.B. Anderson, J.C. Angus, J. Electrochem. Soc. 143 (1996) L133.

[7] Q. Chen, M.C. Granger, T.E. Lister, G.M. Swain, J. Electrochem. Soc. 144 (1997) 3806.

[8] C.H. Goeting, F. Marken, A. Gutiérrez-Sosa, R.G. Compton, J.S. Foord, Diam. Relat. Mater. 9 (2000) 390.

[9] M.C. Granger, G.M. Swain, J. Electrochem. Soc. 146 (1999) 4551.

[10] I. Duo, C. Levy-Clement, A. Fujishima, C. Comninellis, J. Appl. Electrochem. 34 (2004) 935.

[11] F. Montilla, E. Morallon, I. Duo, C. Comninellis, J.L. Vazquez, Electrochim. Acta 48 (2003) 3891.

[12] J. Weng, J.M. Xue, J. Wang, J.S. Ye, H.F. Cui, F.S. Sheu, Q.Q. Zhang, Adv. Funct. Mater. 15 (2005) 639.

[13] L. Hutton, M.E. Newton, P.R. Unwin, J.V. Macpherson, Anal. Chem. 81 (2009) 1023.

[14] K.E. Toghill, L. Xiao, G.G. Wildgoose, R.G. Compton, Electroanalysis 21 (2009) 1113.

[15] X.A. Lu, J.P. Hu, J.S. Foord, Q.A. Wang, J. Electroanal. Chem. 654 (2011) 38.

[16] W.S. Yang, O. Auciello, J.E. Butler, W. Cai, J.A. Carlisle, J. Gerbi, D.M. Gruen, T. Knickerbocker, T.L. Lasseter, J.N. Russell, L.M. Smith, R.J. Hamers, Nat. Mater. 1 (2002) 253.

[17] T. Strother, T. Knickerbocker, J.N. Russell, J.E. Butler, L.M. Smith, R.J. Hamers, Langmuir 18 (2002) 968.

[18] C.E. Nebel, D.C. Shin, B. Rezek, N. Tokuda, H. Uetsuka, H. Watanabe, J. R. Soc. Interface 4 (2007) 439.

[19] Y.L. Zhou, R.H. Tian, J.F. Zhi, Biosensors & Bioelectronics 22 (2007) 822.

[20] D. Shin, B. Rezek, N. Tokuda, D. Takeuchi, H. Watanabe, T. Nakamura, T. Yamamoto, C.E. Nebel, Phys. Status Solidi A-Appl. Mat. 203 (2006) 3245.

[21] H.R. Gu, X. di Su, K.P. Loh, J. Phys. Chem. B 109 (2005) 13611.

[22] F.J. Shang, L. Zhou, K.A. Mahmoud, S. Hrapovic, Y.L. Liu, H.A. Moynihan, J.D. Glennon, J.H.T. Luong, Anal. Chem. 81 (2009) 4089.

[23] M. Wang, M.R. Das, M.S. Li, R. Boukherroub, S. Szunerits, J. Phys. Chem. C 113 (2009) 17082.

[24] T. Watanabe, T.A. Ivandini, Y. Makide, A. Fujishima, Y. Einaga, Anal. Chem. 78 (2006) 7857.

[25] T.A. Ivandini, R. Sato, Y. Makide, A. Fujishima, Y. Einaga, Anal. Chem. 78 (2006) 6291.

[26] G. Siné, G. Fóti, C. Comninellis, J. Electroanal. Chem. 595 (2006) 115.

[27] G. Siné, I. Duo, B.E. Roustom, G. Fóti, C. Comninellis, J. Appl. Electrochem. 36 (2006) 847.

[28] C.A. Martínez-Huitle, N. Suely Fernandes, S. Ferro, A. De Battisti, M.A. Quiroz, Diam. Relat. Mater. 19 (2010) 1188.

[29] P. Gan, R.G. Compton, J.S. Foord, Electroanalysis 25 (2013) 2423.

[30] M. Wei, Y. Liu, Z.-Z. Gu, Z.-D. Liu, J. Chin. Chem. Soc. 58 (2011) 516.

[31] T. Tatsuma, H. Mori, A. Fujishima, Anal. Chem. 72 (2000) 2919.

[32] H.B. Suffredini, V. Tricoli, N. Vatistas, L.A. Avaca, J. Power Sources 158 (2006) 124.

[33] I.B. Dimov, C. Batchelor-McAuley, L. Aldous, R.G. Compton, Phys. Chem. Chem. Phys. 14 (2012) 2375.

[34] J. Hees, R. Hoffmann, N. Yang, C.E. Nebel, Chem. Eur. J. 19 (2013) 11287.

[35] I. Shpilevaya, J.S. Foord, Electroanalysis 26 (2014) 2088.

[36] D.C. Qi, J.T. Sun, X.Y. Gao, L. Wang, S. Chen, K.P. Loh, A.T.S. Wee, Langmuir 26 (2010) 165.

[37] M. Szybowicz, W. Bala, K. Fabisiak, K. Paprocki, M. Drozdowski, Cryst. Res. Technol. 45 (2010) 1265.

[38] T. Kondo, A. Tamura, T. Kawai, J. Electrochem. Soc. 156 (2009) F145.

[39] N.B. MacKeown, Phthalocyanine materials : synthesis, structure and function, Cambridge Univ. Press, Cambridge, 1998.

[40] J.H. Zagal, Coord. Chem. Rev. 119 (1992) 89.

[41] J.H. Zagal, S. Griveau, J.F. Silva, T. Nyokong, F. Bedioui, Coord. Chem. Rev. 254 (2010) 2755.

[42] R. Jasinski, Nature 201 (1964) 1212.

[43] R. Jasinski, J. Electrochem. Soc. 112 (1965) 526.

[44] J. Zagal, P. Bindra, E. Yeager, J. Electrochem. Soc. 127 (1980) 1506.

[45] J. Zagal, M. Paez, A.A. Tanaka, J.R. Dossantos, C.A. Linkous, J. Electroanal. Chem. 339 (1992) 13.

[46] R. Chen, H. Li, D. Chu, G. Wang, J. Phy. Chem. C 113 (2009) 20689.

[47] H.A. Gasteiger, S.S. Kocha, B. Sompalli, F.T. Wagner, Appl. Catal. B Environ. 56 (2005) 9.

[48] Z. Chen, D. Higgins, A. Yu, L. Zhang, J. Zhang, Energ. Environ. Sci. 4 (2011) 3167.

[49] G.M. Swain, A.B. Anderson, J.C. Angus, MRS Bulletin 23 (1998) 56.

[50] J. Xu, M.C. Granger, Q. Chen, J.W. Strojek, T.E. Lister, G.M. Swain, Anal. Chem. 69 (1997) 591A.

[51] E. Yeager, Electrochim. Acta 29 (1984) 1527.

[52] B. Šljukić, C.E. Banks, R.G. Compton, J. Iranian Chem. Soc. 2 (2005) 1.

[53] C. Song, J. Zhang, in: J. Zhang (Ed.), PEM Fuel Cell Electrocatalysts and Catalyst Layers, Springer, London, 2008.

[54] T. Yano, D.A. Tryk, K. Hashimoto, A. Fujishima, J. Electrochem. Soc. 145 (1998) 1870.

[55] M.R. Tarasevich, A. Sadkowski, E. Yeager, in: B. Conway, J.M. Bockris, E. Yeager, S.M. Khan, R. White (Eds.), Comprehensive Treatise of Electrochemistry, Springer US, 1983.

[56] D.R. Lide, CRC Handbook of Chemistry and Physics, 82nd Edition, CRC Press, London, 2001.

[57] M. Gara, R.G. Compton, New J. Chem. 35 (2011) 2647.

[58] S.B. Hall, E.A. Khudaish, A.L. Hart, Electrochim. Acta 44 (1999) 2455.

[59] C.E. Banks, T.J. Davies, R.G. Evans, G. Hignett, A.J. Wain, N.S. Lawrence, J.D. Wadhawan, F. Marken, R.G. Compton, Phys. Chem. Chem. Phys. 5 (2003) 4053.

[60] U. Schröder, F. Scholz, J Solid State Electrochem. 1 (1997) 62.

[61] F. Marken, R.D. Webster, S.D. Bull, S.G. Davies, J. Electroanal. Chem. 437 (1997) 209.

[62] U. Schröder, R.G. Compton, F. Marken, S.D. Bull, S.G. Davies, S. Gilmour, J. Phy. Chem. B 105 (2001) 1344.

[63] J.D. Wadhawan, R.G. Evans, C.E. Banks, S.J. Wilkins, R.R. France, N.J. Oldham, A.J. Fairbanks, B. Wood, D.J. Walton, U. Schröder, R.G. Compton, J. Phy. Chem. B 106 (2002) 9619.

[64] T.J. Davies, R.G. Compton, J. Electroanal. Chem. 585 (2005) 63.

Chapter 5

Nanocarbon Paste Electrodes

Nanocarbon has been demonstrated in Chapter 3 to be an effective electrode modifier. This carbon material is further explored through the construction of a composite electrode in this chapter, which aims to investigate the electrochemical behaviour of carbon paste electrodes prepared using nanocarbon and paraffin oil. The practicality of the carbon paste is established by cyclic voltammetry with several well-characterised redox systems commonly used to test electrode activity. Work related to this chapter has been published in *Electroanalysis* [1].

5.1 Introduction

Carbon paste electrodes (CPEs) in which a carbon, usually graphite powder, is mixed with a pasting liquid ("binder") to form electrodes were first reported by Adams in 1958 [2]. These are very commonly used for electroanalysis, especially in aqueous solutions, since they offer a reproducible, readily renewable electrode surface. Carbon paste electrodes and their properties have been recently reviewed [3,4].

The properties of any carbon paste electrode reflect both the nature (chemical and physical) of the carbon material used, and that of the binder. A huge variety of carbon materials have been used in CPEs ranging from graphite [5,6], charcoal [7], ethyne black [8], glassy carbon powders [9,10], diamond [11], carbon foams [12] and carbon

microspheres [12]. Recently fullerenes [13] and carbon nanotubes [14-17] have extended the list.

Nanocarbon has recently been proposed as a useful electrode material which offers similar advantages to multi-walled carbon nanotubes but at close to zero cost [18]. This material is typically composed of approximately spherical carbon particles, which are often of size ~ 10 nm, commonly aggregated to form clumps of ca ten or more spheres. The particles are available commercially (for instance from Cabot Corporation) in a range of sizes.

This chapter examines the use of nanocarbon in carbon paste electrodes and in particular, makes a comparison of the voltammetric behaviour of the resulting electrodes with those made from the more usual graphite powder as well as the commonly used glassy carbon electrode. The viability of the nanocarbon CPEs is demonstrated through voltammetric measurements for a series of well defined redox systems. At the same time a note of caution is presented: the CPEs can reversibly uptake some analytes giving rise to complex double peak voltammetry.

5.2 Experimental section

5.2.1 Chemicals and Materials

Hexaaminеruthenium(III) chloride ($Ru(NH_3)_6Cl_3$, Aldrich, 98%), potassium hexacyanoferrate(II) trihydrate [$K_2Fe(CN)_6 \cdot 3H_2O$, Sigma-Aldrich, 98.5-102%], potassium hexachloroiridate(IV) (K_2IrCl_6, Sigma-Aldrich, 99.99%), ferrocenemethanol ($C_{11}H_{12}FeO$, Aldrich, 97%), potassium chloride (KCl, Sigma-Aldrich), nanocarbon (diameter 27 ± 10 nm, Monarch 430®, Cabot Corporation), graphite powder (d < 20 μm,

Aldrich, synthetic) and paraffin oil (puriss, Sigma-Aldrich) were used as received without further purification. Prior to experiments, $Ru(NH_3)_6Cl_3$ (RuHex) solutions were purged through nitrogen (N_2, BOC, Surrey) to remove oxygen from the system.

5.2.2 Apparatus

The working electrode in the three electrode arrangement is either a carbon paste electrode or a glassy carbon electrode. Glassy carbon electrodes were polished on soft lapping pads (Kemet Ltd., UK) using alumina powder (Buehler, IL) of sizes 1.0, 0.3 and 0.05 μm, thoroughly rinsed with ultrapure water between each step, then sonicated with ultrapure water and finally left to dry in air. The surface morphology of nano-carbon was characterised by field-emission scanning electron microscopy (SEM, LEO Gemini 1530, Zeiss), using an in-lens detector and a beam voltage of 5 kV. The carbon powder was immobilized on a SEM sample holder using adhesive carbon tape. To reduce electrical charging during the measurement, a thin layer of gold was sputtered (Cressington sputter coater 108 auto) on top of the sample. The SEM sample preparation and procedure were kindly assisted by Dr K. Tschulik.

5.2.3 Preparation of carbon paste electrodes

The carbon paste was prepared by thorough hand pasting of 60% (w/w) of the nanocarbon or graphite, with paraffin oil using a pestle and mortar. The resulting pastes were packed into the well (diameter 3.0 mm) of the working electrode to a depth of 1 mm as depicted in **Figure 5.1**. The body of the working electrode was a Teflon tube tightly packed with the carbon paste and electrical contact was provided by a copper wire. The surface exposed to the solution was polished on a weighing paper to give a smooth finish before use. The pastes were kept at room temperature until used.

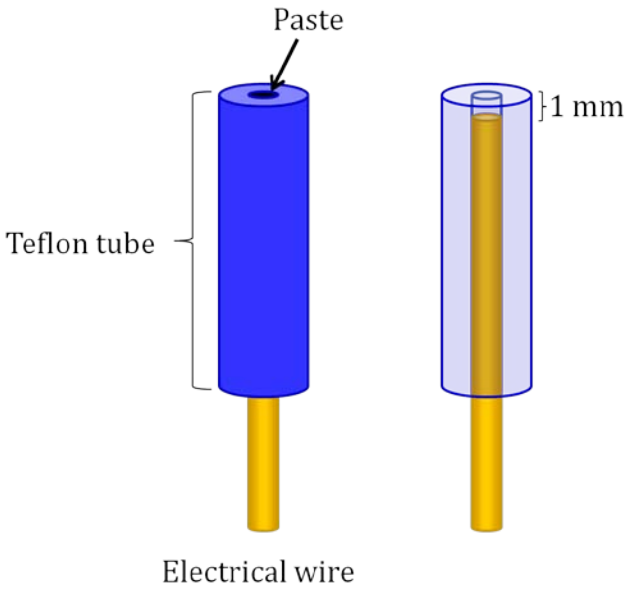

Figure 5.1 Schematic diagram of a carbon paste electrode.

5.3 Results and discussion

The nanocarbon material was first observed using scanning electron microscopy. To test the reactivity of the nanocarbon paste electrode, a series of electrochemical characterisations was conducted using several well-defined redox systems. $Ru(NH_3)_6^{3+/2+}$ represents a positively charged redox mediator couple while $Fe(CN)_6^{4-/3-}$ and $IrCl_6^{3-/2-}$ serve as the anionic analogues. The couple $FcCH_2OH^{+/0}$ was included as a neutral redox probe for study.

5.3.1 Surface characterisation of nanocarbon

The surface morphology of the commercial nanocarbon particles was characterised by scanning electron microscopy (SEM) and the SEM images obtained are shown in **Figure 5.2**. It can be seen that the commercial nano-carbon powder is composed of

spherical carbon particles presenting no topographical features, with diameters ranging from 25 to 37 nm, aggregated to form clumps of spheres.

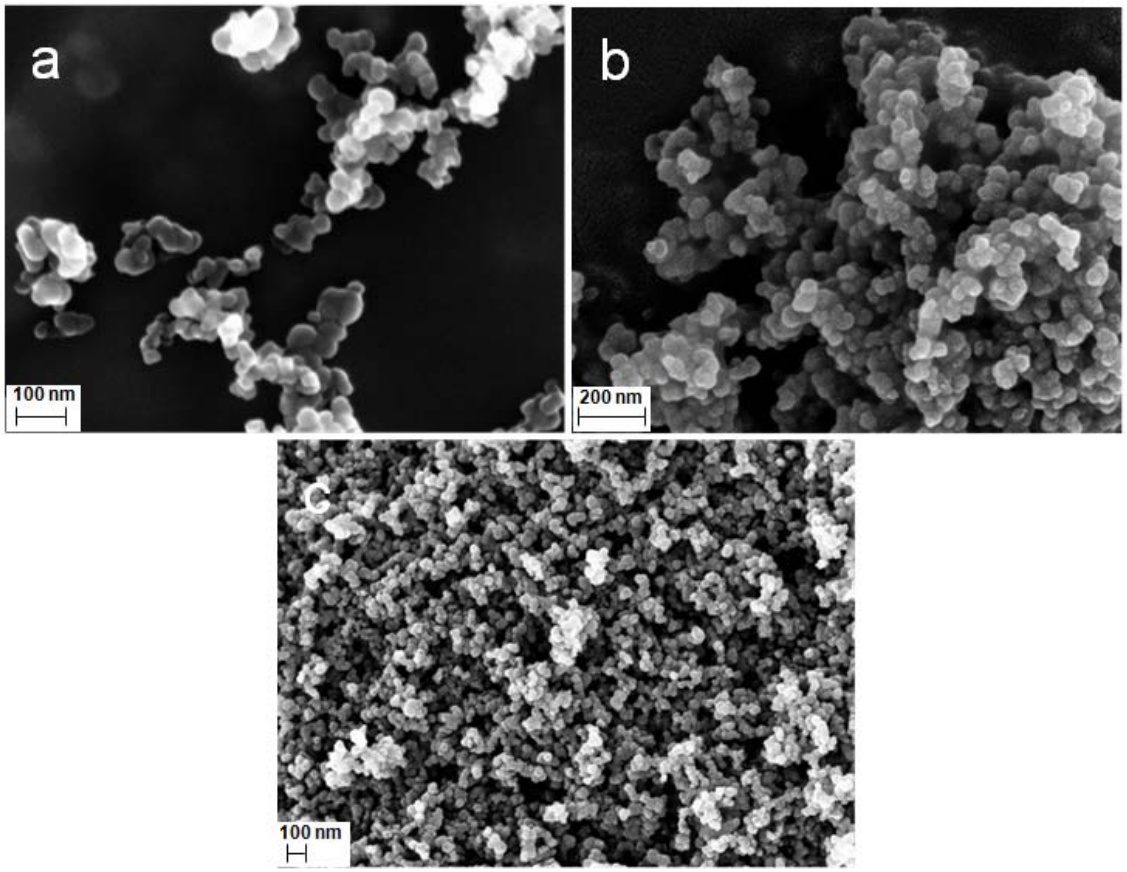

Figure 5.2 (a) High, (b) intermediate and (c) low magnification SEM images of the commercial nano-carbon particles.

Studies of nanocarbon using X-ray photoelectron spectroscopy showed the surface to be predominantly carbon with the presence of a small amount (1.6%) of surface oxygen [19], which is introduced during and after the production process [20] and include functionalities such as carboxylic acids and phenols [21].

5.3.2 Electrochemical characterisation: $Ru(NH_3)_6^{3+/2+}$

The carbon paste electrodes were prepared by mixing nanocarbon or graphite powder with paraffin oil. These were first characterised by cyclic voltammetry using $Ru(NH_3)_6Cl_3$ in aqueous 0.1 M KCl solution, which is a typical redox system often used to test electrode behaviour [22], at a scan rate 100 mV s^{-1}. The commonly used glassy carbon electrode was also included for comparison.

As shown in **Figure 5.3**, the current-potential curve of the nanocarbon paste electrode appears almost identical to that of the graphite version, indicating very similar behaviour towards the redox system:

$$Ru(NH_3)_6^{3+} + e^- \rightleftharpoons Ru(NH_3)_6^{2+}$$

which has been well-studied [23,24]. $Ru(NH_3)_6^{3+/2+}$ is typically considered to be an outer sphere electron transfer redox system with rapid kinetics and is generally insensitive to the electrode surface functionalities and impurities [25,26]. It can also be seen that the background current displayed by both electrodes is lower than that of the glassy carbon electrode, which means that the nanocarbon CPE retains the beneficial feature of low capacitance characteristic of CPEs.

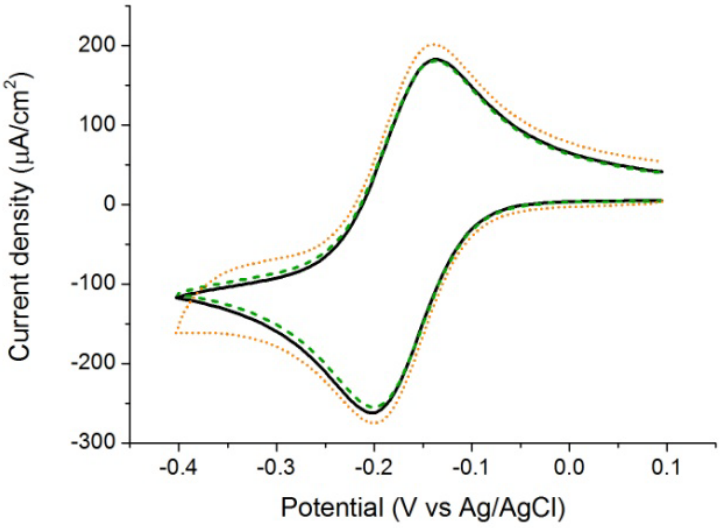

Figure 5.3 Cyclic voltammograms of 1.0 mM $Ru(NH_3)_6Cl_3$ in KCl solution at nanocarbon paste (solid line), graphite paste (dashed line) and glassy carbon electrodes (dotted line). Scan rate: 100 mV s^{-1}.

From the voltammograms, the formal potential, $\Delta E^{0'}$, was obtained as the midpoint of the anodic and cathodic peak potentials while the peak-peak potential separation, ΔE_p, was calculated as the difference between the pair of peak potentials. These values as well as the ratio of the anodic peak current density, $i_{p,a}$, to cathodic peak current density, $i_{p,c}$, are summarised in **Table 5.1**.

Table 5.1 Cyclic voltammetric data for $Ru(NH_3)_6^{3+/2+}$ at 100 mV s^{-1} for different electrodes

Electrode	**$E^{0'}$/V**	**ΔE_p/mV**	**$i_{p,a}/i_{p,c}$**
nano-carbon CPE	−0.17	64	0.92
graphite CPE	−0.17	59	0.91
glassy carbon	−0.17	59	0.89

The formal potentials for the $Ru(NH_3)_6^{3+/2+}$ system in the presence of 0.1 M KCl were found to be −0.17 V and are in line with the values reported in the literature [23,27]. The peak-peak potential separation is an indicator of the heterogeneous charge transfer kinetics and in this case a value close to 57 mV is suggestive of rapid electron transfer at the nanocarbon paste electrode. This is corroborated by the ratio of $i_{p,a}$ to $i_{p,c}$ having a value close to unity.

Cyclic voltammetry was carried out at scan rates over the range of 50 to 800 mV s^{-1} and the voltammetric measurements for the nanocarbon paste electrode are shown in **Figure 5.4**. The current of the cathodic peak for each electrode increases linearly with the square root of the scan rate as depicted in **Figure 5.5**, indicating that the current is controlled by a semi-infinite linear diffusion. With increasing scan rates, the peak-peak potential separation increases for all three electrodes but does not exceed 85 mV, suggesting fast but quasi-reversible charge transfer kinetics at higher scan rates.

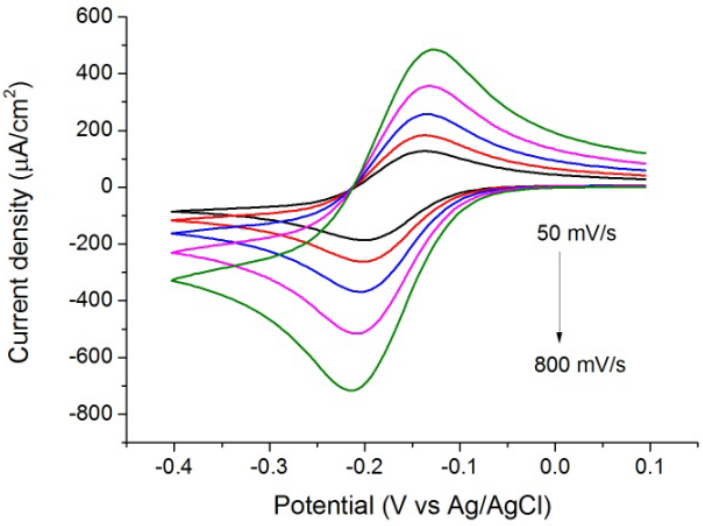

Figure 5.4 Cyclic voltammograms of 1.0 mM $Ru(NH_3)_6Cl_3$ in KCl solution at nanocarbon paste electrode at scan rates from 50 to 800 mV s^{-1}.

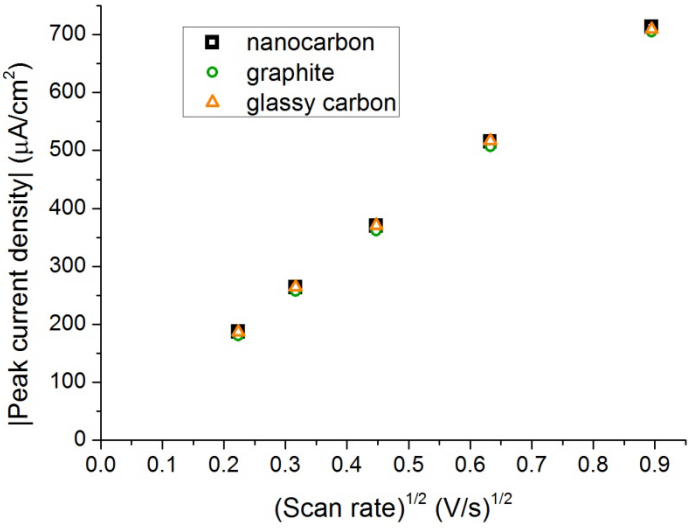

Figure 5.5 Plot of absolute values of cathodic peak current density for $Ru(NH_3)_6Cl_3$ against square root of scan rate at nanocarbon paste, graphite paste and glassy carbon electrodes.

5.3.3 $Fe(CN)_6^{3-/4-}$

Next the voltammetry of the anionic redox species $Fe(CN)_6^{3-/4-}$ was investigated at each of the three electrodes. The ferri/ferrocyanide redox system has been reported to possess some inner sphere characteristics [25,28]. For an inner sphere electron transfer reaction, the process is more sensitive to the electrode surface due to a greater interaction between the reactant and the electrode compared to the outer sphere process.

The resulting current-potential curves at 100 mV s^{-1} are shown in **Figure 5.6**. The peak-peak potential separations were in notable excess of 57 mV (**Table 5.2**), indicating quasi-reversible electron transfer kinetics. For the nanocarbon paste electrode, the anodic and cathodic peak potentials displayed a symmetrical shift towards the positive

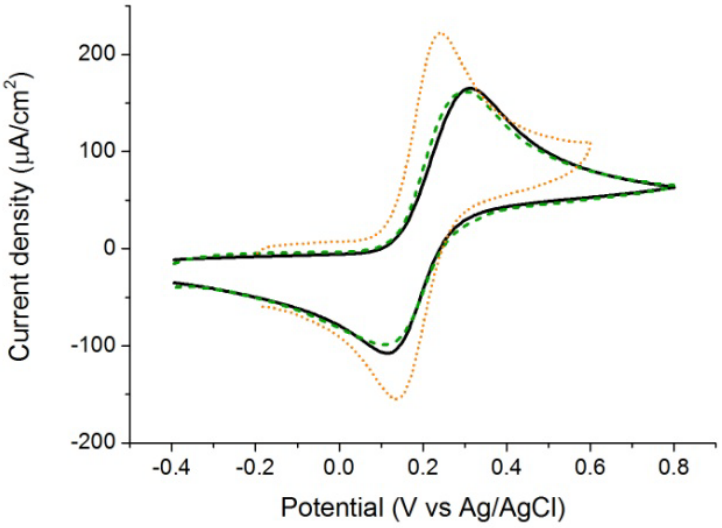

Figure 5.6 Cyclic voltammograms of 1.0 mM potassium ferrocyanide in KCl solution at nanocarbon paste (solid line), graphite paste (dashed line) and glassy carbon electrodes (dotted line). Scan rate: 100 mV s^{-1}.

and negative directions respectively when compared to the glassy carbon electrode, with ΔE_p increasing from 97 to 195 mV and an accompanying ~20% decrease in the anodic and cathodic peak current densities. This larger anodic-cathodic peak separation is reflective of a decrease in the heterogeneous electron transfer rate constant at the nanocarbon CPE, with similar behaviour being observed for the graphite CPE. Moreover the increased deviation from unity of the ratios of $i_{p,a}$ to $i_{p,c}$ further indicates the sluggish kinetics. The lower electrochemical reactivity of the ferri/ferrocyanide redox system at the carbon paste electrodes compared to the glassy carbon electrodes could be attributed to the addition of the hydrocarbon pasting liquid which is known to decrease the heterogeneous electron transfer rate from the “dry” carbon limit [29].

Table 5.2 Cyclic voltammetric data for $Fe(CN)_6^{3-/4-}$ at 100 mV s^{-1} for different electrodes

Electrode	**$E^{0'}$/V**	**ΔE_p/mV**	**$i_{p,a}/i_{p,c}$**
nano-carbon CPE	0.22	195	1.2
graphite CPE	0.21	190	1.3
glassy carbon	0.19	97	1.2

From the plot of the peak anodic current densitites against the square root of scan rate as depicted in **Figure 5.7**, the excellent linearity shown by the three electrodes indicate that the current is limited by the semi infinite linear diffusion of the reactant to the electrode surface. The peak-peak potential separations increased with the scan rate, as expected for quasi-reversible electrode processes, to 313 mV, 268 mV and 137 mV at the highest scan rate (800 mV s^{-1}) for the nanocarbon paste electrode, graphite CPE and glassy carbon electrode respectively.

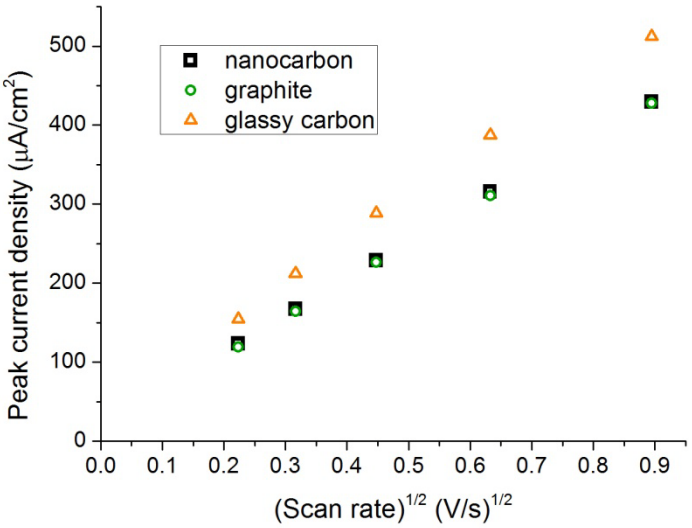

Figure 5.7 Plot of anodic peak current density for potassium ferrocyanide against square root of scan rate at nanocarbon paste, graphite paste and glassy carbon electrodes.

5.3.4 $IrCl_6^{2-/3-}$

The electron transfer kinetics at the nanocarbon paste electrode was further examined with another negatively charged redox analyte $IrCl_6^{2-/3-}$ which is known to be an outer sphere system [25,26]. Cyclic voltammograms of K_2IrCl_6 in 0.1 M KCl at 100 mV s^{-1} for the three different electrodes are given in **Figure 5.8** and relevant data from the CVs are provided in **Table 5.3**.

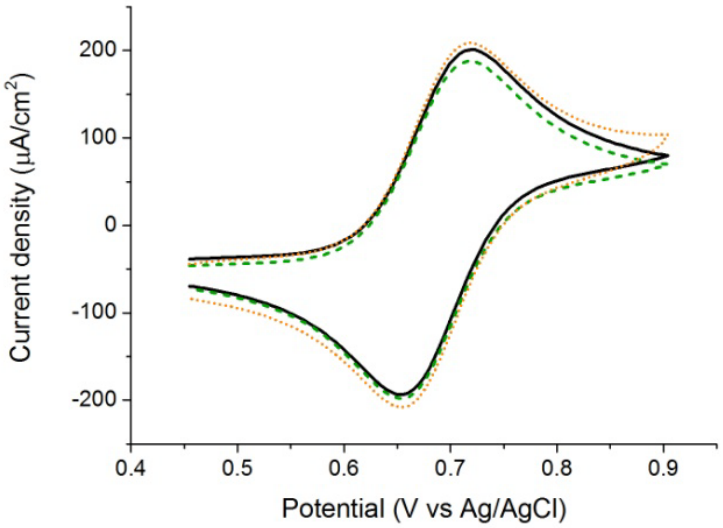

Figure 5.8 Cyclic voltammograms of 1.0 mM K_2IrCl_6 in KCl solution at nanocarbon paste (solid line), graphite paste (dashed line) and glassy carbon electrodes (dotted line). Scan rate: 100 mV s^{-1}.

Table 5.3 Cyclic voltammetric data for $IrCl_6^{2-/3-}$ at 100 mV s^{-1} for different electrodes.

Electrode	**$E^{0'}$/V**	**ΔE_p/mV**	**$i_{p,a}/i_{p,c}$**
nano-carbon CPE	0.69	64	1.1
graphite CPE	0.69	64	1.1
glassy carbon	0.69	59	1.2

The results are very different from the anionic ferri/ferrocyanide redox system. The anodic-cathodic peak separations for the nanocarbon and graphite paste electrodes are both 64 mV and the anodic to cathodic peak current density ratios are close to unity, suggestive of nearly reversible electrode kinetics for the hexachloroiridate(III/II) system at the CPEs. In this case of an outer sphere anionic species, the carbon electrodes mainly function as a source or sink of electrons and the electron transfer kinetics is largely unaffected by the specific electrode surface chemistry therefore no significant difference was observed compared to the glassy carbon electrode, unlike the above anionic case of the ferri/ferro-cyanide system.

Cyclic voltammetry done at different scan rates of 50 to 800 mV s^{-1} showed that the peak anodic current density varied linearly with the square root of the scan rate, as given by the plot in **Figure 5.9**, again indicating a diffusion controlled electrode reaction. At higher scan rates, the electron transfer kinetics remained relatively fast with the peak-peak potential separation increasing to values not beyond 85 mV.

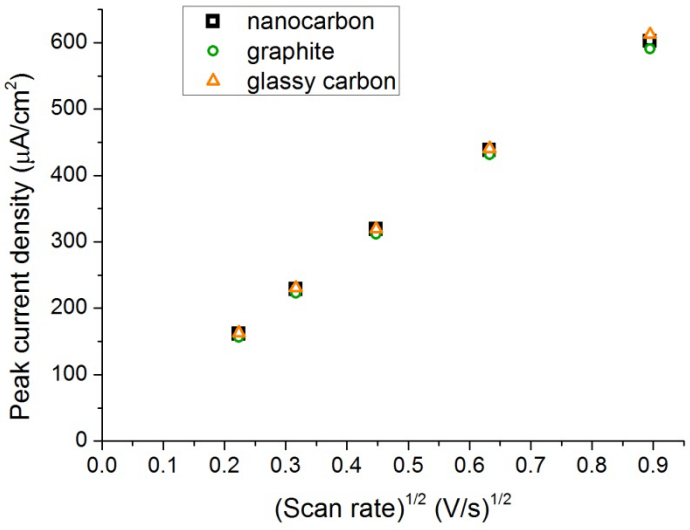

Figure 5.9 Plot of anodic peak current density for K_2IrCl_6 against square root of scan rate at nanocarbon paste, graphite paste and glassy carbon electrodes.

5.3.5 Ferrocenemethanol and its diffusion into the nanocarbon paste electrode

The redox reaction of the neutral molecule ferrocenemethanol

$$FcCH_2OH - e^- \rightleftharpoons FcCH_2OH^+$$

is a well-studied system [30] and this was used to investigate the behaviour of the nanocarbon paste electrode. As illustrated in **Figure 5.10**, the cyclic voltammetric response of the nanocarbon paste electrode recorded at 100 mV s^{-1} closely matched that of the graphite CPE. The values of ΔE_p and the ratio of $i_{p,a}$ to $i_{p,c}$ given in **Table 5.4** points to the reversibility of the ferrocenemethanol system at all three electrodes.

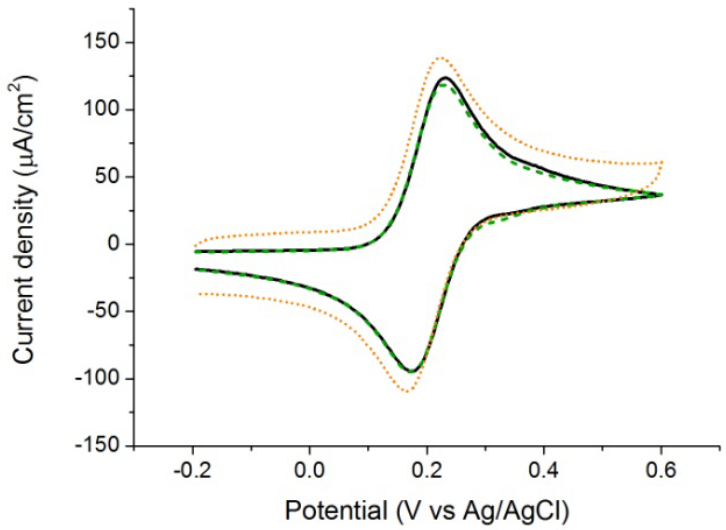

Figure 5.10 Cyclic voltammograms of 0.5 mM ferrocenemethanol in KCl solution at nanocarbon paste (solid line), graphite paste (dashed line) and glassy carbon electrodes (dotted line). Scan rate: 100 mV s^{-1}.

Table 5.4 Cyclic voltammetric data for ferrocenemethnol at 100 mV s^{-1} for different electrodes.

Electrode	**$E^{0'}$/V**	**ΔE_p/mV**	**$i_{p,a}/i_{p,c}$**
nano-carbon CPE	0.20	54	1.1
graphite CPE	0.20	54	1.1
glassy carbon	0.20	59	1.0

Similar to the three redox probes above, a diffusional mechanism operates for the reaction of ferrocenemethanol at the interfacial zone as shown by the square root dependence of the anodic peak current density on the scan rate in **Figure 5.11**. The peak-peak potential separations remained relatively stable, and thus reversible, at all scan rates studied.

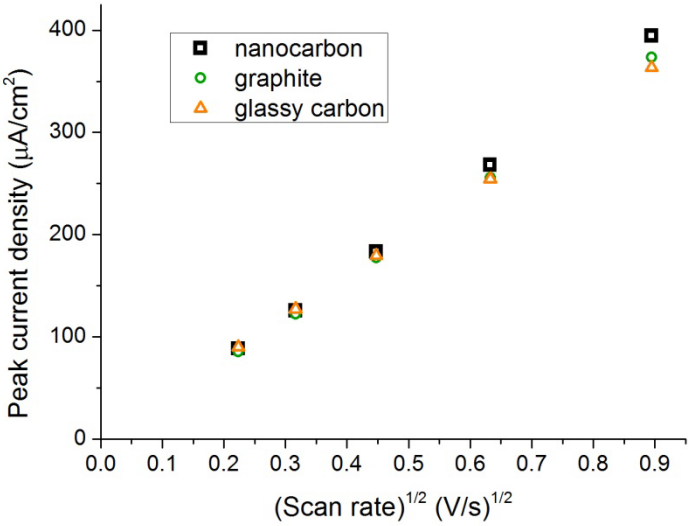

Figure 5.11 Plot of anodic peak current density for ferrocenemethanol against square root of scan rate at nanocarbon paste, graphite paste and glassy carbon electrodes.

During the voltammetric experiments, it was observed that ferrocenemethanol accumulates in the nanocarbon paste electrode. This observation was then studied by obtaining cyclic voltammograms in a 0.1 M KCl solution. The voltammogram A corresponds to the cyclic voltammogram in a 0.1 M KCl solution at the nanocarbon paste electrode. After that, the nanocarbon paste electrode was immersed for 20 mins in a solution containing 0.5 mM $FcCH_2OH$, transferred to 0.1 M KCl solution and the cyclic voltammogram B was obtained. The results are shown in **Figure 5.12**, where two pairs of peaks are clearly seen. The peaks P1a (E = 0.23 V) and P1b (E = 0.17 V)

correspond to the $FcCH_2OH/FcCH_2OH^+$ redox system in aqueous solution (amount of $FcCH_2OH$ dissolved out of the paste to the solution) and the peaks P2a (E = 0.36 V) and P2b (E = 0.32 V) represent probably the same redox system "in" the paste. More specifically it is presumed that the peaks P2 reflect voltammetry at the triple interface formed by nano-carbon, paraffin oil and water (as presented in the literature [31]). Similar behaviour was observed when a graphite CPE was used. This phenomenon will be further explored in the next chapter.

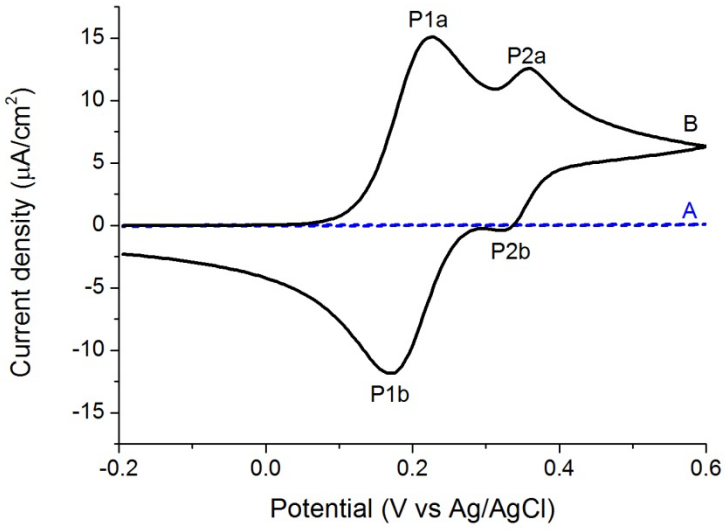

Figure 5.12 Cyclic voltammograms in 0.1 M KCl (A) before and (B) after 20 min the nanocarbon paste electrode was dipped in 0.5 mM ferrocenemethanol and transferred to KCl solution. Scan rate: 50 mV s^{-1}.

5.4 Conclusions

In this chapter, the electrochemical behaviour of a carbon paste electrode produced from nanocarbon or graphite mixed with paraffin oil has been investigated. The study of the electrochemical properties of these electrodes toward four different redox probes ($Ru(NH_3)_6^{3+}$, $Fe(CN)_6^{4-}$, $IrCl_6^{3-}$, and $FcCH_2OH$) was carried out showing good performance, rather similar to a glassy carbon electrode. Rapid electron transfer kinetics were observed for $Ru(NH_3)_6^{3+}$, $IrCl_6^{3-}$ and $FcCH_2OH$ while $Fe(CN)_6^{4-}$ exhibited a quasi-reversible electrochemical response, with all displaying diffusion limited peak currents. The diffusion of $FcCH_2OH$ into the nanocarbon paste electrode is a very interesting aspect that will be further examined electrochemically in the next chapter.

It can be concluded that nanocarbon and graphite CPEs had almost the same results for all four systems. Based on the series of electrochemical characterisations, nanocarbon has been demonstrated to be a valid alternative to graphite powder in the construction of carbon paste electrodes not least because the cost of nano-carbon (~$1/kg [32]) is ca. 50 times cheaper than graphite (~$50/kg [33]).

References

[1] D. Lowinsohn, P. Gan, K. Tschulik, J.S. Foord, R.G. Compton, Electroanalysis 25 (2013) 2435.

[2] R.N. Adams, Anal. Chem. 30 (1958) 1576.

[3] I. Švancara, K. Vytřas, K. Kalcher, A. Walcarius, J. Wang, Electroanalysis 21 (2009) 7.

[4] I. Švancara, A. Walcarius, K. Kalcher, K. Vytřas, Cent. Eur. J. Chem. 7 (2009) 598.

[5] K. Kalcher, J.M. Kauffmann, J. Wang, I. Švancara, K. Vytřas, C. Neuhold, Z. Yang, Electroanalysis 7 (1995) 5.

[6] I. Svancara, K. Kalcher, A. Walcarius, K. Vytras, Electroanalysis with Carbon Paste Electrodes, CRC Press, London, 2012.

[7] R.N. Adams, Electrochemistry at solid electrodes, Marcel Dekker, New York, 1969.

[8] G. Li, C. Wan, Z. Ji, K. Wu, Sens. Actuators, B 124 (2007) 1.

[9] I. Švancara, M. Hvízdalová, K. Vytřas, K. Kalcher, R. Novotný, Electroanalysis 8 (1996) 61.

[10] J. Wang, Ü. Anik Kirgöz, J.-W. Mo, J. Lu, A. Nasser Kawde, A. Muck, Electrochem. Commun. 3 (2001) 203.

[11] R.I. Stefan, S.G. Bairu, Anal. Chem. 75 (2003) 5394.

[12] A.J.G. Zarbin, Quim Nova 30 (2007) 1469.

[13] M. Miranda-Hernández, M.E. Rincón, I. González, Carbon 43 (2005) 1961.

[14] F. Ricci, A. Amine, D. Moscone, G. Palleschi, Anal. Lett. 36 (2003) 1921.

[15] R. Antiochia, I. Lavagnini, F. Magno, F. Valentini, G. Palleschi, Electroanalysis 16 (2004) 1451.

[16] N.S. Lawrence, R.P. Deo, J. Wang, Talanta 63 (2004) 443.

[17] M.D. Rubianes, G.A. Rivas, Electroanalysis 17 (2005) 73.

[18] T.W.B. Lo, L. Aldous, R.G. Compton, Sens. Actuators, B 162 (2012) 361.

[19] J. Panchompoo, L. Aldous, M. Baker, M.I. Wallace, R.G. Compton, Analyst 137 (2012) 2054.

[20] H.O. Pierson, Handbook of Carbon, Graphite, Diamond, and Fullerenes: Properties, Processing, and Applications, Noyes Publications, New Jersey, 1993.

[21] J. Panchompoo, L. Aldous, R.G. Compton, New J. Chem. 34 (2010) 2643.

[22] J.G. Limon-Petersen, J.T. Han, N.V. Rees, E.J.F. Dickinson, I. Streeter, R.G. Compton, J. Phy. Chem. C 114 (2010) 2227.

[23] C.E. Banks, R.G. Compton, A.C. Fisher, I.E. Henley, Phys. Chem. Chem. Phys. 6 (2004) 3147.

[24] M.C. Granger, G.M. Swain, J. Electrochem. Soc. 146 (1999) 4551.

[25] P. Chen, R.L. McCreery, Anal. Chem. 68 (1996) 3958.

[26] P. Chen, M.A. Fryling, R.L. McCreery, Anal. Chem. 67 (1995) 3115.

[27] C.E. Banks, N.V. Rees, R.G. Compton, J. Electroanal. Chem. 535 (2002) 41.

[28] K.R. Kneten, R.L. McCreery, Anal. Chem. 64 (1992) 2518.

[29] M.E. Rice, Z. Galus, R.N. Adams, J. Electroanal. Chem. Interfac. Electrochem. 143 (1983) 89.

[30] P. Liljeroth, C. Johans, C.J. Slevin, B.M. Quinn, K. Kontturi, Electrochem. Commun. 4 (2002) 67.

[31] C.E. Banks, T.J. Davies, R.G. Evans, G. Hignett, A.J. Wain, N.S. Lawrence, J.D. Wadhawan, F. Marken, R.G. Compton, Phys. Chem. Chem. Phys. 5 (2003) 4053.

[32] L. Dai, Carbon Nanotechnology: Recent Developments in Chemistry, Physics, Materials Science and Device Applications, Elsevier Science, Amsterdam, 2006.

[33] http://www.sigmaaldrich.com/united-kingdom.html.

Chapter 6

The Measurement of the Gibbs Energy of Transfer Between Oil and Water Using a Nanocarbon Paste Electrode

Progressing from the previous chapter, this chapter reports the use of nanocarbon paste electrodes for the measurement of Gibbs energies of transfer between oil and aqueous phases. In this method the oil of interest is used as the binder for the nanocarbon paste electrodes and the molecule of interest is dissolved in the organic or aqueous phase. Voltammetry is performed over a period of time and used to monitor the transfer of the molecule between the two phases. The method is illustrated for the transfer of ferrocenemethanol between water and oil using the ferrocenemethanol/ ferroceniummethanol ($FcCH_2OH/FcCH_2OH^+$) redox couple. When supporting electrolyte containing the anions Cl^-, NO_3^- or SCN^- was used, an expulsion of the oxidised ferrocene occurred and the difference in midpoint potentials (E_{mid}) between the peaks of interest observed in these experiments allowed the calculation of the Gibbs energy ($\Delta G°$) of transfer of ferrocenemethanol from water to oil. The average $\Delta G°$ value thus obtained was $-(12.7 \pm 0.2)$ kJ mol $^{-1}$. For more hydrophobic anions (X^- = PF_6^-, AsF_6^-), the electron transfer is coupled to the transfer of the anion into the oil and the $\Delta G°$ for the transfer of the ion pair of $FcCH_2OH^+$ and X^- ions from water to oil was found to be −1.3 and −3.9 kJ mol^{-1} for PF_6^- and AsF_6^- respectively. This work has been published in *Electroanalysis* [1].

6.1 Introduction

The energetics of molecule and ion transfer between two liquid phases are key to understanding many phenomena including essential biological processes [2]. Electrochemical measurements have proved extremely powerful in the area starting with the 4-electrode approach extensively developed by Samec and colleagues [3-5]. In this method a counter and a reference electrode are placed in each of the two phases and used to perform voltammetry at the liquid-liquid interface from which ion and molecule transfer energetics can be inferred. Note that the approach requires the two phases to contain electrolyte so that diffusion controlled voltammetry can be performed; this limits the wider use of the method, excluding systems of low or zero ionic strength.

An alternative strategy, which makes the use of oil phase droplet(s), has been developed by Scholz (large volume drops) [6-9] and by Marken (femtolitre volumes) [10,11]. These allow a three electrode methodology in which the counter and reference are placed in an aqueous phase whilst potential is applied via a potentiostat to the (working) electrode supporting the droplet(s). In the case of small oil droplets supported on a layer electrode in a bulk aqueous phase electron transfer is thought to occur at the triple boundary formed between the water, the oil and the electrode. The electron transfer is strongly coupled with ion transfer between the two phases induced by the need to preserve local electroneutrality [11-17]. Similar experiments have been reported using tiny water droplets supported on a large electrode in a bulk non-aqueous solvent [18].

In this chapter an approach is considered which is complementary to those above and which enables the energetics of transfer of neutral species to be inferred, in addition to further data relating to ion transfer. In particular a nanocarbon paste electrode (n-CPE)

[19] is used in which the oil phase of interest is used as a binder. The solute of interest is then dissolved with in the oil or an aqueous phase and voltammetry used to study the interface formed between the carbon paste electrode and an aqueous phase. This is used to monitor the transfer of species between the two phases and, indirectly, provides information on the energetics of transfer. As background the very early work of Kuwana and French [20] in using a CPE to release molecules into aqueous solutions for electrochemical studies is noted.

6.2 Experimental

6.2.1 Chemicals and materials

Ferrocenemethanol (97%, Sigma Aldrich), paraffin oil (puriss, Sigma-Aldrich), potassium chloride (99.5%, Fluka), potassium nitrate (99%, Aldrich), potassium hexafluorophosphate (98%, Aldrich), potassium hexafluoroarsenate (V), (98%, Aldrich), potassium thiocyanate (98%, Hopkin & Williams) and commercial nanocarbon (diameter 27 ± 10 nm, Monarch 430®, Cabot Corporation) were used as received. All aqueous solutions were prepared using ultra pure water (~18.2 MΩ cm at 25°C).

6.2.2 Preparation of the carbon paste electrodes

Unmodified carbon paste was prepared by hand-pasting nanocarbon with paraffin oil in a ratio of 60:40 (w/w) using a mortar and pestle. The resulting paste was packed into the well of the working electrode as described in the previous chapter. Modified carbon paste was prepared in a similar manner using paraffin oil which contained ferrocenemethanol at concentrations from 5 to 50 mM.

6.3 Results and discussion

6.3.1 Accumulation of ferrocenemethanol in an unmodified carbon paste electrode

As described in the previous chapter, when a nano-carbon paste electrode, made with paraffin oil, was pretreated by dipping for 20 min in a solution containing 0.5 mM ferrocenemethanol ($FcCH_2OH$), $FcCH_2OH$ was found to accumulate in the electrode during the pretreatment. To further investigate this uptake process, the unmodified nano carbon paste electrode was first pretreated by contact in a 0.1 M KCl solution containing 0.5 mM $FcCH_2OH$ for different times from 1 to 20 min. After this, the electrode was removed and briefly rinsed with ultra pure water before immersion in a 0.1 M KCl solution for cyclic voltammetry (CV). **Figure 6.1** shows the cyclic voltammograms in the KCl solution measured with the unmodified carbon paste electrode without (dotted line) and with (solid line) pretreatment for 1 to 20 min. After 1 min of contact with the $FcCH_2OH$ solution, a pair of peaks can be clearly seen in the KCl solution. The peaks P1a (E = 0.23 V vs Ag/AgCl) and P1b (E = 0.17 V vs Ag/AgCl) correspond to the redox couple $FcCH_2OH/[FcCH_2OH]^+$, as described in Equation (6.1), which has dissolved out from the paste to the aqueous solution.

$$FcCH_2OH\ (aq) - e \rightleftharpoons FcCH_2OH^+\ (aq) \qquad (6.1)$$

This assignment is made since these peak potentials are consistent with those obtained in CV for an unmodified electrode (without pretreatment) in a solution of $FcCH_2OH$ (**Figure 6.1** inset). However, after 20 min of contact with $FcCH_2OH$, an additional pair of peaks, P2a (E = 0.36 V vs Ag/AgCl) and P2b (E = 0.32 V vs Ag/AgCl), appears and represents probably the same redox couple but with one or more components not in the aqueous phase. The explanation of the P2 peaks will be explored further below. The

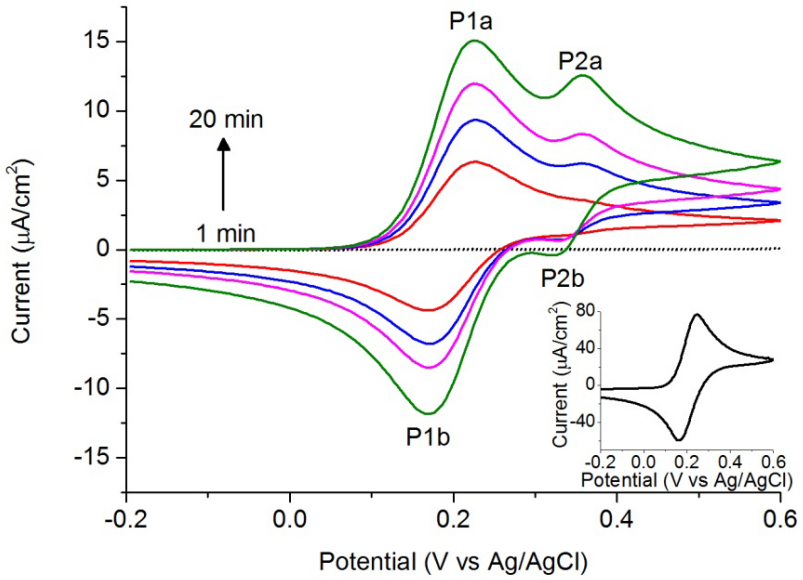

Figure 6.1 Cyclic voltammograms of the unmodified nanocarbon paste electrode in 0.1 M KCl without (dotted line) and with (solid line) pretreatment of contact in 0.5 mM ferrocenemethanol for 1, 5, 10 and 20 min. Inset: Cyclic voltammogram of unmodified CPE in 0.5 mM ferrocenemethanol (supporting electrolyte: 0.1 M KCl). Scan rate: 50 mV s^{-1}.

peak currents of both peaks P1 and P2 increased with the pretreatment time, which implies a diffusion of $FcCH_2OH$ from the aqueous solution into the carbon paste and a continual accumulation of the compound in the paste during the period of pretreatment.

Next, after an unmodified carbon paste electrode was pretreated in 0.5 mM $FcCH_2OH$ solution for 20 min, it was transferred to a 0.1 M KCl solution and cyclic voltammetry was performed immediately (time = 0 min) and at subsequent times up to 10 min. These consecutive cyclic voltammograms from 0 to 10 min are shown in **Figure 6.2**.

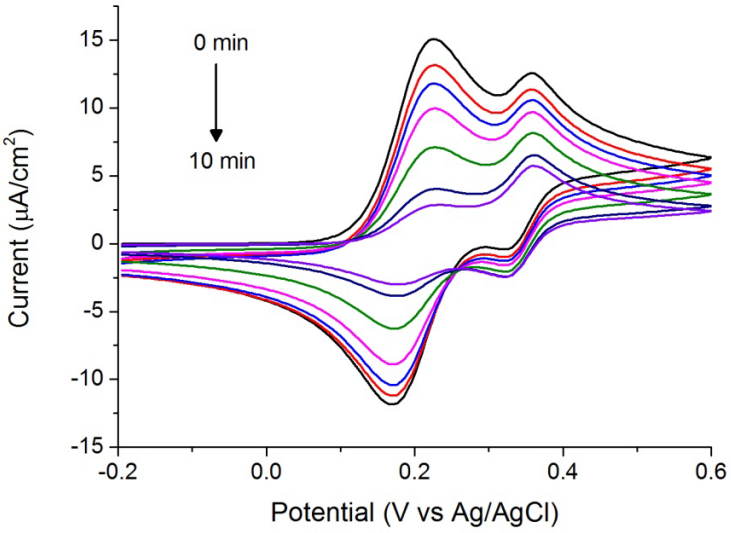

Figure 6.2 Cyclic voltammograms of the unmodified nanocarbon paste electrode (previously pretreated for 20min) at 0, 1, 2, 4, 6, 8 and 10 min in 0.1 M KCl. Scan rate: 50 mV s^{-1}.

The peak currents for peaks P1a and P1b decreased with time due to diffusion of some $FcCH_2OH$ molecules into the bulk aqueous solution and the depletion likely reflects that local to the electrode surface in aqueous solution. As for peaks P2a and P2b, little change was observed with time. Noting the partition coefficient of $FcCH_2OH$ (P = 82) in the system of 1,2-dichlorobenzene and aqueous HCl [21], $FcCH_2OH$ is likely to be much more soluble in the organic phase than in the aqueous phase. For other pretreatment times of 1 to 10 min, peaks P1 and P2 behaved in a similar manner.

6.3.2 Electrochemical behaviour of a modified carbon paste electrode

In order to investigate the $FcCH_2OH$ / $[FcCH_2OH]^+$ redox couple within the carbon paste electrode, a modified carbon paste electrode was fabricated using paraffin oil containing 20 mM of dissolved $FcCH_2OH$. **Figure 6.3**a shows the cyclic voltammograms when the $FcCH_2OH$-modified carbon paste electrode was immersed in

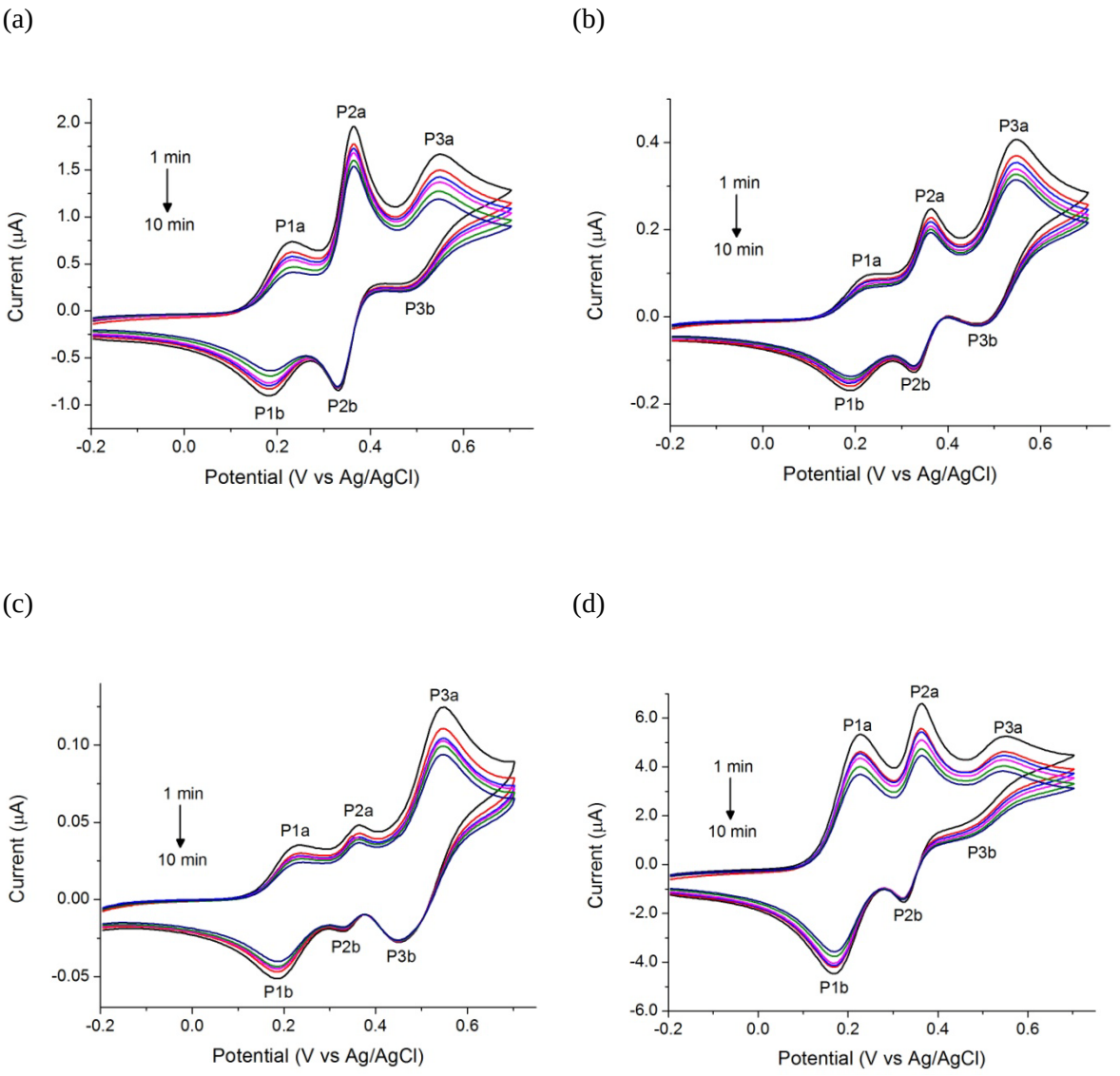

Figure 6.3 Cyclic voltammograms of modified nano-carbon paste electrode at 1, 2, 4, 6, 8 and 10 min in 0.1 M KCl for different concentrations of ferrocenemethanol in oil of (a) 20 mM, (b) 10 mM, (c) 5 mM, (d) 50 mM. Scan rate: 50 mV s^{-1}.

a 0.1 M KCl solution at different times from 1 to 10 min. In addition to the pairs of peaks P1a, P1b, P2a and P2b, a third pair of peaks, P3a (E = 0.55 V vs Ag/AgCl) and P3b (E = 0.46 V vs Ag/AgCl), could also be observed. Subsequent scans up to 10 min revealed the decrease in peak currents with time for peaks P1a, P1b, P3a and P3b, while the peak currents of peaks P2a and P2b remained relatively constant. The trends for peaks P1 and P2 are similar to those found above whereas peak P3 will be explored below. As the concentration of $FcCH_2OH$ in the paraffin oil was varied from 5 mM to 50 mM, similar behaviour was found as shown in **Figure 6.3**b-d, with the peak currents all increasing with greater amounts of $FcCH_2OH$ in the paste.

Next, the effect of scan rate on the peak current was studied to understand the mechanism of the electrochemical process. For the peaks P1 and P3, the variation of the peak current with scan rate was compounded with the rapid drop in peak current with time due to the material loss of the $FcCH_2OH$ / $[FcCH_2OH]^+$ redox couple from the oil into the aqueous phase and so was not pursued further. As for the peak P2, its peak current dependence on scan rate was studied at a time of 3 hours after immersion of the modified nano-carbon paste electrode into the KCl solution, when the current was nearly stable between consecutive scans. Cyclic voltammetric measurements at this time are depicted in **Figure 6.4**a for scan rates of 50 to 800 mV s^{-1} while **Figure 6.4**b shows that the corresponding peak current for peak P2a increased apparently linearly with the square root of the scan rate, suggesting a diffusive process for this peak.

(a)

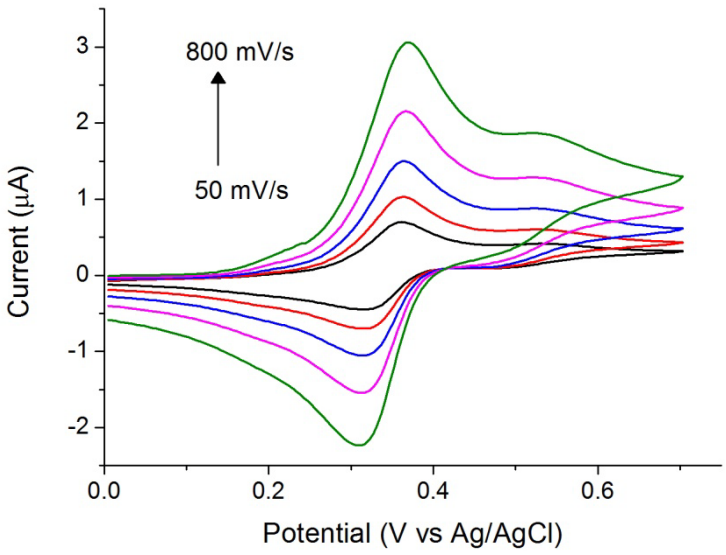

(b)

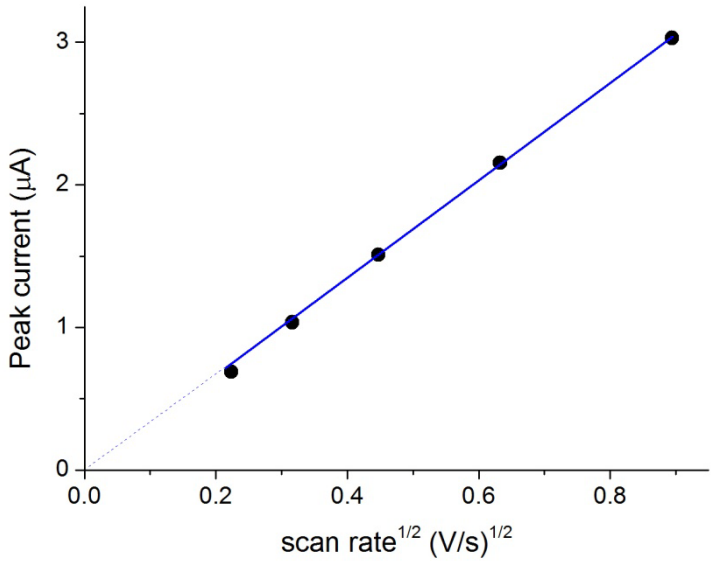

Figure 6.4 (a) Cyclic voltammograms after 3-hour immersion of modified nanocarbon paste electrode in 0.1 M KCl at scan rates of 50 to 800 mV s^{-1}; (b) Plot of peak current against square root of scan rate for peak P2a.

6.3.3 Effect of solution stirring and peak assignment

Experiments were performed with solution stirring to help to understand the origin of the redox species involved in reaction for each set of peaks. The solution was stirred with a mechanical stirrer at a speed of 2000 rpm and the resulting movement of the liquid improved the mass transport within the aqueous phase. As shown in **Figure 6.5**, peaks P1a and P1b were removed during stirring, indicating that the species leading to these peaks both existed in the aqueous phase. The agreement of the peak potential values with those obtained from an unmodified carbon paste electrode in an aqueous solution of $FcCH_2OH$ provides further evidence for this. Therefore, the P1 pair of peaks can be assigned to the reaction in equation (6.1).

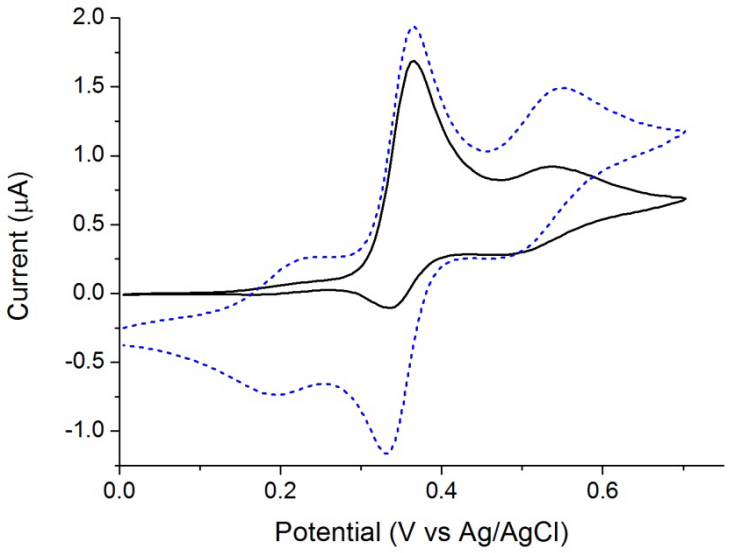

Figure 6.5 Cyclic voltammograms of modified nanocarbon paste in 0.1 M KCl with (solid line) and without (dashed line) solution stirring. Scan rate: 50 mV s^{-1}. Concentration of ferrocenemethanol in oil: 20 mM.

Peak P2a remained unaffected while peak P2b became diminished during stirring. The anodic reaction due to peak P2a thus has its source in the paste and the product which undergoes the cathodic reaction resulting in peak P2b enters the solution. This corresponds to the following reaction in equation (6.2):

$$FcCH_2OH\ (o) - e \rightleftharpoons FcCH_2OH^+(aq) \qquad (6.2)$$

where (o) represents the species in the organic phase.

Note that this process likely occurs at the triple boundary formed between the oil, the aqueous phase and the carbon as proposed for a variety of other processes [2,10,12,13].

Both peaks P3a and P3b showed a drop in peak current upon stirring but did not disappear. The species involved could possibly originate from the paste and exist in equilibrium with the aqueous phase, with the transfer being driven towards the aqueous upon agitation of the solution. The nature of the peak P3 is considered below with further experiments designed to further explore this issue.

6.3.4 Paste composition with different carbon content; assignment of peak P3

The influence of the modified paste composition was studied by varying the carbon content from 50% to 65% (w/w) and mixing with the corresponding amounts of paraffin oil containing 10 mM $FcCH_2OH$. **Figure 6.6** shows the cyclic voltammograms in 0.1 M KCl solution on the resulting carbon paste electrode. The peak currents of peaks P1a and P1b decreased with an increase in carbon content. As the $FcCH_2OH$-containing oil content decreases, a lower amount of $FcCH_2OH$ from the paste enters the

aqueous phase. This results in less molecules diffusing from within the paste towards the oil/water interface hence a lower current response.

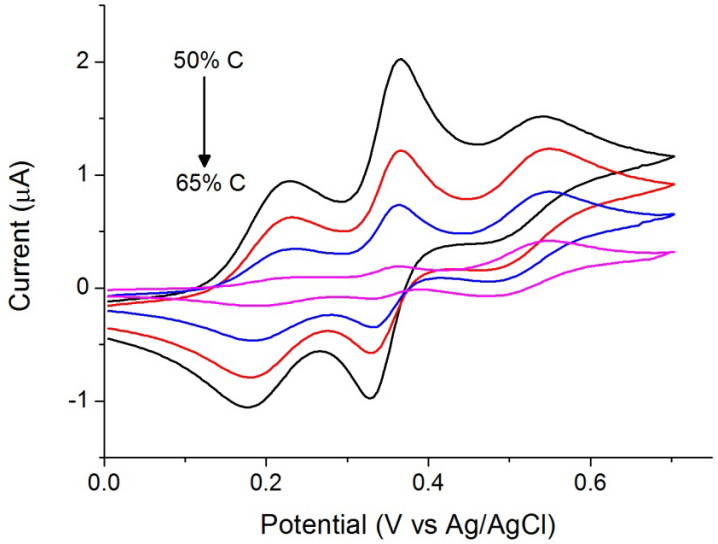

Figure 6.6 Cyclic voltammograms in 0.1 M KCl of modified nanocarbon paste containing 50%, 55%, 60% and 65% carbon (w/w). Scan rate: 50 mV s^{-1}. Concentration of ferrocenemethanol in oil: 10 mM.

Since the relative current of peak P3a to that of peak P2a increases with greater amounts of carbon, the former is likely to arise from $FcCH_2OH$ associated with the nanocarbon particles, which have been shown to display strong adsorptive behaviour [22-25]. The $FcCH_2OH$ molecules are likely to be stabilised on the nanocarbon thereby only undergoing oxidation at a more positive potential.

6.3.5 Effect of anion in supporting electrolyte

The oxidation of $FcCH_2OH$ generates a positively charged $FcCH_2OH^+$ species and for electroneutrality to be maintained in the organic phase, either the electrolyte anion is transported across the water|oil interface or the $FcCH_2OH^+$ cation is expelled into the

aqueous phase. This will depend on the Gibbs energy of ion transfer across the water|oil interface [2,6]. Other than Cl^-, different supporting electrolytes containing other anions, namely NO_3^-, SCN^-, PF_6^- and AsF_6^-, were investigated for their effect on this anodic process.

Figure 6.7 shows the cyclic voltammograms on the modified carbon paste electrode in the four supporting electrolytes. The electrochemical behaviour of $FcCH_2OH$ in KNO_3, KPF_6 or $KAsF_6$ solutions was similar to that in KCl. For KSCN, only peaks P1 and P2 were observed due to the limit in potential window arising from oxidation of the electrolyte after +0.5 V. The peaks P1a and P1b all occur at the same potential as those in KCl, providing additional evidence for the assignment of the process to equation (6.1).

Since the peak P2 involves the redox reaction of $FcCH_2OH$ in the organic phase, the average midpoint potential (E_{mid}) values (at least three runs each) of this peak in each electrolyte are summarised in **Table 6.1**. From **Table 6.1**, E_{mid} values in KNO_3 and KSCN are very close to the value in KCl, it is likely that the expulsion of the $FcCH_2OH^+$ cation occurs in these three electrolyte systems. These anions are strongly hydrophilic therefore the Gibbs energy of transfer into the oil phase is expected to be positive, making it energetically unfavourable.

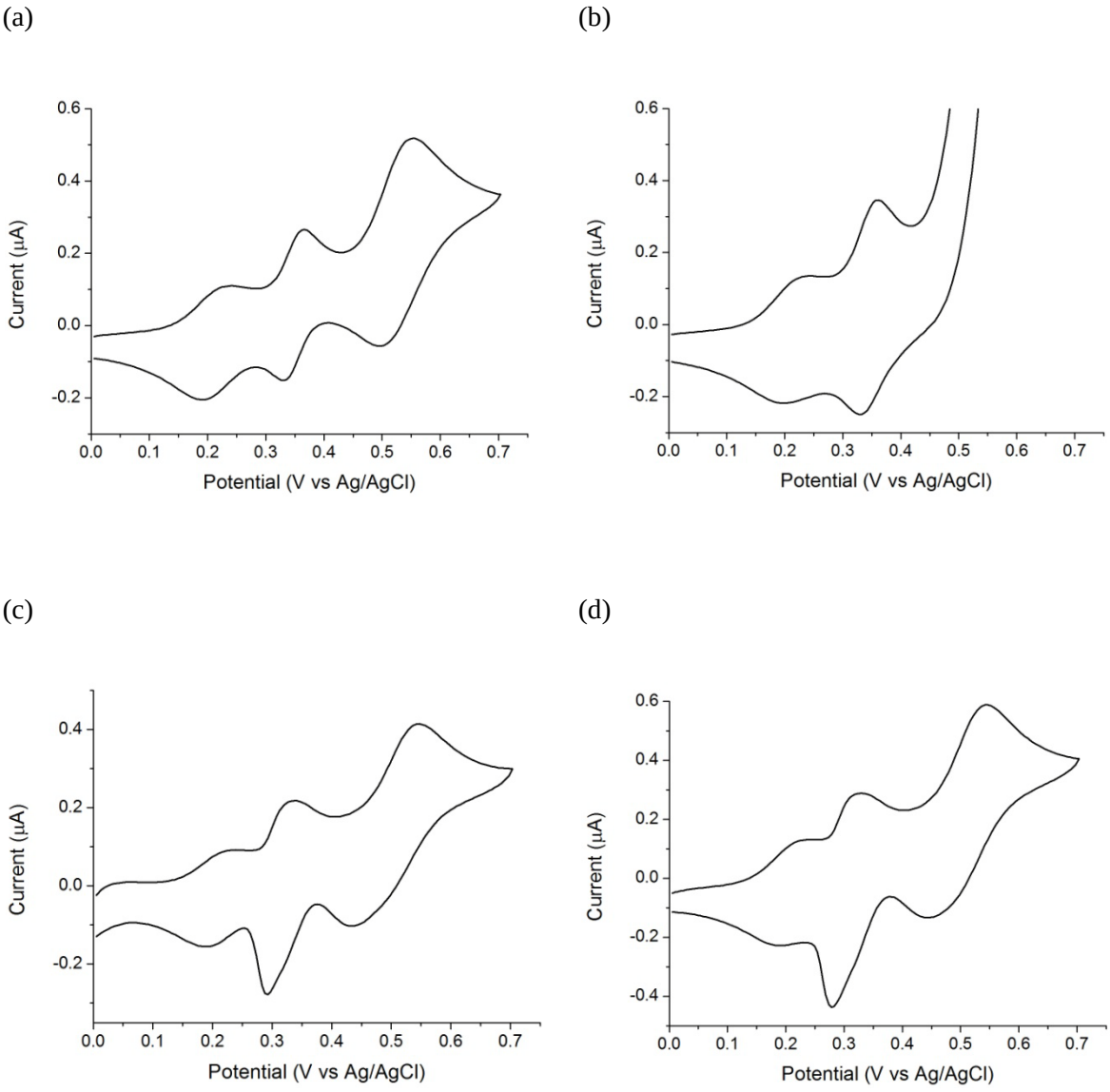

Figure 6.7 Cyclic voltammograms of modified nano-carbon paste electrode in 0.1 M of (a) KNO_3, (b) KSCN, (c) KPF_6, (d) $KAsF_6$. Scan rate: 50 mV s^{-1}. Concentration of ferrocenemethanol in oil: 10 mM.

Table 6.1 Average values of midpoint potential (E_{mid}) of peak P2 for different supporting electrolyte.

Electrolyte (0.1 M)	E_{mid} **(V)**
KCl	0.349 ± 0.001
KNO_3	0.347 ± 0.002
KSCN	0.345 ± 0.001
KPF_6	0.336 ± 0.005
$KAsF_6$	0.309 ± 0.004

As for KPF_6 and $KAsF_6$, the midpoint potential values displayed a shift from those in the KCl system. Due to the greater hydrophobicity of these two anions, it can be expected that a different process could possibly take place, that is, an electron transfer coupled to an ion transfer, which can be expressed in equation (6.3):

$$FcCH_2OH\ (o) - e + X^-\ (aq) \rightleftharpoons FcCH_2OH^+X^-\ (o) \qquad (6.3)$$

where (o) denotes the species in the organic phase and X^- refers to the anion present in the electrolyte.

6.3.6 Calculation of Gibbs energy of transfer

From the voltammetric data obtained, the Gibbs energy of transfer of $FcCH_2OH$ from the organic phase to the aqueous phase, $\Delta^{o\rightarrow w}G$, can be calculated. Taking the difference between the reactions described in equations (6.1) and (6.2) leads to the following equation (6.4).

$$FcCH_2OH\ (o) \rightleftharpoons FcCH_2OH\ (aq) \qquad (6.4)$$

The value of $\Delta^{o\rightarrow w}G$ can thus be found from the potential difference between the E_{mid} values of peaks P1 and P2 (ΔE_{mid}), in the cases of the electrolyte anions Cl^-, NO_3^- and SCN^- when the oxidised ferrocene enters the aqueous phase, through the equation (6.5).

$$\Delta^{o\rightarrow w}G = -nF\Delta E_{mid} \quad (6.5)$$

where n is the number of electrons transferred (n = 1 here) and F is the Faraday constant.

With the potential values from such experiments involving the above anions, the average $\Delta^{o\rightarrow w}G$ value thus obtained is (−12.7 ± 0.2) kJ mol $^{-1}$, which is similar to those shown in **Table 6.2** listing the values of Gibbs energy of transfer of ferrocene and its derivatives from various organic phases into the aqueous phase. Paraffin oil has a lower polarity than dichlorobenzene consistent with the value derived herein being lower than that for ferrocenemethanol in the dichlorobenzene system.

Table 6.2 Gibbs energy of transfer of some ferrocenium compounds

Compound	Organic Phase	Aqueous Phase	$\Delta^{o\rightarrow w}G$ / kJ mol^{-1}	Ref
$FcCH_2OH$	Paraffin oil	0.1 M $KCl_{(aq)}$	−12.7 ± 0.2 [a]	This work
$FcCH_2OH$	Dichlorobenzene	10 mM $HCl_{(aq)}$	−10.9 [b]	[21]
FcC_2H_4OH	Nitrobenzene	Water	−14.8 [b]	[26]
Fc	Nitrobenzene	Water	−21.9 [b]	[26]
Fc	Dodecane	Water	−19.7 ± 0.2 [b]	[27]
Fc^+	Nitrobenzene	Water	−7.2 [a]	[28]

[a]from electrochemical data
[b]from partition data

As for the electrolyte anions PF_6^- and AsF_6^-, the subtraction of equation (6.2) from equation (6.3) leads to equation (6.6):

$$FcCH_2OH^+ (aq) + X^- (aq) \rightleftharpoons FcCH_2OH^+ (o) + X^- (o) \quad (6.6)$$

From the potential difference between the peak P2 for ion transfer into the aqueous phase (Cl^-, NO_3^- and SCN^-) and into the oil phase (PF_6^- and AsF_6^-), the calculated values of Gibbs energy for the reaction described in equation (6.6) are −1.3 and −3.9 kJ mol^{-1} for PF_6^- and AsF_6^- respectively.

6.4 Conclusions

The voltammetric behaviour of an unmodified nanocarbon paste electrode (CPE), after pretreatment by contact in ferrocenemethanol ($FcCH_2OH$) solution, has been studied to understand the accumulation of $FcCH_2OH$ in the CPE. Through the modification of the carbon paste by dissolution of $FcCH_2OH$ in the oil, details concerning the interaction of $FcCH_2OH$ with the carbon paste electrode were revealed. The investigation of the effects of solution stirring and paste composition enabled the determination of the three pairs of voltammetric peaks observed with the $FcCH_2OH$-modified CPE in a 0.1 M KCl solution. These have been assigned to the oxidation of the $FcCH_2OH$ species found in the aqueous solution, originating in the oil and adsorbed on the nanocarbon respectively.

From the voltammetric studies involving the modified CPE, the calculation of the Gibbs energy of transfer of $FcCH_2OH$ from oil to water can be achieved, with an average value of (-12.7 ± 0.2) kJ mol^{-1} being found. The use of supporting electrolytes with different anions showed the influence of the anion on the direction of ion transfer across the water|oil interface during the oxidation of $FcCH_2OH$. By employing anions of greater hydrophobicity ($X^- = PF_6^-$, AsF_6^-), it is possible to obtain information regarding the Gibbs energy of transfer of $FcCH_2OH^+$ and X^- from water to oil. It is concluded that the CPE approach can give complementary information to existing methods for studying liquid-liquid interfaces.

References

[1] P. Gan, D. Lowinsohn, J.S. Foord, R.G. Compton, Electroanalysis 26 (2014) 351.

[2] C.E. Banks, T.J. Davies, R.G. Evans, G. Hignett, A.J. Wain, N.S. Lawrence, J.D. Wadhawan, F. Marken, R.G. Compton, Phys. Chem. Chem. Phys. 5 (2003) 4053.

[3] Z. Samec, V. Mareček, J. Koryta, M.W. Khalil, J. Electroanal. Chem. Interfac. Electrochem. 83 (1977) 393.

[4] Z. Samec, V. Mareček, J. Weber, J. Electroanal. Chem. Interfac. Electrochem. 96 (1979) 245.

[5] Z. Samec, E. Samcová, H.H. Girault, Talanta 63 (2004) 21.

[6] F. Scholz, Š. Komorsky-Lovrić, M. Lovrić, Electrochem. Commun. 2 (2000) 112.

[7] Š. Komorsky-Lovrić, K. Riedl, R. Gulaboski, V. Mirčeski, F. Scholz, Langmuir 18 (2002) 8000.

[8] Š. Komorsky-Lovrić, M. Lovrić, F. Scholz, J. Electroanal. Chem. 508 (2001) 129.

[9] R. Gulaboski, A. Galland, G. Bouchard, K. Caban, A. Kretschmer, P.-A. Carrupt, Z. Stojek, H.H. Girault, F. Scholz, J. Phy. Chem. B 108 (2004) 4565.

[10] F. Marken, R.D. Webster, S.D. Bull, S.G. Davies, J. Electroanal. Chem. 437 (1997) 209.

[11] F. Marken, R.G. Compton, C.H. Goeting, J.S. Foord, S.D. Bull, S.G. Davies, Electroanalysis 10 (1998) 821.

[12] U. Schröder, R.G. Compton, F. Marken, S.D. Bull, S.G. Davies, S. Gilmour, J. Phy. Chem. B 105 (2001) 1344.

[13] J.D. Wadhawan, R.G. Evans, C.E. Banks, S.J. Wilkins, R.R. France, N.J. Oldham, A.J. Fairbanks, B. Wood, D.J. Walton, U. Schröder, R.G. Compton, J. Phy. Chem. B 106 (2002) 9619.

[14] U. Schröder, J. Wadhawan, R.G. Evans, R.G. Compton, B. Wood, D.J. Walton, R.R. France, F. Marken, P.C. Bulman Page, C.M. Hayman, J. Phy. Chem. B 106 (2002) 8697.

[15] J.D. Wadhawan, A.J. Wain, A.N. Kirkham, D.J. Walton, B. Wood, R.R. France, S.D. Bull, R.G. Compton, J. Am. Chem. Soc. 125 (2003) 11418.

[16] F. Marken, A.N. Blythe, J.D. Wadhawan, R.G. Compton, S.D. Bull, R.T. Aplin, S.G. Davies, J Solid State Electrochem 5 (2001) 17.

[17] D. Rayner, N. Fietkau, I. Streeter, F. Marken, B.R. Buckley, P.C. Bulman Page, J. del Campo, R. Mas, F.X. Muñoz, R.G. Compton, J. Phy. Chem. C 111 (2007) 9992.

[18] T.J. Davies, S.J. Wilkins, R.G. Compton, J. Electroanal. Chem. 586 (2006) 260.

[19] D. Lowinsohn, P. Gan, K. Tschulik, J.S. Foord, R.G. Compton, Electroanalysis 25 (2013) 2435.

[20] T. Kuwana, W.G. French, Anal. Chem. 36 (1964) 241.

[21] P. Peljo, L. Qiao, L. Murtomäki, C. Johans, H.H. Girault, K. Kontturi, ChemPhysChem 14 (2013) 311.

[22] T.W.B. Lo, L. Aldous, R.G. Compton, Sens. Actuators, B 162 (2012) 361.

[23] M. Bele, A. Kodre, I. Arčon, J. Grdadolnik, S. Pejovnik, J.O. Besenhard, Carbon 36 (1998) 1207.

[24] E.M. Cuerda-Correa, J.R. Domínguez-Vargas, F.J. Olivares-Marín, J.B. de Heredia, J. Hazard. Mater. 177 (2010) 1046.

[25] H.T. Wang, A.A. Keller, F.T. Li, J. Environ. Eng.-ASCE 136 (2010) 1075.

[26] K. Nakatani, M. Wakabayashi, K. Chikama, N. Kitamura, J. Phy. Chem. 100 (1996) 6749.

[27] M.H. Abraham, N. Benjelloun-Dakhama, J.M.R. Gola, J.W.E. Acree, W.S. Cain, J. Enrique Cometto-Muniz, New J. Chem. 24 (2000) 825.

[28] J. Hanzlík, Z. Samec, J. Hovorka, J. Electroanal. Chem. Interfac. Electrochem. 216 (1987) 303.

Chapter 7

Ionic Liquid-Carbon Nanotube Modified Screen-Printed Electrodes and Their Potential for Adsorptive Stripping Voltammetry

It was demonstrated in the previous chapter that the constituents of the nanocarbon paste electrode were able to exert certain effects on the voltammetric behaviour due to their interaction with solution species. This chapter examines some aspects regarding the influence of the components of the carbon composite material towards adsorptive stripping voltammetry. Compared with paraffin oil, the use of ionic liquids as a binder in carbon paste type electrodes was shown to greatly enhance the accumulation of analytes, as illustrated with 17α-ethynylestradiol as a model. The ionic "liquid" *n*-octyl-pyridinium hexafluorophosphate [C_8py][PF_6] was most efficient among several ionic liquids investigated. Such preconcentration showed a [C_8py][PF_6]-multi-walled carbon nanotubes (MWCNTs) (95:5 w/w) composite electrode to be useful for adsorptive stripping voltammetry. Screen-printed electrodes modified with [C_8py][PF_6]-MWCNTs were developed and were able to achieve high sensitivity during adsorptive stripping voltammetric measurements under optimised conditions. This work has been published in *Electroanalysis* [1].

7.1 Introduction

Ionic liquids can be defined as organic salts with melting points below 100°C, with typical structures based on an asymmetric heterocyclic cation such as *N*,*N*-dialkylimidazolium and *N*-alkylpyridinium ions, and a poorly coordinating anion such as tetrafluoroborate (BF_4^-), hexafluorophosphate (PF_6^-), and bis(trifluoromethylsulfonyl)imide [$N(Tf)_2^-$] [2]. With properties including nonvolatility, high thermal stability and ionic conductivity, increasing research has been carried out with ionic liquids in areas such as green solvents for organic synthesis, analytical separation and extraction, as well as electrochemical studies and applications [2-5].

The use of ionic liquids for electrode modification has been reported on various substrates such as glassy carbon [6,7], gold [6], carbon fibre microelectrode [8] and basal plane pyrolytic graphite [9]. In combination with carbon powders, ionic liquids have been employed as a binder in the preparation of carbon paste and composite electrodes [10-14] for the detection of different types of compounds such as glucose, ascorbic acid, dopamine, NADH and phenols. Carbon as a versatile and economical material can also lend itself to the fabrication of screen printed electrodes (SPEs), which have utility as disposable electrochemical sensors [15-17]; the merits of SPEs have recently been reviewed [18]. So far, relatively limited work has been done on applying ionic liquids to the modification of SPEs for electroanalysis, apart from a few reports on using ionic liquids as a bulk modifier [19,20] and as a surface modifier [21-23] for the detection of mainly dopamine as well as alkylphenols.

The aim in this chapter is to explore the use of ionic liquids on SPEs for adsorptive stripping voltammetry. For the purpose of illustration the electrochemical sensing of the

endocrine disruptor 17α-ethynylestradiol (EE2) as a model is reported. The effect of different ionic liquids as binder for carbon-ionic liquid composite electrodes is studied and it is shown that the sensitivity of SPEs modified with the carbon-ionic liquid composite can be greatly enhanced. The use of ionic liquid is seen to provide a significant benefit in respect of adsorptive stripping voltammetry and for SPEs in particular and the ideas presented are intended to have generic value rather than aimed at EE2 in particular. Further experiments of the use of CNT/IL composite are summarised in **Table 7.1**.

Table 7.1 Some simple applications of ionic liquid-carbon nanotube composites for non-enzymatic electroanalysis. GC: glassy carbon.

Target	**Substrate**	**Ref**
dopamine	GC	[7]
hydroquinone, catechol	GC	[24]
hydrogen peroxide, iodate	GC	[25]
estradiol	GC	[26]
p-nitroaniline	GC	[27]

7.2 Experimental

7.2.1 Chemicals and materials

$K_2HPO_4 \cdot 3H_2O$ (≥99.0%, Sigma Aldrich), KH_2PO_4 (≥99.0%, Sigma Aldrich), 17α-ethynylestradiol (≥98%, Sigma), 17β-Estradiol (≥98%, Sigma), 4-nonylphenol (99.9%, Fluka), graphite (1-2μm, Aldrich), multi-walled carbon nanotubes (30 ± 10nm, NanoLab Inc.), paraffin oil (puriss, Sigma-Aldrich), *n*-hexyl-pyridinium hexafluorophosphate $[C_6py][PF_6]$ (97+%, Acros Organics) and 1-butyl-3-

methylimidazolium hexafluorophosphate [C_4mim][PF_6] (≥97.0% Aldrich) were used as received. *N*-octyl-pyridinium hexafluorophosphate [C_8py][PF_6], and *n*-butyl-pyridinium bis(trifluoromethylsulfonyl)imide [C_4py][NTf_2] were prepared in high purity and kindly donated by QUILL, Belfast. Standard solutions of each compound (1.0 mmol dm^{-3}) were prepared in methanol and diluted with phosphate buffer solutions (0.10 mol dm^{-3}) to obtain the appropriate concentrations. All aqueous solutions were prepared using ultra pure water (~18.2 MΩ cm at 25°C).

Screen printed electrodes (SPEs) (DropSens, Spain) [28] used in the experiments consisted of a graphite working electrode, a graphite counter electrode and a silver reference electrode. The electrodes were all ink jet deposited onto a ceramic strip of dimensions 34×10 mm, with a disc of diameter 3.8 mm as the working electrode. In place of the silver reference electrode, a Ag/AgCl (1.0 M KCl) reference electrode was used instead.

7.2.2 Apparatus

The working electrode for the standard three-electrode configuration used in this work was either a carbon paste electrode or a SPE graphite electrode, with the counter electrode being a platinum coil or graphite respectively.

7.2.3 Preparation of electrodes

Carbon paste was prepared by hand-pasting graphite and binder (either paraffin oil or ionic liquid) in a ratio of 50:50 (w/w) using a mortar and pestle. The resulting paste was packed into the well (diameter 3.0 mm) of the working electrode to a depth of 0.80 mm and smoothed using a spatula, with the structure of the electrode as explained in

Chapter 5. Where the ionic “liquid” exists as a solid at room temperature, this was first mixed with carbon powder (either graphite or carbon nanotubes) in the required weight loading using a mortar and pestle to form a composite which was then heated to a temperature above the melting point prior to packing into the electrode cavity. For preparation of the modified SPE, 2.0 mg of the carbon nanotubes-[C_8py][PF_6] (5:95 w/w) composite was melted and deposited in liquid form onto the surface of the working electrode where it solidified before use.

7.3 Results and discussion

Modified screen-printed electrodes for adsorptive stripping voltammetry are developed using carbon paste electrodes. The section first investigates how the choice of binder influences the voltammetric response, with particular attention to ionic liquids. This is followed by an optimisation of the electrode for adsorptive stripping voltammetry. The optimised material is then applied to screen-printed electrodes for electroanalysis using 17α-ethynylestradiol as an illustration.

7.3.1 Effect of binder

Based on the observations from the earlier chapters as well as other work from the literature, the binder in a carbon paste electrode was shown in some cases to be able to accumulate material such as ferrocenemethanol [29], N,N’-dimethylaniline [30] and butylated hydroxyanisole [31]. To compare the effect of the binder on the possible accumulation of the estrogenic compound 17α-ethynylestradiol, two different binders – paraffin oil and the ionic “liquid” *n*-octylpyridium hexafluorophosphate [C_8py][PF_6] (melting point 64-65°C [11]) – were combined with graphite (50% w/w loading). The resulting carbon paste electrodes were immersed into an unstirred solution of 0.05 mM

EE2 at pH 7.0 for 0 min and 10 min respectively at open circuit before the start of cyclic voltammetry. The pH is chosen such that it is below the pK_a value of EE2, reported to be 10.40±0.01 [32], so that the compound exists predominantly in the neutral form. Furthermore, pH 7.0 is selected in part because the use of higher pH lowers the oxidation potential and hence the possibility of interference from other reductants in "real" samples. **Figure 7.1** displays the resulting cyclic voltammograms at a scan rate of 100 mV s^{-1}. Each of the forward sweeps shows an anodic peak likely corresponding to the oxidation of the phenolic hydroxyl group on EE2 [33] while no reduction wave can be observed. This indicates that the overall oxidation reaction is chemically irreversible under the conditions of these experiments.

For the graphite-paraffin oil paste electrode (**Figure 7.1**a), the anodic peak potential is at +0.69 V, with a peak current of 0.95 μA when the voltammetry was started immediately after immersion of the electrode into the EE2 solution. When the electrode was left for 10 min in the EE2 solution prior to voltammetry, the peak current increased by 20%. As for the graphite-$[C_8py][PF_6]$ composite electrode (**Figure 7.1**b), the anodic peak seen on immediate immersion occurs at +0.51 V, with a peak current of 5.9 μA. At 10 min, the peak current increased to 46.6 μA, a nearly eightfold increase. Despite the rising capacitive current, the electrode fabricated using $[C_8py][PF_6]$ is superior to that made from paraffin oil given the much greater increase in peak current under the same conditions. This demonstrates that the adsorptive uptake is much stronger for $[C_8py][PF_6]$ than for paraffin oil.

(a)

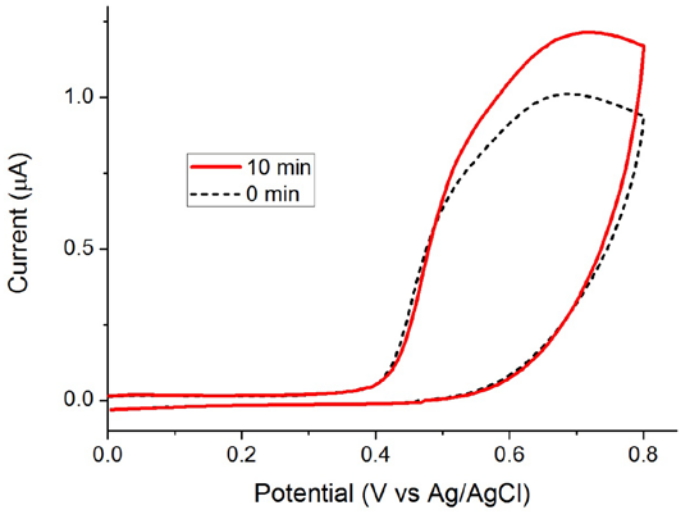

(b)

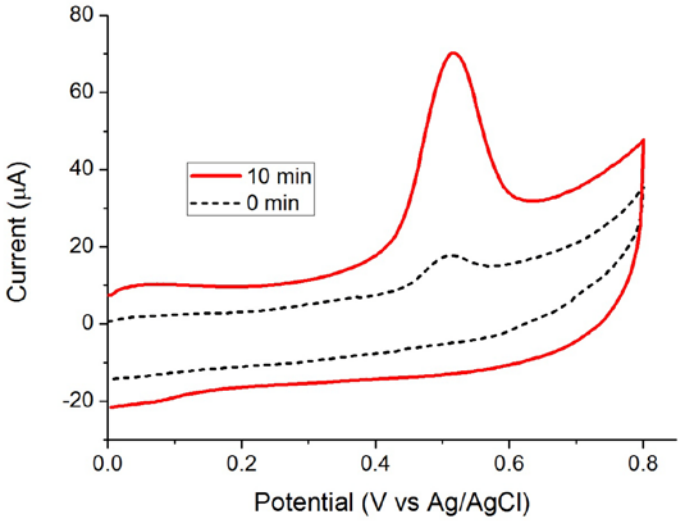

Figure 7.1 Cyclic voltammograms of carbon paste electrode with (a) paraffin oil and (b) $[C_8py][PF_6]$ as binder at 0 and 10 min of immersion in 0.05 mM EE2 in phosphate buffer pH 7. Scan rate: 100 mV s^{-1}.

The accumulation was then carried out under forced convection with a mechanical stirrer at a speed of 2000 rpm to improve the mass transport for different lengths of time prior to voltammetry. **Figure 7.2** shows the cyclic voltammograms measured from 0 min to 120 min at a scan rate of 0.1 Vs^{-1} for the graphite-$[C_8py][PF_6]$ composite electrode. There is a rapid initial rise of the peak current before leveling at 120 min, thus this time of preconcentration under forced convection is used in subsequent experiments. The increasing capacitative current over time is likely associated with water uptake. Heated electrodes are known to reduce capacitative effects in certain cases [10].

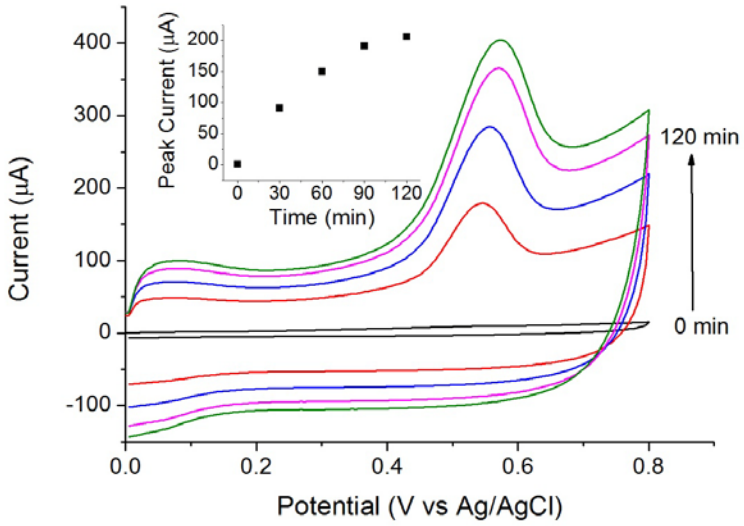

Figure 7.2 Cyclic voltammograms of graphite:$[C_8py][PF_6]$ electrode after immersion for 0 min, 30 min, 60 min, 90 min and 120 min in 5.0 µM EE2 in phosphate buffer pH 7 with stirring. Scan rate: 100 mV s^{-1}. Inset: Graph showing peak current at times from 0 to 120 min.

The behaviour of the endocrine disruptors, namely estradiol and 4-nonylphenol, was also compared under the same conditions. From the cyclic voltammograms shown in

Figure 7.3, the oxidation of these compounds occurs at almost the same peak potential, therefore voltammetric methods can at least provide the total estrogenic content of a sample, rather than distinguish between each of the species.

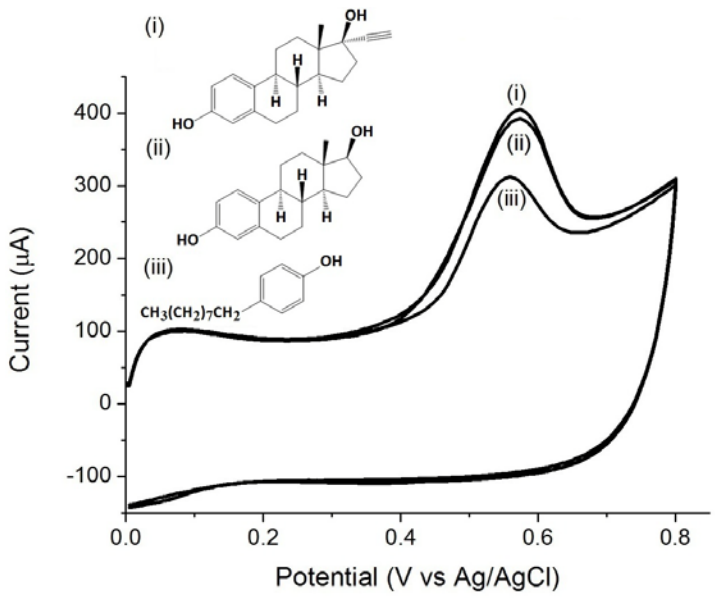

Figure 7.3 Cyclic voltammograms of graphite:$[C_8py][PF_6]$ composite electrode in 5.0 μM (i) EE2, (ii) estradiol and (iii) 4-nonylphenol in phosphate buffer pH 7. Scan rate: 100 mV s^{-1}. Inset: corresponding structures of compounds studied.

7.3.2 Comparison of different ionic liquids

As the binder plays an important role in the accumulation of the analyte, four different ionic liquids were next studied to compare their effect. These are *n*-octyl-pyridinium hexafluorophosphate $[C_8py][PF_6]$, *n*-hexyl-pyridinium hexafluorophosphate $[C_6py][PF_6]$, 1-butyl-3-methylimidazolium hexafluorophosphate $[C_4mim][PF_6]$ and *n*-butyl-pyridinium bis(trifluoromethylsulfonyl)imide $[C_4py][NTf_2]$, with their respective chemical structures given in **Figure 7.4**. $[C_8py][PF_6]$ and $[C_6py][PF_6]$ have melting

points of 64-65°C [11] and 45-48°C [34] respectively and thus as exist as solid at room temperature while [C_4mim][PF_6] and [C_4py][NTf_2] are liquids at room temperature.

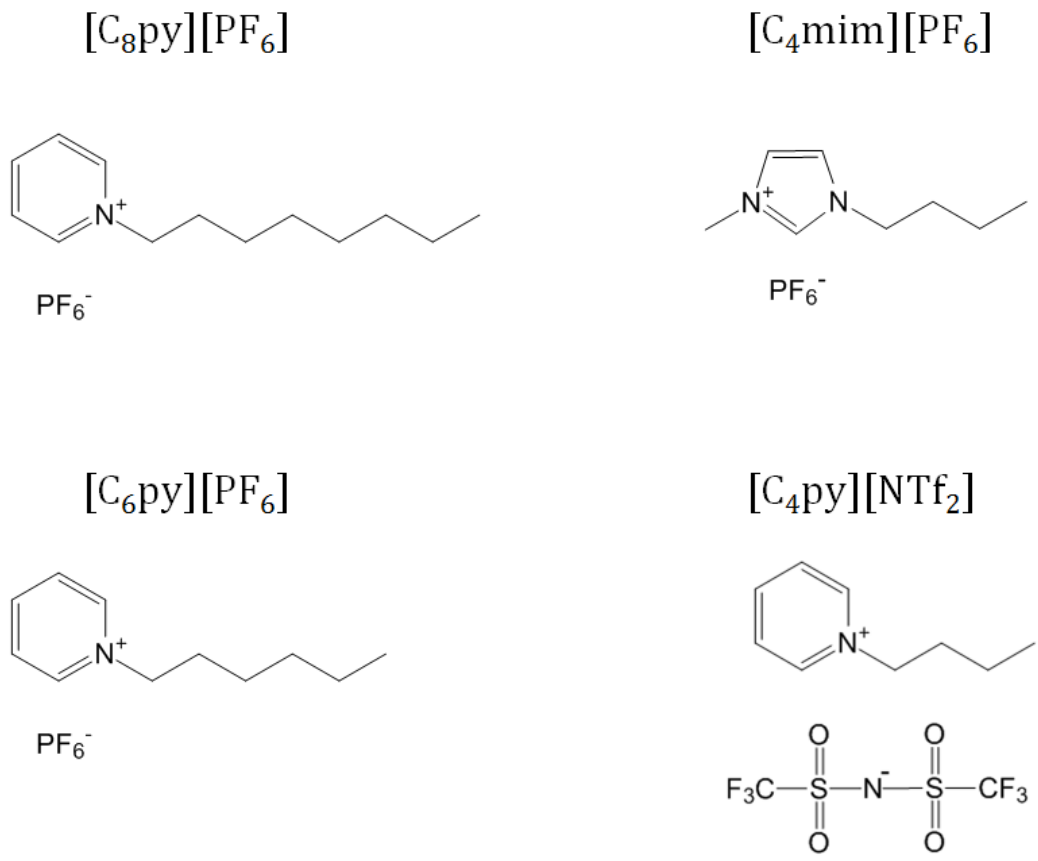

Figure 7.4 Chemical structures of the ionic liquids studied.

Figure 7.5 shows the cyclic voltammetric anodic peak currents at times of accumulation from 60 min to 120 min in 5.0 μM of EE2 in phosphate buffer solution at pH 7.0 for carbon paste electrodes made from each of the ionic liquids as binder. The peak current, which reflects the accumulation ability, consistently decreases in the order: [C_8py][PF_6] > [C_6py][PF_6] > [C_4mim][PF_6] > [C_4py][NTf_2] for each time. This trend might be due to the number of carbon atoms found on the substituent chains, with an increase in the carbon leading to greater hydrophobic interaction with the organic

analyte of a steroidal structure. [C_8py][PF_6] shows superior performance as binder among these ionic liquids and was selected for further study.

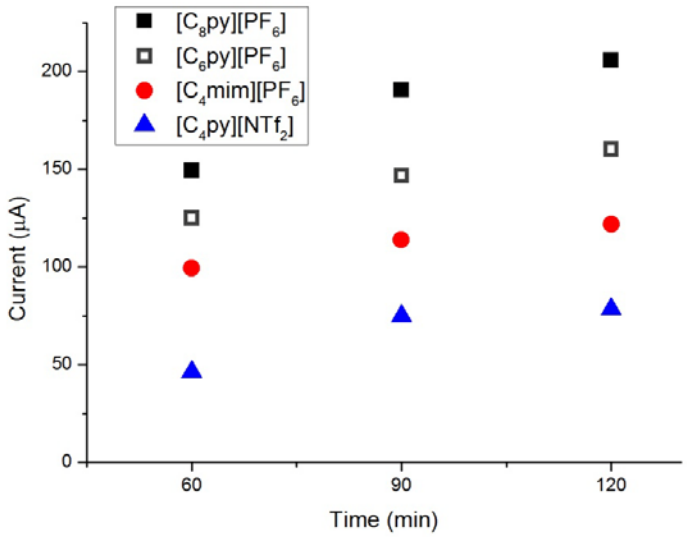

Figure 7.5 Peak currents for voltammetric scans in 5.0 μM EE2 in phosphate buffer pH 7 on graphite paste electrode made with different ionic liquids: ■ [C_8py][PF_6], □ [C_6py][PF_6], ● [C_4mim][PF_6], ▲ [C_4py][NTf_2]) as binder at different times of 60 min, 90 min and 120 min of solution stirring. Scan rate: 100 mV s^{-1}.

7.3.3 Optimisation of electrode composition

After the selection of [C_8py][PF_6] as binder, the composition was varied to obtain the optimal graphite content for subsequent work. **Figure 7.6** illustrates the effect of different carbon content on the cyclic voltammetric responses for 5.0 μM EE2 in phosphate buffer solution at pH 7.0. The increase in background with the increased graphite content likely arises from an increase in the double-layer capacitance and charge build-up at the double-layer interface [12]. Initially the peak current rises and reaches a maximum value at 50% before decreasing. As the electron transfer at the composite electrode can only occur across the carbon|aqueous electrolyte interface, the organic analyte accumulated at the solid ionic “liquid” needs to be spatially adjacent to

the carbon particles for electrochemical oxidation to take place. Therefore the loading of 50% represents the optimal interfacial area for the matrix of graphite and ionic "liquid".

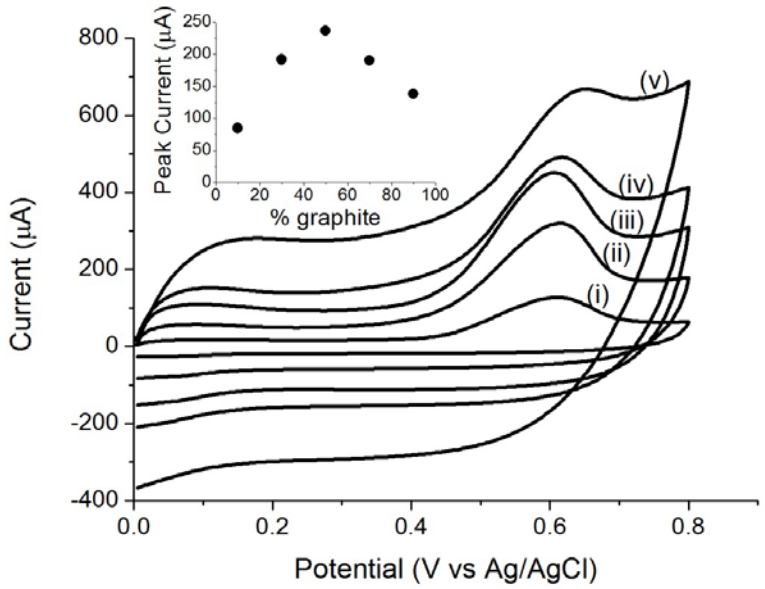

Figure 7.6 Cyclic voltammograms of carbon-[C_8py][PF_6] electrode with (i) 10%, (ii) 30%, (iii) 50%, (iv) 70% and (v) 90% graphite (w/w) in 5.0 μM EE2 in phosphate buffer pH 7. Scan rate: 100 mV s^{-1}. Inset: Plot of peak currents as a function of different percentages of graphite.

Multi-walled carbon nanotubes (MWCNTs) have been shown to provide a high surface area for adsorptive stripping voltammetry [35,36]. Thus a MWCNTs-[C_8py][PF_6] composite electrode was used to compare the effects of using a different carbon powder and optimisation of the carbon content was carried out. From **Figure 7.7**, a similar trend to graphite is seen, but the maximum peak current occurs at a much lower weight loading of 5% and its value is 87% greater than that using graphite. This can be attributed to the larger surface area for the MWCNTs and hence a greater relative adsorptive ability.

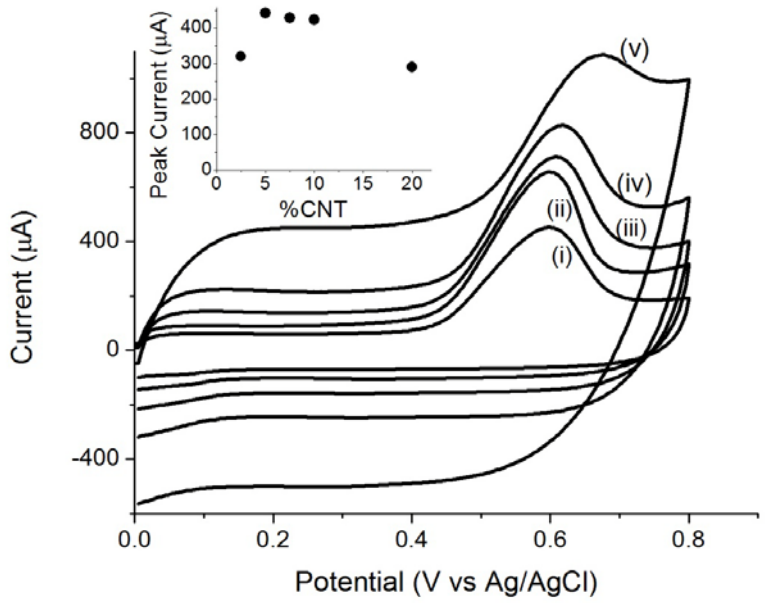

Figure 7.7 Cyclic voltammograms of carbon-[C_8py][PF_6] electrode with (i) 2.5%, (ii) 5%, (iii) 7.5%, (iv) 10% and (v) 20% MWCNTs (w/w) in 5.0 μM EE2 in phosphate buffer pH 7. Scan rate: 100 mV s^{-1}. Inset: Plot of peak currents as a function of different percentages of MWCNTs.

An increase in electrode resistance could exert certain effects on the electrochemical response as the effective potential at the interface differs from the applied potential. Such effects due to the ohmic drop include peak broadening, peak potential displacement and a drop in peak current during cyclic voltammetry [37,38]. In addition, non-faradaic processes could lead to a significant rise in the charge current at the base of the current-potential curve. The considerable charging current observed at the MWCNTs-[C8py][PF6] composite electrodes likely arises from the large double layer capacitance as a result of the high surface area of the MWCNTs. Increasing the loading of the MWCNTs led to an increase in the capacitance (up to values of mF/cm^2) as shown by the rising background current. Studies in which the effects owing to ohmic

drop and charging current are diminished could be carried out through the use of steady state techniques for instance by electrochemical measurements at microelectrodes.

7.3.4 Adsorptive stripping voltammetry on MWCNTs-[C_8py][PF_6] composite electrodes

The optimised MWCNTs loading of 5% was used to make composite electrodes for the adsorptive stripping voltammetric analysis of EE2. **Figure 7.8** shows the standard curve obtained for the optimised MWCNTs-[C_8py][PF_6] electrodes at different concentrations of EE2 in phosphate buffer solution (pH 7.0) and the corresponding linear sweep voltammograms from which the peak current values were derived. Fresh electrodes were used to eliminate any possibility of carry-over. The peak current values exhibited good linearity from 0.08 to 2.0 μM, with a correlation coefficient of 0.991 and a slope of 75.2 ± 2.9 μA μM^{-1}.

The electroanalysis of estrogenic compounds is commonly carried out on carbon electrodes, which mostly require surface modification to achieve greater sensitivity, and the relevant data from the literature are summarised in **Table 7.2** [26,39-45]. It can been seen from **Table 7.2** that the sensitivity obtained with the unmodified MWCNTs-[C_8py][PF_6] composite electrode is the highest among various carbon electrodes. The limit of detection (LOD) was calculated with 3σ to slope [46] to be 4 nM, which is one of the lowest reported for the electrochemical determination of estrogenic compounds on carbon electrodes, as shown in **Table 7.2**.

(a)

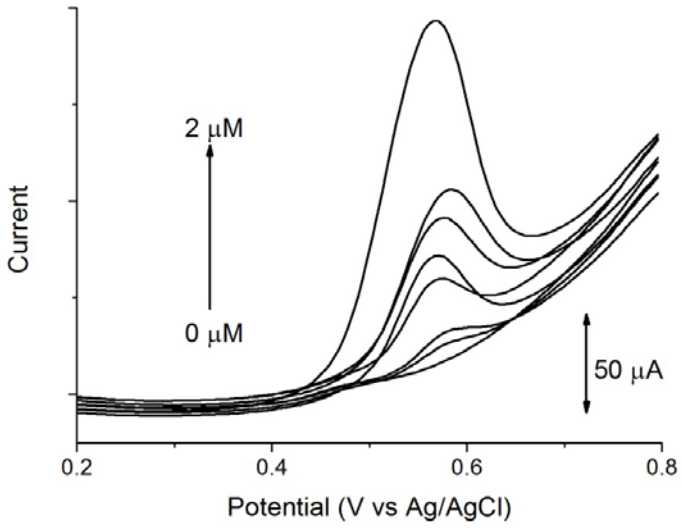

(b)

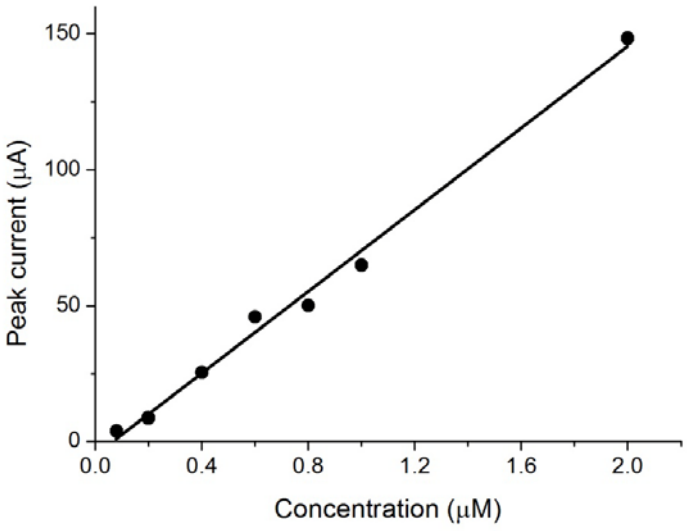

Figure 7.8 (a) Linear sweep voltammograms at EE2 concentrations of 0.0, 0.08, 0.2, 0.4, 0.6, 0.8, 1.0 and 2.0 μM. Scan rate: 100 mV s^{-1}; (b) Calibration curve for MWCNTs-[C_8py][PF_6] composite electrode (5:95 w/w) in EE2 in phosphate buffer pH 7 at concentrations from 0.08 μM to 2 μM.

7.3.5 MWCNTs-[C_8py][PF_6]-modified screen printed electrodes (SPEs)

The MWCNTs-[C_8py][PF_6] composite was then applied to screen printed electrodes (SPEs) as a route to disposable sensors. To modify the SPE, the MWCNTs-[C_8py][PF_6] (5:95 w/w) composite was melted to deposit onto the graphite working electrode. The resulting MWCNTs-[C_8py][PF_6]/SPEs were then immersed in different concentrations of EE2 in phosphate buffer solution (pH 7.0) prior to linear sweep voltammetry. In **Figure 7.9**, the peak current values showed a linear increase from 0.05 to 2.0 μM, with a correlation coefficient of 0.991 and a slope of 66.5 ±2.6 μA μM^{-1}. This sensitivity value is similar to that obtained above, and very high in comparison with the alternates listed in **Table 7.2**. The LOD, calculated as 3σ to slope, is 2 nM and among the lowest of such values found in **Table 7.2**.

(a)

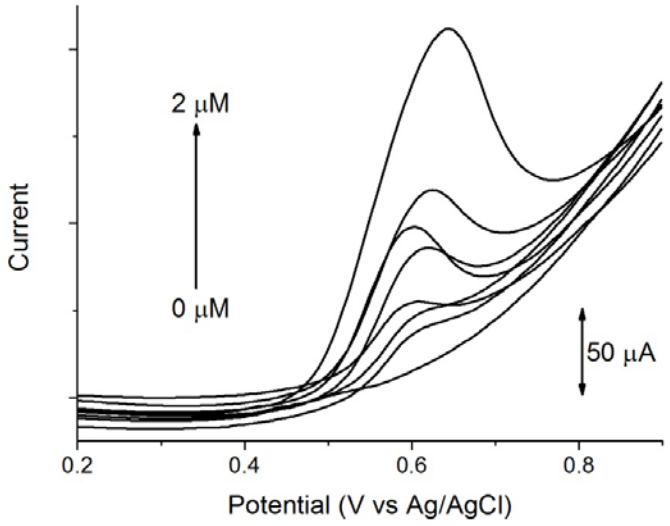

(b)

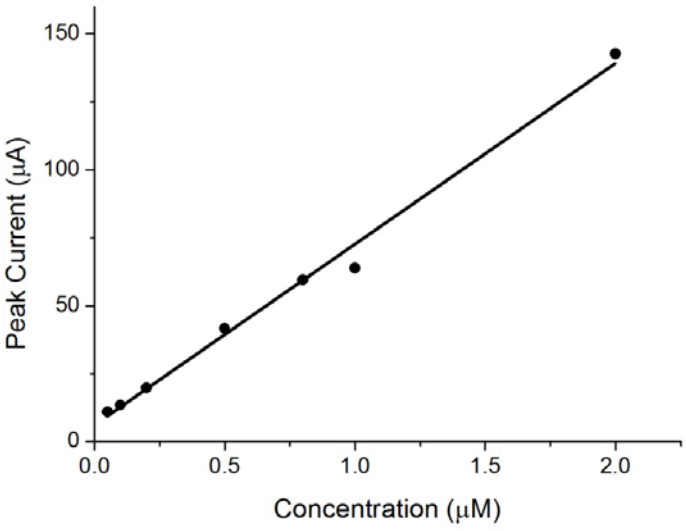

Figure 7.9 (a) Linear sweep voltammograms at EE2 concentrations of 0.0, 0.05, 0.1, 0.2, 0.5, 0.8, 1.0 and 2.0 μM. Scan rate: 100 mV s^{-1}; (b) Calibration curve for MWCNTs-[C_8py][PF_6]-modified graphite SPE in EE2 in phosphate buffer pH 7 at concentrations from 0.05 μM to 2 μM.

Table 7.2 Literature for electroanalysis of endocrine disruptors at different electrodes.

The following abbreviations are used: multi-walled carbon nanotubes (MWCNTs), screen-printed electrode (SPE), glassy carbon electrode (GCE), Ni(II)tetrakis(4-sulfonatophenyl) porphyrin (NiTPPS), nanocarbon (NC), boron-doped diamond (BDD), 1,4,8,11,tetraazacyclotetradecane (cyclam), 17α-ethynylestradiol (EE2), estradiol (E2), estrone (E1), estriol (E3), linear sweep voltammetry (LSV), square wave voltammetry (SWV), hydrodynamic amperometry (HyAm), not reported (NR).

Electrode	**Endocrine disruptor**	**Electrolyte (pH)**	**Technique**	**Linear dynamic range (M)**	**Sensitivity (μA/ μM)**	**LOD (M)**	**Ref**
MWCNTs-[C_8py][PF_6] composite	EE2	PBS (pH 7)	LSV	8.0×10^{-8}—2.0×10^{-6}	75.2 ± 2.9	4×10^{-9}	This work
MWCNTs-[C_8py][PF_6]/SPE	EE2	PBS (pH 7)	LSV	5.0×10^{-8}—2.0×10^{-6}	66.5 ± 2.6	2×10^{-9}	This work
MWCNTs/GCE	EE2	PBS (pH 7)	HyAm	1.0×10^{-6}—1.0×10^{-4}	0.07 ± 0.01	3.4×10^{-7}	[39]
NiTPPS/MWCNTs/GCE	EE2	NaOH	HyAm	2.0×10^{-7}—6.0×10^{-5}	0.12 ± 0.0093	1.2×10^{-7}	[40]
MWCNTs-ionic liquid/GCE	E2	PBS (pH 7)	LSV	1.0×10^{-8}—1.0×10^{-6} 1.0×10^{-6}—7.5×10^{-6}	30.6 6.3	5×10^{-9}	[26]

NC/BDD	E2	PBS (pH 12)	SWV	5.0×10^{-9}—1.0×10^{-7}	28 ± 0.2	2.2×10^{-9}	[41]
Ni(cyclam)/MWCNTs/GCE	E2	NaOH	SWV	5.0×10^{-7}—4.0×10^{-5}	1.92 ± 0.14	6×10^{-8}	[42]
MWCNTs-Nafion/GCE	E2	PBS (pH 7)	SWV	2.5×10^{-7}—1.0×10^{-5}	(1)	1×10^{-8}	[43]
Pt nanoparticles/	E2	PBS (pH 7)	SWV	5.0×10^{-7}—1.5×10^{-5}	0.79	1.8×10^{-7}	[44]
MWCNTs/GCE	E1			2.0×10^{-6}—5.0×10^{-5}	NR	8.4×10^{-7}	
	E3			1.0×10^{-6}—7.5×10^{-5}	NR	6.2×10^{-7}	
BDD	E3	NaOH (pH 12)	SWV	2.0×10^{-7}—2.0×10^{-5}	0.1 ± 0.0008	1.7×10^{-7}	[45]

7.4 Conclusions

Some ionic liquids have been shown to offer benefits in comparison to oil in the fabrication of carbon paste type electrode due to an increased adsorption of analytes, as illustrated with 17α-ethynylestradiol (EE2) as a model. In particular, the solid ionic "liquid" $[C_8py][PF_6]$ is most effective among several ionic liquids studied. The combination of $[C_8py][PF_6]$ with MWCNTs can be used as a composite electrode or as a modifier to a screen-printed electrode to greatly enhance the sensitivity of detection. The limits of detection obtained compare favourably with state-of-the-art values (in the low nM range) for electroanalysis of estrogenic compounds on carbon electrodes as a case in point. In general, SPEs modified with solid ionic "liquid" can be expected to show generic benefits for sensitive electroanalysis via adsorptive stripping voltammetry.

References

[1] P. Gan, J.S. Foord, R.G. Compton, Electroanalysis 26 (2014) 1886.

[2] L.E. Barrosse-Antle, A.M. Bond, R.G. Compton, A.M. O'Mahony, E.I. Rogers, D.S. Silvester, Chem. Asian J. 5 (2010) 202.

[3] J.-f. Liu, G.-b. Jiang, J.-f. Liu, J.Å. Jönsson, TrAC, Trends Anal. Chem. 24 (2005) 20.

[4] M.J. Earle, K.R. Seddon, Pure Appl. Chem. 72 (2000) 1391.

[5] M. Galiński, A. Lewandowski, I. Stępniak, Electrochim. Acta 51 (2006) 5567.

[6] F. Zhao, X. Wu, M. Wang, Y. Liu, L. Gao, S. Dong, Anal. Chem. 76 (2004) 4960.

[7] Y. Zhao, Y. Gao, D. Zhan, H. Liu, Q. Zhao, Y. Kou, Y. Shao, M. Li, Q. Zhuang, Z. Zhu, Talanta 66 (2005) 51.

[8] Y. Liu, X. Zou, S. Dong, Electrochem. Commun. 8 (2006) 1429.

[9] S.-F. Ding, W. Wei, G.-C. Zhao, Electrochem. Commun. 9 (2007) 2202.

[10] N. Maleki, A. Safavi, F. Tajabadi, Anal. Chem. 78 (2006) 3820.

[11] M.M. Musameh, R.T. Kachoosangi, L. Xiao, A. Russell, R.G. Compton, Biosens. Bioelectron. 24 (2008) 87.

[12] R.T. Kachoosangi, M.M. Musameh, I. Abu-Yousef, J.M. Yousef, S.M. Kanan, L. Xiao, S.G. Davies, A. Russell, R.G. Compton, Anal. Chem. 81 (2009) 435.

[13] H. Liu, P. He, Z. Li, C. Sun, L. Shi, Y. Liu, G. Zhu, J. Li, Electrochem. Commun. 7 (2005) 1357.

[14] A. Safavi, N. Maleki, F. Tajabadi, Analyst 132 (2007) 54.

[15] J.P. Hart, S.A. Wring, TrAC, Trends Anal. Chem. 16 (1997) 89.

[16] J. Wang, M. Musameh, Analyst 129 (2004) 1.

[17] M. Li, Y.-T. Li, D.-W. Li, Y.-T. Long, Anal. Chim. Acta 734 (2012) 31.

[18] N. Thiyagarajan, J.-L. Chang, K. Senthilkumar, J.-M. Zen, Electrochem. Commun. 38 (2014) 86.

[19] J. Ping, J. Wu, Y. Wang, Y. Ying, Biosens. Bioelectron. 34 (2012) 70.

[20] J. Ping, J. Wu, Y. Ying, Electrochem. Commun. 12 (2010) 1738.

[21] D.V. Chernyshov, N.V. Shvedene, E.R. Antipova, I.V. Pletnev, Anal. Chim. Acta 621 (2008) 178.

[22] J.-L. Chang, G.-T. Wei, J.-M. Zen, Electrochem. Commun. 13 (2011) 174.

[23] A.-M. Gurban, L. Rotariu, M. Baibarac, I. Baltog, C. Bala, Talanta 85 (2011) 2007.

[24] C. Bu, X. Liu, Y. Zhang, L. Li, X. Zhou, X. Lu, Colloids Surf., B 88 (2011) 292.

[25] B. Haghighi, H. Hamidi, L. Gorton, Electrochim. Acta 55 (2010) 4750.

[26] H. Tao, W. Wei, X. Zeng, X. Liu, X. Zhang, Y. Zhang, Microchim. Acta 166 (2009) 53.

[27] F. Zhao, L. Liu, F. Xiao, J. Li, R. Yan, S. Fan, B. Zeng, Electroanalysis 19 (2007) 1387.

[28] http://www.dropsens.com.

[29] D. Lowinsohn, P. Gan, K. Tschulik, J.S. Foord, R.G. Compton, Electroanalysis 25 (2013) 2435.

[30] C.A.H. Chambers, J.K. Lee, J. Electroanal. Chem. Interfac. Electrochem. 14 (1967) 309.

[31] J. Wang, B.A. Freiha, Anal. Chem. 56 (1984) 849.

[32] A.R. Hurwitz, S.T. Liu, J. Pharm. Sci. 66 (1977) 624.

[33] L. Papouchado, R.W. Sandford, G. Petrie, R.N. Adams, J. Electroanal. Chem. Interfac. Electrochem. 65 (1975) 275.

[34] http://www.fishersci.com/ecomm/servlet/fsproductdetail_10652_632226__-1_0.

[35] R.T. Kachoosangi, G.G. Wildgoose, R.G. Compton, Anal. Chim. Acta 618 (2008) 54.

[36] M.J. Sims, Q. Li, R.T. Kachoosangi, G.G. Wildgoose, R.G. Compton, Electrochim. Acta 54 (2009) 5030.

[37] J. Navarro-Laboulais, J. Vilaplana, J. Lopez, J.J. Garcıa-Jareno, D. Benito, F. Vicente. J. of Electroanal. Chem. 484, (2000) 33.

[38] D. O'Hare, J.V. Macpherson, A. Willows, Electrochem. Commun. 4, (2002) 245.

[39] D. Vega, L. Agüí, A. González-Cortés, P. Yáñez-Sedeño, J.M. Pingarrón, Talanta 71 (2007) 1031.

[40] X. Liu, H. Feng, X. Liu, D.K.Y. Wong, Anal. Chim. Acta 689 (2011) 212.

[41] P. Gan, R.G. Compton, J.S. Foord, Electroanalysis 25 (2013) 2423.

[42] X. Liu, D.K.Y. Wong, Anal. Chim. Acta 594 (2007) 184.

[43] N. Terui, B. Fugetsu, S. Tanaka, Anal. Sci. 22 (2006) 895.

[44] X. Lin, Y. Li, Biosens. Bioelectron. 22 (2006) 253.

[45] K.D. Santos, O.C. Braga, I.C. Vieira, A. Spinelli, Talanta 80 (2010) 1999.

[46] C.M.A. Brett, A.M.O. Brett, Electroanalysis, Oxford University Press, Oxford, 1998.

Chapter 8

Conclusions

This thesis has looked at aspects of the electrochemistry at carbon-based electrodes, in particular those made from boron-doped diamond and carbon composite materials, especially for electrochemical sensing and energetics studies.

An important feature of boron-doped diamond electrodes in electrochemical studies is the surface chemical termination. In the study on the endocrine disrupting compounds, which belong to a class of increasingly important pollutants in environmental waters, the precise tuning of the surface chemical termination has been shown to be able to control the electrochemical mechanism of the reactions of these compounds. The oxygenated (hydrophilic) surface exhibited a diffusional process whilst the hydrogenated (hydrophobic) surface displayed adsorptive behaviour towards the reacting molecules.

The surface modification of boron-doped diamond electrodes by physical immobilisation of microcrystalline copper phthalocyanine was concluded to be sensitive to the surface chemical termination in relation to the oxygen reduction reaction. Oxygen was found to undergo a two-electron cathodic reaction via the peroxide pathway on the modified hydrogen-terminated BDD electrode with a significant lowering of the overpotential whereas such electrocatalytic effect was not

observed on the modified oxygenated BDD, indicating the increased interaction of the molecular modifier with the hydrogenated surface compared to the oxygenated one.

Another material, nanocarbon, has been investigated as a surface modifier to boron-doped diamond, leading to the preconcentration of analyte such that the limit of detection could be improved down to nanomolar levels. Such levels are as good as those offered by other relatively more expensive carbon modifiers such as carbon nanotubes. Nanocarbon has also been concluded to be useful as a bulk electrode in the form of a carbon paste electrode. Its practicality was established by a series of electrochemical characterizations with well-defined redox probes and compared with graphite paste as well as the typical glassy carbon electrode. This material has proven to be a viable alternative to the traditional graphite formulation, exhibiting comparable electron transfer kinetics. In addition, the uptake of solute was observed at the nanocarbon paste electrode. Further examination of this uptake phenomenon allowed the voltammetric study of the interfacial processes taking place and enabled the derivation of the Gibbs energy of transfer between oil and water from the resulting data. Finally the carbon nanotube ionic liquid composite modified screen printed carbon electrode has been shown to be highly sensitive for adsorptive stripping voltammetry.

The above results have demonstrated the significance of the surface chemical termination on boron-doped diamond. Whilst the studies are conclusive, several questions still remain for future experiments. In Chapter 3, the cathodic pretreatment of the BDD electrode resulted in a lowering of the anodic overpotential, to a lesser extent compared to the hydrogen plasma pretreatment. Can the cathodic pretreatment process be improved to achieve the same results as the hydrogen plasma method? To what

extent is the hydrogenation offered by each method? Other than the more commonly accessible terminations of oxygen and hydrogen, what are the effects of other less prevalent surface chemical terminations such as nitrogen towards the electrochemical mechanism and ease of physical modification? These are some areas which merit further research towards greater understanding of the influence of the surface chemical termination of BDD electrodes.

Nanocarbon has received relatively scant attention in the area of electroanalysis until rather recent emerging interest for such use. This work has shown its utility as a surface modifier as well as a bulk electrode in this regard. Further functionalisation of the nanocarbon can be studied to extend its use in electrochemical sensing. The incorporation of bio-recognition compounds onto the nanocarbon particles or within the bulk of the carbon composite electrodes represents an area to explore for biosensing. Catalytic nanoparticles can also be deposited onto the nanocarbon surface to achieve improved properties. Such further research will surely broaden the understanding and applications of this highly accessible and ultra low cost material.